4-2001

Enhancing Commercial Aircraft Survivability via Active Venting

Roger L. Veldman
Western Michigan University

ENHANCING COMMERCIAL AIRCRAFT SURVIVABILITY VIA ACTIVE VENTING

by

Roger L. Veldman

A Dissertation
Submitted to the
Faculty of The Graduate College
in partial fulfillment of the
requirements for the
Degree of Doctor of Philosophy
Department of Mechanical and Aeronautical Engineering

Western Michigan University
Kalamazoo, Michigan
April 2001

ENHANCING COMMERCIAL AIRCRAFT SURVIVABILITY VIA ACTIVE VENTING

Roger L. Veldman, Ph.D.

Western Michigan University, 2001

A new technique for enhancing aircraft safety in the event of an on-board explosion was studied. The method under study employs deployable vent panels located on the fuselage which are activated by an array of pressure sensors in the aircraft interior. In the event that an explosion is detected, appropriate vent panels are rapidly released from the aircraft. This approach seeks to provide timely relief of explosive pressures within an aircraft to prevent catastrophic structural failure.

In this study, the approximate time scale of an explosive detonation and the subsequent sensing and electronic processing was determined. Then, the actuation response times of several vent panel systems were determined through analytical modeling and scale-model experimental testing with good correlation achieved.

A scale-model experimental analysis was also conducted to determine the decompression venting time of an aircraft fuselage under a variety of conditions. Two different sized pressure vessels were used in the experimental work and the results correlated quite favorably with an analytical model for decompression times.

Finally, a dynamic finite element analysis was conducted to determine the response of a portion of a typical commercial aircraft fuselage subjected to explosive

pressure loading. It was determined from this analysis that the pre-stressing of the fuselage from cabin pressurization increases the damage vulnerability of a commercial aircraft fuselage to internal explosions. It was also learned from the structural analysis that the peak fuselage strains due to blast loading occur quickly (within approximately 2 milliseconds) while it was conservatively estimated that approximately 5 to 7 milliseconds would be required to sense the explosion, to actuate selected vent panels, and to initiate the release of cabin pressure from the aircraft. Additionally, since it was determined that predicted fuselage strains for both pressurized and unpressurized load cases remained well below the material strain limit, ultimate failure of the aircraft under blast loading may occur later than originally thought due to secondary explosive pressure reflections and the significant overall increase in cabin pressure after detonation. This delayed onset of failure indicates that an active venting system may indeed be capable of functioning rapidly enough to reduce significant fuselage explosive damage.

INFORMATION TO USERS

This manuscript has been reproduced from the microfilm master. UMI films the text directly from the original or copy submitted. Thus, some thesis and dissertation copies are in typewriter face, while others may be from any type of computer printer.

The quality of this reproduction is dependent upon the quality of the copy submitted. Broken or indistinct print, colored or poor quality illustrations and photographs, print bleedthrough, substandard margins, and improper alignment can adversely affect reproduction.

In the unlikely event that the author did not send UMI a complete manuscript and there are missing pages, these will be noted. Also, if unauthorized copyright material had to be removed, a note will indicate the deletion.

Oversize materials (e.g., maps, drawings, charts) are reproduced by sectioning the original, beginning at the upper left-hand corner and continuing from left to right in equal sections with small overlaps.

Photographs included in the original manuscript have been reproduced xerographically in this copy. Higher quality 6" x 9" black and white photographic prints are available for any photographs or illustrations appearing in this copy for an additional charge. Contact UMI directly to order.

Bell & Howell Information and Learning
300 North Zeeb Road, Ann Arbor, MI 48106-1346 USA
800-521-0600

ACKNOWLEDGEMENTS

There are many people who I would like to thank for their contributions to this project. First of all, I would like to thank my dissertation advisor Dr. Judah Ari-Gur for his initial vision for this study, his keen insights on the project, and his support and encouragement on this project from start to finish. I would also like to thank Dr. Naghshineh, Dr. VandenBrink, and Dr. Waas for serving on my dissertation committee. Additionally, I would like to thank Dr. VandenBrink for serving as my master's project advisor and for teaching me a great deal about the finite element method. A large debt of gratitude is owed to Brad Mulder, Hope College instrument maker, for his mastery in turning experimental ideas into reality. Dr. Vipperla Venkayya, Director of the Flight Structures Division of the Air Force Research Lab at Wright-Patterson Air Force Base in Dayton, Ohio, was also a great help in providing specific aircraft design information and background materials on previous research work.

Financially, this work was assisted by a research seed grant from the Michigan Space Consortium and through the support of a Hope College faculty development grant.

Finally, and most of all, I want to thank my wife, Cheryl, who believed in me more than I believed in myself. You have made all the difference.

Roger L. Veldman

TABLE OF CONTENTS

Table of Contents – Continued

Table of Contents – Continued

CHAPTER

Table of Contents – Continued

CHAPTER

Table of Contents – Continued

LIST OF TABLES

List of Tables-Continued

LIST OF FIGURES

List of Figures-Continued

CHAPTER I

BACKGROUND

Background on Research Into Aircraft Protection From Explosions

From 1960 to 1997, there were 33 cases of commercial aircraft being damaged or destroyed due to in-flight detonation of explosive devices (Aoude, 1999). Twelve of these incidents have resulted in a complete loss of the aircraft. One such catastrophic aircraft failure occurred on Pan Am Flight 103 over Lockerbie, Scotland, on December 21, 1988. An extensive investigation of the Pan Am 103 tragedy attributed the catastrophic failure of the plane to the detonation of an improvised explosive device located in a metal luggage container in the plane cargo hold (Anon., 1990). Subsequent to these findings, United States President George Bush formed the Commission on Aviation Security with two major goals: to determine the explosive limits of current aircraft, and to propose measures to prevent a similar occurrence (Kurtz, 1993).

Over the past decade, largely as a result of this initiative, there has been an increase in research targeted at mitigating the effects of explosions on commercial aircraft. This research effort focuses on finding ways to protect an aircraft against relatively small quantities of explosives which are difficult to detect, because, typically, explosives weighing less than three pounds cannot be reliably detected

using current airport security systems (Ashley, 1992). It is generally believed that the explosive device which caused the catastrophic failure of the Boeing 747 of Pan Am Flight 103 contained less than one pound of explosives (Wald, 1997).

Therefore, aircraft hardening researchers are tasked with proposing measures to allow an aircraft to better withstand the blast effects of relatively small quantities of explosives. Research approaches have been generally targeted at methods of absorbing or redirecting explosive pressures away from the aircraft structure. These blast control techniques usually require design changes in the aircraft, aircraft luggage containers, or both.

Because data from historical bombings indicate that in about half of reported cases, explosive devices were placed outside of the cargo hold (Aviation Security: Development, 1994), both the cargo area and passenger cabin should be considered as potential bomb locations. New design features are needed to minimize the damage caused to a commercial aircraft by the internal detonation of an explosive device in order to prevent a catastrophic failure of the structure.

Currently Proposed Methods of Solution

As a result of research efforts in recent years, several potential solutions for protecting aircraft structures from explosions have been proposed. Solution approaches can be categorized in three groups: 1) methods for luggage containers; 2) Methods for the aircraft cargo bay; and 3) methods for the aircraft fuselage.

Methods for Luggage Containers

One proposed solution involves modifying conventional luggage containers, or unit load devices (ULDs), in an attempt to absorb energy from an explosion, and thereby protect the aircraft structure.

Luggage containers, used on wide body aircraft, allow increased efficiency in loading and unloading materials into the cargo area. Luggage containers are filled with baggage or other materials outside of the aircraft and then the entire container is loaded onto the plane. Conventional luggage containers are constructed of thin aluminum sheet metal or plastic. In their current form, luggage containers provide little protection from internal explosions. In an effort to enhance the bomb-resistance of ULDs, a method of strengthening or hardening luggage containers has been proposed by various commercial interests (Ashley, 1992).

Several design concepts of hardened luggage containers have been modeled, built, and tested. In an effort to resist container rupturing, Mlakar (1997) proposed a preliminary luggage container design with a strengthened door closure that engages with increasing force in the event of an internal explosion. Mlakar and Smith (1997) further proposed a ULD constructed of composite panels with integral reinforcing fibers. These panels are secured to the container door by means of an interlocking grip which tightens under internal pressures. Both designs suggest the use of slightly perforated container walls to allow controlled pressure release. This indicates that pure containment of an explosive pressure within a luggage container may not be feasible

and that allowing for a controlled pressure release is necessary to prevent container rupturing.

Test results of a prototype composite container were published by Mlakar, Klein, and Smith (1992). Initial explosive tests demonstrate the ability of the container to withstand a blast from a small quantity of explosive material. Although no explicit explosive quantities were given, typical explosive weights for this testing are assumed to be less than three pounds.

Another approach to hardened luggage containers has been presented by Sanai and Greenfield (1993). The first of their proposed hardened luggage containers is constructed of two layers. The inside layer, constructed of lightweight foam, is designed for debris capture. The inner layer is surrounded by an outer pressure mitigation layer which is designed to be flexible in order to change from a rectangular to a circular cross-section under explosive internal loading, and to withstand blast induced hoop stresses. The outer flexible layer would also be porous to allow a controlled rate of venting of the gaseous detonation products. This semi-permeable outer shell construction allows a slow release of explosive pressures in order to increase the time duration of loading on the aircraft. This approach is intended to eliminate explosive shock loading.

In addition, Sanai and Greenfield (1993) suggested that their luggage container could employ weaker end sections which are designed to fail during an internal explosion. As the end members fail, they allow blast pressures to escape into adjacent containers. Special consideration would be needed for the outermost luggage containers which have no adjacent container in which to vent. This could require

aircraft modifications in areas adjacent to the outermost containers in order to prevent direct blast loading of the aircraft structure. Reported scale model testing of this Sanai and Greenfield container has shown "promising results" (Anon., 1992).

Methods for Cargo Bay

A second proposed explosion counter-measure involves lining the cargo area of an aircraft with energy-absorbing materials. This approach is intended to absorb the energy of an explosion. It attempts to either contain, slow, or redirect the blast before it reaches the passenger cabin and the aircraft frame (Anon., 1990).

Researchers at Britain's Royal Ordnance Factories in London have proposed the installation of a honeycomb construction of metal and plastic foam panels to line the walls of aircraft cargo holds. These energy-absorbing and reflecting materials are intended to contain and redirect the initial blast away from the aircraft structure. Additionally, it has been suggested that the reflected blast pressures could be directed out of the plane via a blowout panel in the fuselage (Ashley, 1992).

The cargo hold lining concept was tested in a full-scale explosive test of a pressurized Boeing 747 in Leicestershire, England, on May 17, 1997. Initial test results indicate that linings may offer an improvement in blast protection versus an unlined cargo area. (Wilson, 1997).

Methods for Fuselage

A third proposed solution involves using blowout panels for aircraft structures. A blowout panel is a structural element incorporated into the fuselage and

designed to be weaker than the surrounding airframe. In the event of an internal explosion, a blowout panel is designed to fail in order to allow pressure release before the plane itself suffers significant damage. Blowout panels are also designed so that, during an explosion, the aircraft structure fails in a controlled manner, thereby avoiding cracks in the aircraft skin at the aperture boundaries which can propagate rapidly through the fuselage (Anon., 1990). The blowout panel approach has been suggested by several parties (Ashley, 1992), and findings presented by researchers at NKF Engineering conclude that, upon preliminary analysis, blowout panels are a feasible concept. (Moyer, McNaight, and Miller, 1992).

Shortcomings of Existing Solutions

Although each of the proposed solutions have shown some promise in reducing the severity of particular explosions, none presents a comprehensive approach to protecting commercial aircraft.

The hardened luggage container solution has been widely modeled and tested, and seems to offer adequate protection for cases where explosives occur *inside* the ULD. This solution may succeed in protecting wide-body aircraft which utilize luggage containers; unfortunately, however, approximately three-quarters of terrorist bombings in recent years have occurred aboard the larger fleet of narrow body aircraft which generally do not use luggage containers (Ashley, 1992). Additionally, even aircraft that use luggage containers often carry un-containerized baggage, leaving them vulnerable to damage from on-board explosions. Furthermore, hardened luggage containers are irrelevant to explosions which occur in the passenger cabin.

Another concern with hardened luggage containers is the added weight to an aircraft. A U.S. government report estimates that composite containers would add an average of 3,200 pounds to the weight of a wide-body aircraft when compared to conventional aluminum containers (Anon., 1994). There are also durability concerns with luggage containers made from composite materials, which could result in shortened service life.

Although the concept of lining the cargo bay with blast-absorbing materials shows promise in structurally protecting the aircraft, this approach introduces a significant weight increase due to the addition of large quantities of explosion-absorbing materials. Additionally, research has been primarily focused on linings for the cargo area, without consideration for the passenger cabin. It is possible that linings for the passenger cabin may not be feasible due to potential harm to passengers and flight crew caused by the containment of explosive pressures.

The final explosive protective measure, blowout panels, has the advantage of being adaptable to various aircraft styles without adding significant weight. The major concern with blowout panels, however, is response time. During an explosion, internal aircraft pressures must be relieved rapidly before major structural failure occurs. Blowout panels, which are considered passive vents, fail only after a threshold value of pressure is exceeded inside the aircraft. In this scenario, pressure venting begins only after significant pressure has built up, in which case structural damage to the aircraft may have already occurred. Thus, it appears that blowout panels may not provide adequate response time for optimum explosive pressure release from the aircraft.

Additionally, blowout panels would require a major redesign of the aircraft structure in the form of perimeter-strengthened support members. Blowout panels may also pose durability concerns under multi-cycle flight loadings as they are designed to be weaker than the surrounding aircraft structure and would be suspect for early or inadvertent failure.

The Need for a New Approach

Clearly, a need exists for a comprehensive method of mitigating the effects of an on-board aircraft explosion on an aircraft structure. The ideal solution would apply to either explosions in the passenger cabin or cargo areas of all types of aircraft, without adding significant weight. It would be additionally advantageous if the new explosive countermeasure could be retrofitted onto existing aircraft.

Unique Contribution of This Study

Since the bombing of Pan Am Flight 103 in 1988, there have been extensive investigations into methods of increasing the resistance of commercial aircraft structures to damage from on-board explosions. Many of these prior studies have stated the potential benefits of an aircraft venting system for releasing cabin pressurization and explosive pressures. In nearly every case, however, the venting concept is listed as a topic for future research and, as of this writing, no comprehensive studies of the feasibility of aircraft venting have been published.

The earliest modern mention of aircraft venting is found in the accident investigation report by the British Government in the wake of the Pan Am 103

disaster. In an appendix titled, "Potential Remedial Measures", the British report concludes that since the pure containment of explosive energy would not be viable in actual practice (such as through the use of hardened luggage containers), a combination of partial containment and venting of the blast through pre-determined blow-out regions in the fuselage skin should be pursued. The blow-out regions are described as passive structural members which would fail in a controlled manner at a pre-determined pressure differential (Anon, 1990).

In 1992, Moyer, McNaight, and Miller published the only known study that directly addresses the aircraft venting concept. In this work, a finite element analysis is used to model the failure behavior of a stiffened, riveted vent panel. Although this study gives a useful examination of the local effects of the failure of a single passive vent panel, it addresses neither the feasibility of such a system in light of required system response time nor the concept of actively releasing vent panels.

Also in 1992, it was reported that researchers at Britain's Royal Ordnance Factories were considering the combined use of blast absorbing linings and passive fuselage vent panels or "cat flaps" in the cargo area (Ashely, 1992). Since this concept was initially mentioned in 1992, no published results of this work have appeared.

In 1996, Moon, Bharatram, Schimmels, and Venkayya concluded an extensive study intended to define a vulnerability map of a commercial aircraft structure for detonations of various quantities of explosives originating at various locations inside the fuselage. In concluding this work, two of the goals for future research were stated as; 1) The need to better define the effects of internal pressure (cabin pressurization)

and 2) A study of the effectiveness of blowout panels at carefully selected locations. These written recommendations were emphasized again in a personal conversation with Dr. Vipperla Venkayya at the Air Force Research Lab at Wright Patterson Air Force Base in Dayton, Ohio, on October 5, 1999.

Arising from these and other suggestions for an investigation of the venting concept, this dissertation research represents the first known attempt to systematically address the effectiveness of an aircraft venting system. In particular, a feasibility assessment of whether such a system could respond rapidly enough to reduce aircraft structural damage from an on-board explosion is conducted. Further, this study introduces for the first time the concept of active venting as a method of increasing the system response time over passive vents or blowout panels.

In sum, this research represents a first attempt at quantitatively assessing the feasibility of utilizing active pressure venting to improve the resistance of commercial aircraft to on-board explosions in an effort to enhance the overall safety of the traveling public.

CHAPTER II

INTRODUCTION

New Method – Active Explosive Venting for Commercial Aircraft

A new technique for improving commercial aircraft survivability is investigated here which utilizes deployable, or active vent panels. In the event of an explosion on-board an aircraft, these vent panels would be released or forcefully separated from the aircraft fuselage by a system of pressure sensors, electronic processing units, and panel actuators located throughout the aircraft. The rapid release of these selected vent panels would allow immediate venting of internal cabin pressures in order to minimize damage to the aircraft structure.

The use of active vent panels presents many advantages over previously proposed solutions. First, active venting can be applied to all portions of an aircraft and used on all types of aircraft, without adding significant weight. Additionally, active vent panels can be designed to provide adequate reliability and strength without causing weakened structural areas such as required by blowout panels. Finally, by design, active vent panels allow for rapid activation to overcome the slow response time of blowout panel.

Research Plan

The effectiveness of a rapid venting system in reducing structural damage from an on-board explosion depends on the speed at which internal pressures can be relieved. The first goal of this study is to establish the time duration and sequence of events which occur during the detonation of an explosion on an aircraft and during the subsequent functioning of an active venting system. Once the time sequence of events has been determined, the structural response of an aircraft will be evaluated, both with and without an active venting system in place. The results of the structural analysis will be used to evaluate the overall merit of the active venting approach. The sequence of research tasks used in this study is given in Figure 1. A brief description of each of the major research activities in this study follows:

Determination of Time Duration of Events

The time of response of the individual events associated with the aircraft venting process must be determined. This will be accomplished in several ways (Table 1). By combining the response times for the individual events outlined in Table 1, an overall system response time can be established (Figure 2).

Dynamic Structural Response of Aircraft

Once a time scale of events has been determined, the appropriate transient pressure profile will be used in a dynamic structural analysis. For this task, a portion of the aircraft fuselage will be modeled using the finite element method. The pressure profile typical of an explosive blast will then be applied to the fuselage model.

Initially, the structural response and resulting fuselage damage will be determined for the control case (without active venting). The results from this case will then be compared with those from the active venting model which includes the release of a panel member and the subsequent decaying pressure profile inside the fuselage.

Table 1

Methods Used to Determine the Response Time of Various Events

Event	Methods Used to Determine Response Time
Explosive Detection	• Explosive Propagation Velocities • Pressure Transducer Response Times
Control System Processing	• Published Research Data
Panel Actuation	• Scale Model Testing • Analytical Models • Published Research Results
Aircraft Decompression Time	• Scale Model Testing • Analytical Model

Evaluation of Venting System Effectiveness

The dynamic structural analysis results will be used to evaluate the effectiveness of the active venting system. By comparing the structural damage from the un-vented fuselage model to that of the vented fuselage, the merit of the active venting process can be evaluated.

Sequence of Research Tasks Used in this Study

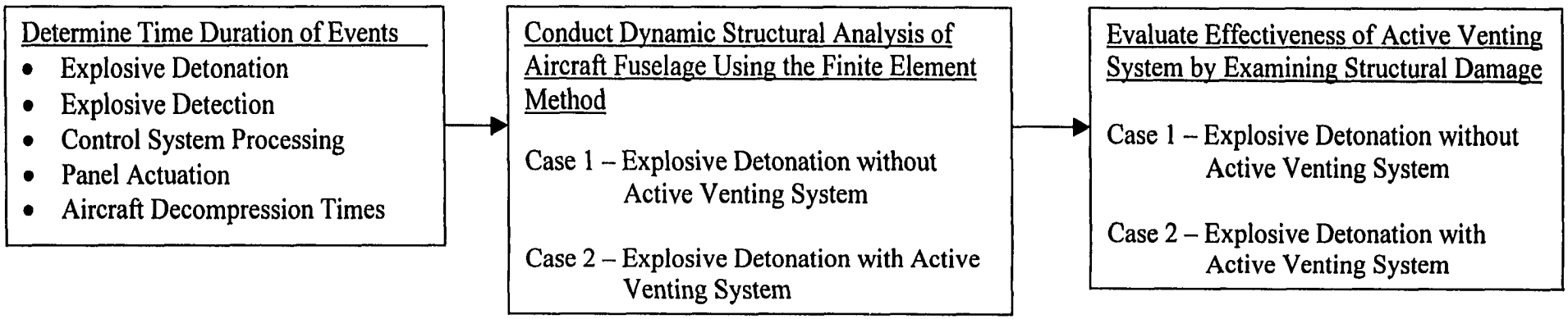

Figure 1. Flow Chart Indicating the Sequence of Research Tasks Involved in This Study.

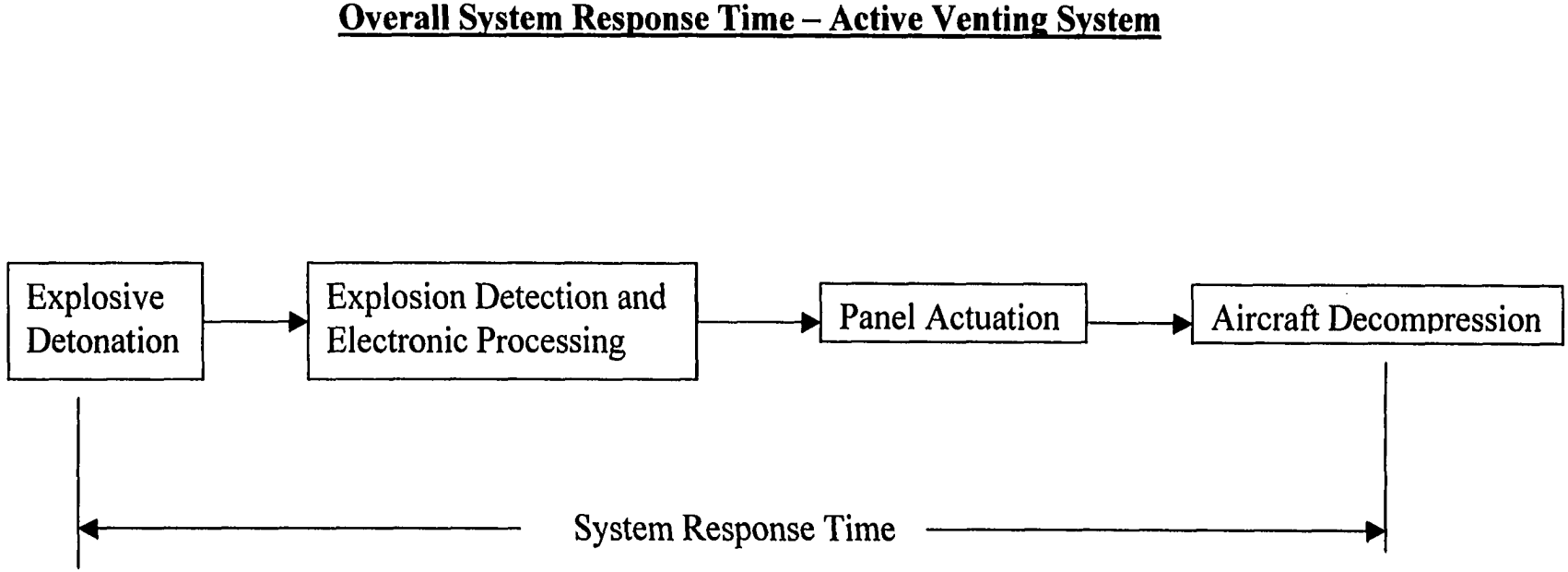

Figure 2. Sequence of Events Which Comprise Overall System Response Time.

CHAPTER III

EXPLOSIVE DETECTION AND CONTROL SYSTEM

Introduction

Active venting employs a system of sensors, actuators, and processors to detect an on-board explosion and to rapidly release portions of the aircraft fuselage in order to relieve internal pressures. An effective active venting system requires rapid and accurate functioning of all components. Due to the fast nature of an explosive event, a system response time on the order of a few milliseconds is required. This challenging design parameter demands the use of uniquely selected components in order to ensure effective functioning of the system.

The typical sequence of events involved in the deployment of an active venting system is depicted in Figure 3. In order to determine the response time of the detection, processing, and output control signal events, one must first understand the nature of an explosive detonation.

Explosion Characterization

Background on Explosive Detonations

In order to design an effective explosion detection system, it is important to understand the types of explosive detonations which the system may encounter. It has

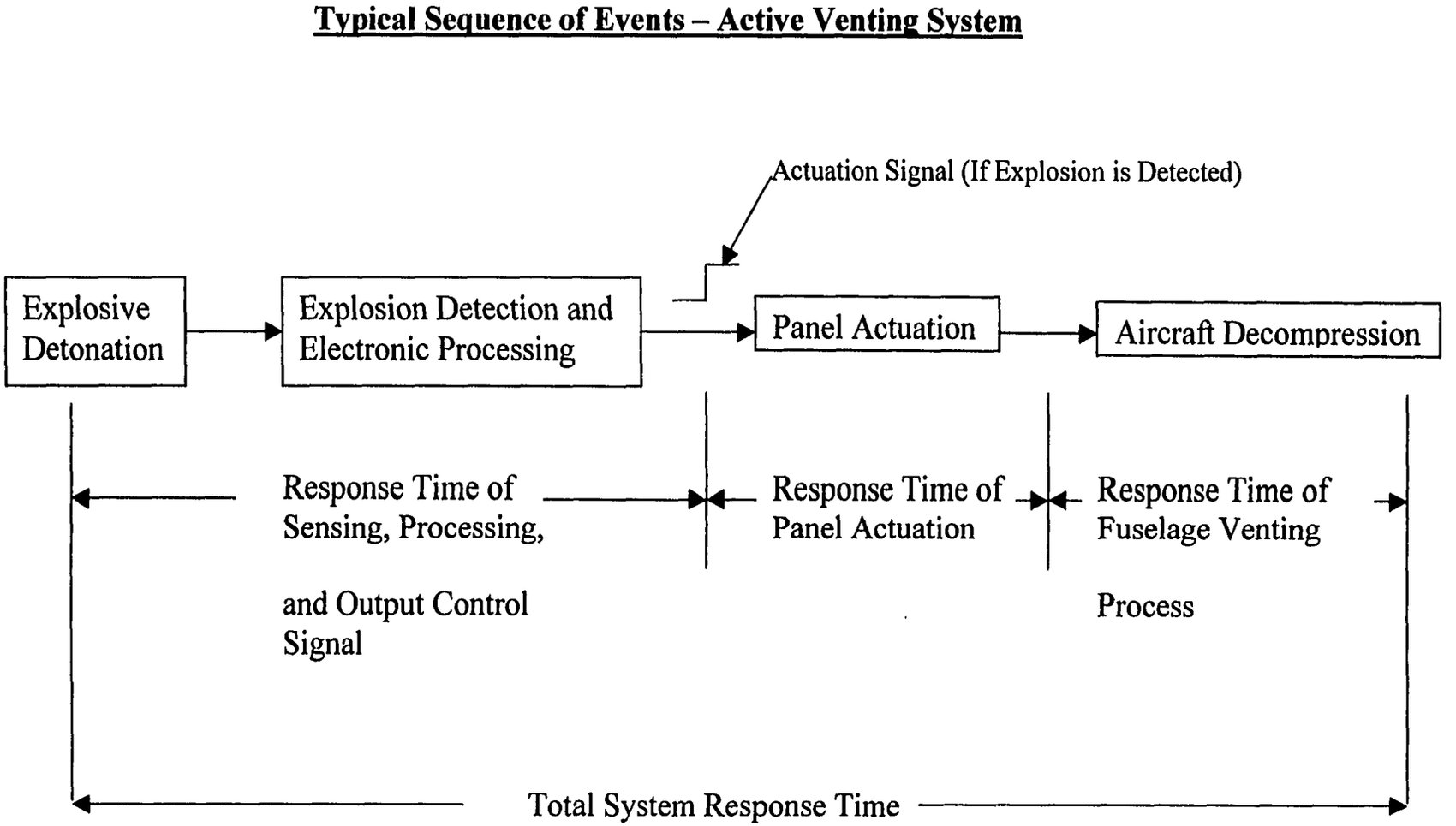

Figure 3. Sequence of Events for Active Venting System.

been established that existing airport security measures are typically capable of detecting explosives weighing 3 pounds (1.4 kg) or more (Ashley, 1992); thus, the primary threat to aircraft are posed by smaller devices. These explosives can contain a wide variety of explosive materials including plastic explosives such as PETN, HMX, and RDX (Anon., 1993) which are especially difficult to detect with existing airport security measures.

It has also been established that the detonation of even relatively small explosive devices can cause tremendous damage to the structure of existing commercial aircraft due to the pressure wave resulting from an explosion. The detonation of an explosive produces a rapid release of energy into the surrounding air. This energy release creates a sudden pressure increase which propagates through space as a pressure wave. The propagation proceeds (in the case of an ideal, spherically shaped explosive) radially outward from the explosive device. As the pressure wave passes through space, a nearly discontinuous increase in pressure, known as a shock wave, develops across the wave front due to the compressible nature of air. If an ideal pressure transducer, capable of perfectly tracking instantaneous changes in pressure were placed at a fixed distance from the explosion, the pressure response shown in figure 4 would be observed (Baker, 1973).

An approximate expression for the velocity of a shock wave traveling through

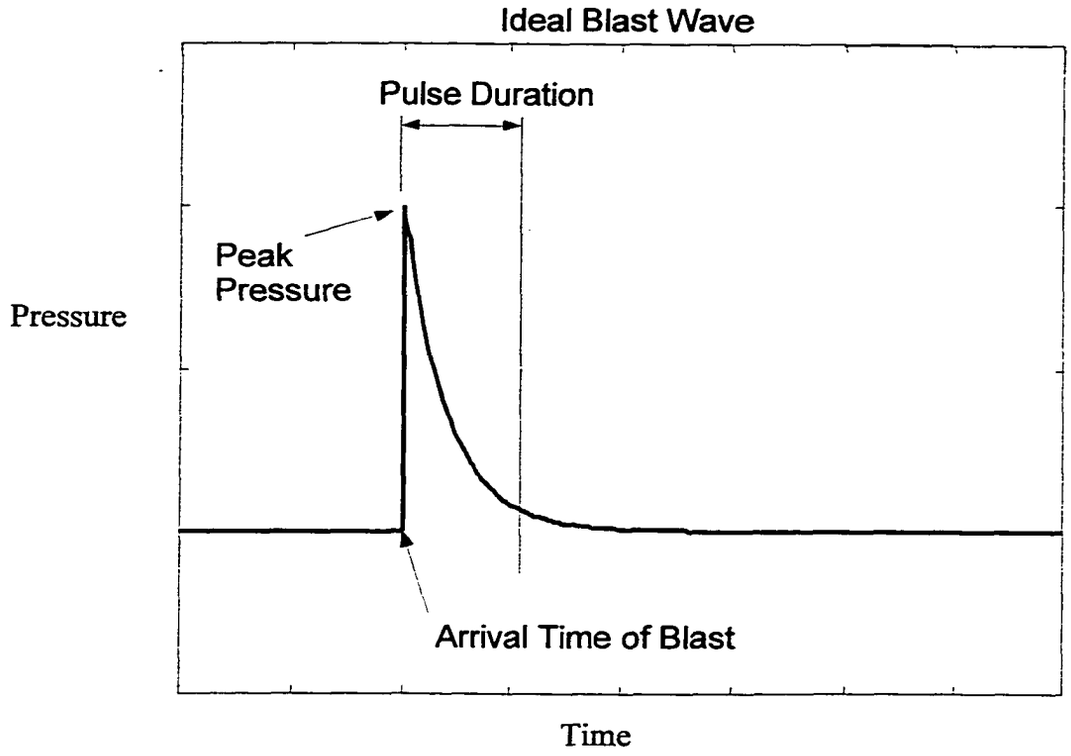

Figure 4. Idealized Pressure Profile for a Sensor Located a Fixed Distance From an Explosive Detonation. (Adapted from Baker, 1973).

air has been given by Glasstone (1977) as:

$$S = c_0\left(1+\frac{6p}{7p_0}\right)^{1/2} \tag{3.1}$$

Where: S = Speed of explosive shock wave
P = Explosive overpressure
P_0 = Atmospheric pressure
C_0 = Speed of sound in air (335 m/s at standard atmosphere)

Thus, for typical overpressures from a small explosive device (as described in greater detail in the following section), shock velocities on the order of 2 to 3.5 times the speed of sound (670 to 1170 meters/second) can be expected.

It is worth noting that, in most cases, shock wave propagation in air is significantly slower than the detonation velocity, V_e, within the explosive material itself. Values of V_e for selected explosive materials are given in Table 2 (Bangash, 1993; Zukas, 1998). It is further noted that explosives are often characterized as low explosives or high explosives. Low explosives, such as black powder, detonate at a relatively slow rate with detonation velocities on the order of a few hundred meters per second. High explosives, on the other hand, are characterized by very high rates of reaction and pressure release, with detonation velocities in the range of 5,000 to 9,000 meters per second (Zukas, 1998).

Table 2

Initial Shock Wave Velocities of Selected Explosive Materials

Explosive Material	Velocity of Detonation (meters/second)
AG Dynamite	6600
Black Powder	1350
HMX	9110
PETN	7980
RDX -	8640
TNT – Trinitrotoluene	6800

Shock wave propagation is quite predictable when the explosion occurs in free space. Eventually, especially in the interior of an aircraft, a propagating blast wave will contact a solid object or surface. When this happens, consideration must be given to reflections and recombinations of shock waves. For purposes of designing an active venting system, however, understanding these effects is not essential. The active venting system is designed to detect the initial free air blast and to immediately

actuate pressure relief panels on the fuselage. This activity should typically occur well before the onset of secondary shock wave reflections.

Background on Measured Explosive Detonation Pressures

With this background, some important parameters can be established to help characterize an explosive detonation. First, the peak pressures associated with an explosion on a commercial aircraft must be established. Ewing, Kivity, and Lenselink (1992) have conducted experimental explosive tests on a stiffened aluminum cylinder. They detonated a spherical, 90 gram (0.2 pound) mass of C4 high explosive at a central location within the closed cylinder. Pressure gages at 0.685 meters (27 inches) from the explosive source measured peak pressures of around 3.17 MPa (460 psi). In this test, it was believed that direct impact of debris on the sensor caused an increase in peak pressures, as handbook calculations had predicted peak pressures of about 1.7 MPa (250 psi).

Another peak pressure reference point was given by Strang (1992), who cites experimental and predicted pressures for the detonation of a "medium-sized explosive" within a 1.52 meter (60 inch) diameter cylinder. A peak pressure of .586 MPa (85 psi) is given at a distance of 0.76 meters (2.5 feet) from the blast. At a distance of 1.52 meters (5 feet), a peak pressure of 0.12 MPa (17 psi) was reported.

Another peak pressure reference is given by White, Bharatram, and Venkaya (1992) who conducted blast tests on a retired B-52 fuselage. At distances of 0.61 meters (2 feet) from a "medium sized charge," a peak pressure of 1.45 MPa (210 psi) was measured. At distances of 1.22 to 1.82 meters (4 to 6 feet) from the explosive,

peak pressures of 0.345 to 0.483 MPa (50-70 psi) were measured, while at a distance of 7.62 meters (25 feet) from the explosive, peak pressures were about 0.069 MPa (10 psi).

From these references it is clear that typical peak pressures in the vicinity of the explosive would be on the order of 0.345 to 1.38 MPa (50-200 psi) or higher. Pressures greater than 1.38 MPa (200 psi) are also expected if explosive debris impacts the sensors directly.

Although peak explosive pressures are significant, they typically remain in contact with the structure for only a short time duration. For the three peak pressure references previously cited, the duration of initial pressure pulse on the cylinder walls was on the order of 0.4-1.1 milliseconds, and the rise times (time for pressures to reach peak values) were in the range of 0.2 to 0.5 milliseconds. The reported time durations required for the measured pressures to return to ambient levels, defined as end time, were in the range of 0.4 to 1.1 milliseconds. Thus, an active venting system must be capable of detecting these strong, but brief, pressure spikes (Figure 5).

Another important characteristic of an explosion detonation is the resulting acceleration imparted on the structure. Kanninen, Marchand, and O'Donoghue (1992) have published calculations of accelerations based on the experimental data from the explosive test on the B-52 aircraft (White, 1992). Predicted peak accelerations of the fuselage wall in the vicinity of the blast of 10,000g to 16,000g are reported. Typical duration of these load pulses are about 1 millisecond. Chen (1997) has also reported experimental and predicted fuselage wall accelerations of 8,000g to 10,000g.

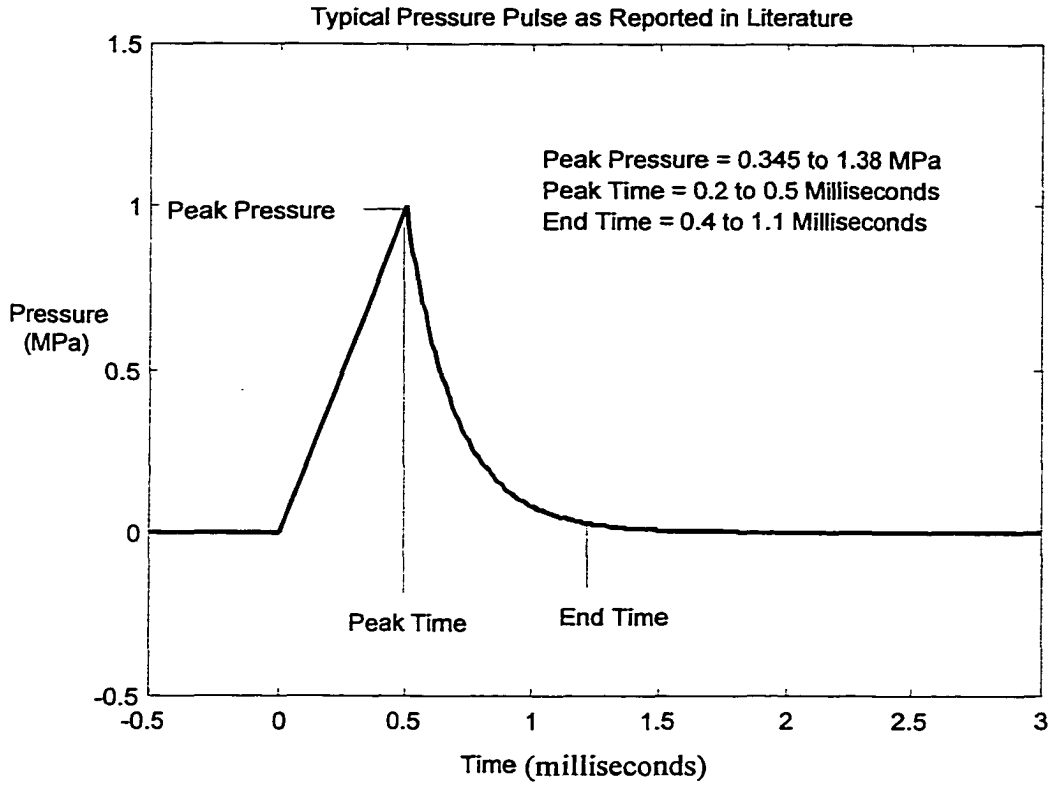

Figure 5. Typical Pressure Profile for a Sensor Located a Fixed Distance From an Explosive Detonation as Described in Literature. (Ewing, 1992; Strang, 1992; White, 1992).

Pressure Sensors

The pressure sensors used in active venting must be uniquely selected for the explosive sensing application. First, the sensors should be small and lightweight. They must also exhibit a fast response time to accurately monitor sudden increases in pressure. The selected sensors must be capable of accurately measuring the full range of anticipated pressures and be rugged enough to withstand the accelerations imparted by the explosive shock front. Finally, the sensors should be unaffected by (non-explosive) mechanical shock and accelerations to eliminate potential false triggers of the system.

A search of a wide variety of sensors and manufacturers has revealed several pressure sensor manufacturers who produce pressure sensors which are suited for use in an active venting system. Four of these manufacturers are included here for reference (Table 3).

The function of dynamic pressure transducers is to convert a pressure input into an electrical output. This typically occurs when a pressure increase gives rise to a proportional displacement or strain. This strain is then transmitted to an electrical transduction element which generates the required electrical output signal. Thus, a typical pressure transducer contains both mechanical and electrical elements. The mechanical component is usually a diaphragm member and the electrical component consists of a quartz crystal or a silicon bridge.

Table 3

Manufacturers of Dynamic Pressure Sensors

Manufacturer	United States Location	Comments/ *World-Wide Web Address*
Endevco	San Juan Capistrano, California, USA	Part of Meggit Aerospace http://www.endevco.com/
Entran Devices, Inc.	Fairfield, New Jersey, USA	Aerospace and Military Background, Worldwide Company http://www.entran.com/
Kistler Instrument Corp.	Amherst, New York, USA	Subsidiary of Kristal Instrumente AG of Winterthur, Switzerland http://www.kistler.com/
PCB Piezotronics, Inc.	Depew, New York, USA	http://www.pcb.com

A variety of mechanical diaphragms for converting pressure into displacement are available. Typical pressure diaphragms are fabricated from welded stainless steel but can also be machined in a one-piece design for high pressure applications. Quartz is used in pressure sensors for the electrical element due to its excellent long-term stability, high rigidity, wide measuring range, and wide temperature range. Quartz-based pressure transducers are ideally suited for measuring dynamic events. Typically, a charge amplifier or signal conditioner is needed to change the electrical output of the quartz element into a readily-usable electrical signal (Kistler, 1995).

Another type of pressure sensor, called a piezoresistive transducer, utilizes the elastic deformation of a silicon diaphragm under pressure loading and a strain gage bridge (Wheatstone Bridge) which is diffused into the surface of the diaphragm. This type of pressure transducer shows good dynamic response and has been used widely for high frequency applications. The piezoresistive pressure transducer, unlike the quartz type sensor, requires a constant current or constant voltage supply for proper operation of the bridge circuit.

Both quartz and piezoresistive pressure transducers can be effectively used to measure explosive pressures for the active venting application. As a practical example, one commercially available sensor of each type has been selected for closer examination. A piezoresistive pressure transducer suitable for use in active venting is model # 8530B-500 sold by Endevco, and a similar quartz piezoelectric pressure sensor is model #113A26 sold by PCB Piezotronics. Table 4 compares some key performance specifications of these two pressure transducers to the proposed design requirements for the pressure sensor needed in an active venting system. Both of the

selected sensors appear well matched to the requirements of a pressure sensor for explosive detection in an active venting system.

Another advantage of the two selected pressure sensors is their small size. This is an important consideration for implementation of an active venting system as the sensors must be small enough to allow unobtrusive placement throughout the interior of existing commercial aircraft. Both selected sensors are cylindrically shaped with a diaphragm diameter of less than 6.4 millimeters (0.25 inches) and an overall length of less than 35.6 millimeters (1.4 inches).

Electronics And Processing

The heart of an effective venting system is the ability to rapidly and accurately process explosive pressure sensor signals, and to make appropriate decisions about which panels to actuate. This processing must account for all possible scenarios which may be encountered and eliminate the possibility of inadvertent system deployment. These logic requirements can be adequately handled by an electronic control module which utilizes a programmable microprocessor and a control algorithm.

In the event of an explosion on-board an aircraft, an active venting sensing and processing unit must first confirm the occurrence of an actual explosion. This can be accomplished in several ways. First, the system can monitor the aircraft interior for large positive pressures which exceed a fixed threshold value. This value can be assumed based on existing explosive test data and on design criteria for commercial aircraft. For example, consider a commercial aircraft fuselage at maximum altitude

Table 4

Performance Characteristics of Two Dynamic Pressure Sensors

Specification	Endevco Piezoresistive Model 8530B-500	PCB Piezotronics Quartz Piezoelectric Model 113A26	Desired for Active Venting System
Weight	2.3 grams	6.0 grams	Minimum
Pressure Range	0 - 3.45 MPa (0 - 500 psi)	0 - 3.45 MPa (0 - 500 psi)	0 - 3.45 MPa (0 - 500 psi)
Operating Temperature Range	-64°C to 121°C	-73°C to 135°C	-60°C to 120°C (Proposed)
Max. Shock	20,000 g (100 microsec. Pulse)	20,000 g	15,000 g (Proposed)
Natural Frequency	1,000,000 Hz	>500,000 Hz	500,000 Hz (Proposed)
Rise Time	0.25 microseconds *	< 1 microsecond	< 10 microseconds (Proposed)

* Rise time not given. Calculated as inverse of 25% of natural frequency.

which experiences a differential pressure of 0.0621 MPa (9.0 psi). A cabin relief valve is used to limit the maximum pressure differential on the fuselage to 0.0684 MPa (9.4 psi) (Niu, 1988). Assuming a safety factor of 1.25, the ultimate load rating for a fuselage with door openings, windows, etc., is 0.0814 MPa (11.8 psi). Next, considering previously cited pressure measurements for explosions within fuselage constructions, it is reasonable to assume that peak pressures of at least 0.345 MPa (50 psi) would be experienced at locations close (within 1.2 – 1.8 meters (4-6 feet)) to the blast. This peak explosive pressure is thus more than five times greater than the

maximum static working pressure for an aircraft fuselage and about four times greater than the ultimate design load rating. Thus, a pressure of 0.345 MPa (50 psi) appears to be a reasonable threshold value for indicating the detonation of an explosion.

Another determination which can be used to detect an explosion is a large, positive rate of change of pressure. As previously cited, the rise times for typical explosive pressures is 0.2 to 0.5 milliseconds. During this brief time period, measured pressure at a fixed point in space will increase from ambient to peak values. An active venting processor could thus monitor for pressure rises which exceeds a specified rate of change. For example, a peak pressure of 0.345 MPa (50 psi) with a rise time of 0.5 milliseconds could be described as having a positive pressure rate of change of 0.69 MPa/millisecond (100 psi/millisecond). Thus, it could be proposed that a measured pressure rate of change in excess of 0.345 MPa/millisecond (50 psi/millisecond) indicates the occurrence of an explosion. In order to maximize accurate explosion detection, it may be necessary for the processing unit to detect both pressure threshold and pressure rate of change events. In other words, if both criteria are met, then an explosive event can be confirmed.

The active venting processing system would likely involve the use of multiple or redundant sensors. It is envisioned, for example, that two pressure sensors could be located in approximately the same position in the aircraft interior. The output of both sensors would then be required to satisfy the criteria for explosion detection. This procedure would guard against reliance on a single sensor for the critical function of explosion detection. A block diagram of such a system is shown in Figure 6. For use

in an aircraft interior, such redundant pairs of pressure sensors would likely be distributed throughout the aircraft to provide protection for explosions regardless of location.

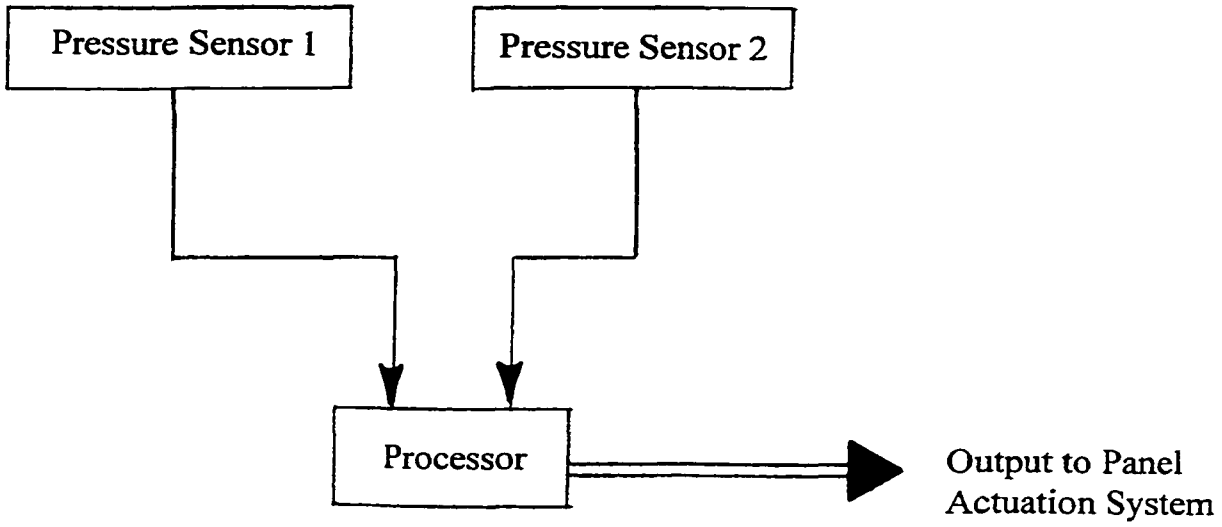

Figure 6. Block Diagram Representation of a Redundant Pressure Sensor Configuration.

When designing an explosion detection system it is important to consider that an explosive blast could damage a sensor or sensor cabling which would interfere with proper pressure measurements. To overcome this problem, the processor control logic could monitor for cases in which one sensor output matches the explosion criteria while the other sensor signal disappears. Such an event could also be used to confirm the detonation of an explosive. Figure 7 illustrates two possible scenarios in which an explosive event is confirmed by the processing system.

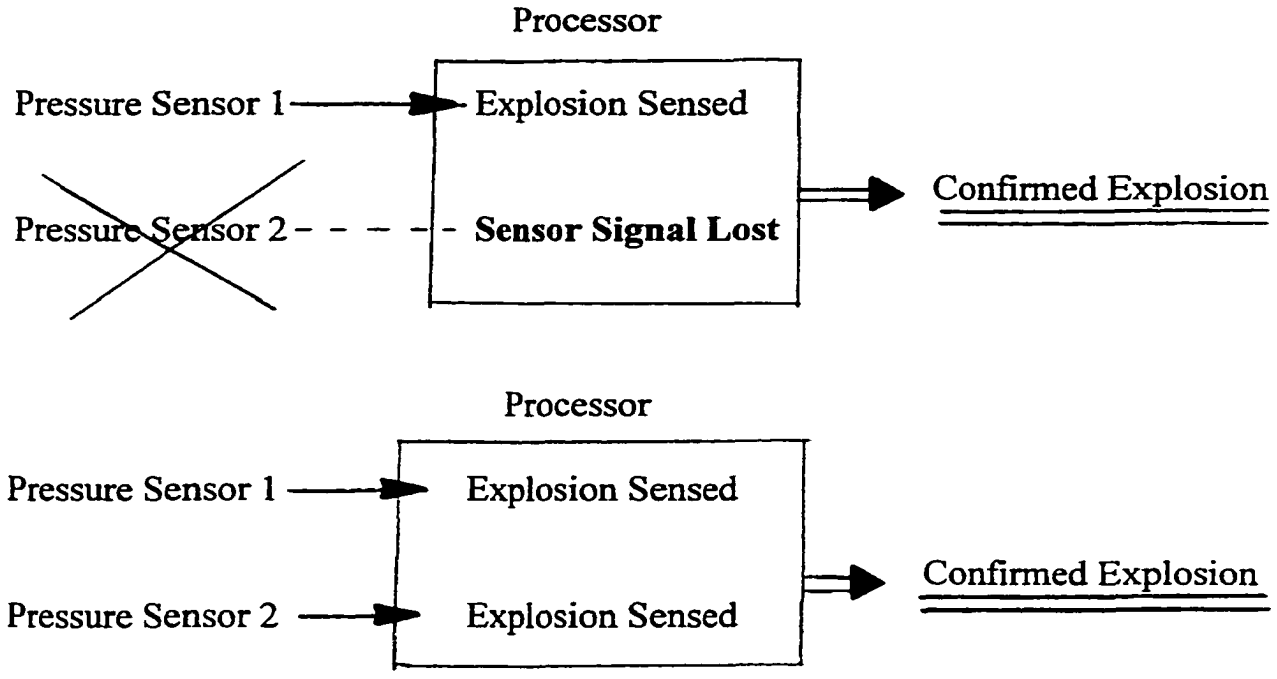

Figure 7. Block Diagram Representation Two Possible Confirmations of an Explosive Event.

Another possible scenario which the active venting system may encounter involves explosive damage to the processing unit itself. To provide protection for the system in this case, multiple or redundant processors can be connected in parallel to a number of pressure sensor pairs. Figure 8 shows a possible configuration for a system with two redundant processors.

These processors would ideally be spaced apart from each other within the aircraft to minimize the possibility of damage to both units. The output signals of both processors would be connected to the panel actuation system. In this design, the actuation system could be activated by the output signal of either one or both of the processors.

In addition to handling the previously described processing functions required for active venting, an electronic control module could also contain signal processing capability for handling pressure sensor output signals. If piezoresistive pressure sensors are used, the electronic module would additionally need to provide either a constant current or constant voltage supply to activate the semiconductor bridge of the pressure sensor.

Projected Response Time of Sensing and Processing

The system response time for the sensing and processing unit can be described as the total elapsed time from the instant of the explosive detonation to the time at which the processing unit sends an activation signal to the vent panel actuation system. The first portion of this time sequence depends upon the physical spacing of

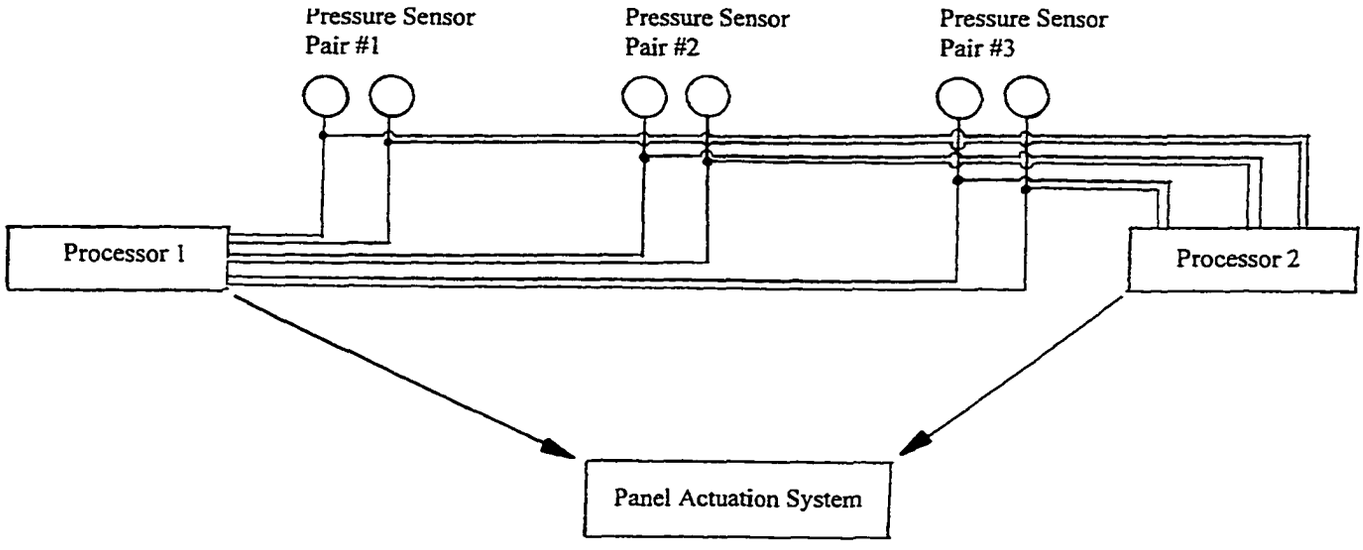

Figure 8. Block Diagram Representation of a Redundant Processor Configuration.

the array of pressure sensors inside the aircraft. In order to examine a typical pressure sensor configuration, consider the passenger cabin of a Boeing 737-700 aircraft (Figure 9). In this configuration, three rows of pressure sensors are located at approximately 1.0 meter spacing across the aircraft. These three rows of sensors consist of staggered spacing of pressure sensors at 2.0 meter intervals along the aircraft longitudinal axis. These three rows of sensors are shown in a single plane of elevation inside the passenger cabin approximately mid-way between the floor and the top of the fuselage.

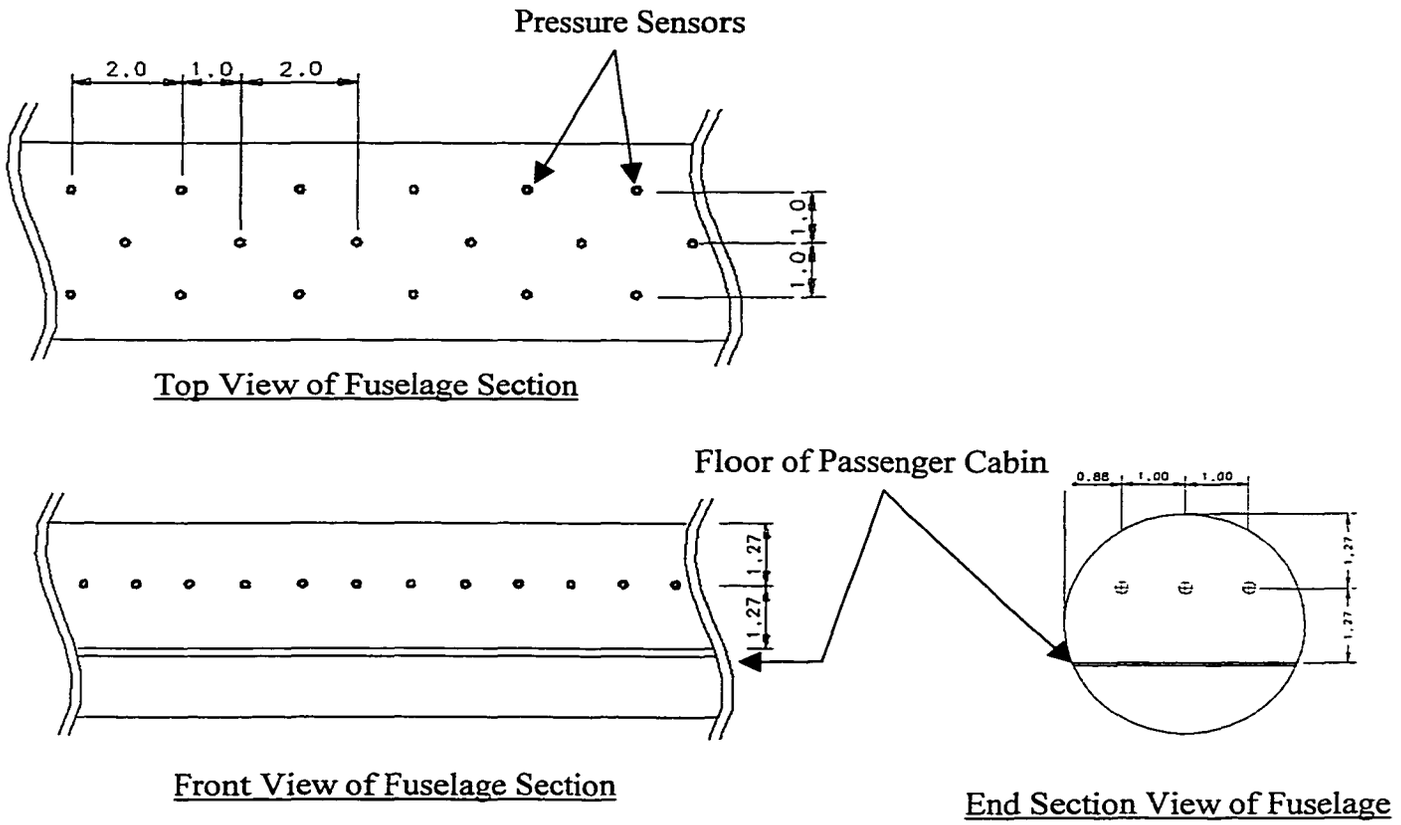

Figure 9. One Possible Configuration of Pressure Sensors in the Interior of the Passenger Cabin of a Boeing 737-700 (All Dimensions in Meters).

In this example configuration, approximately 36 pressure sensor locations would be used (along the interior cabin length of approximately 25.0 meters). Using this spacing of sensors, it can be estimated that for an explosion occurring anywhere inside the passenger cabin, the nearest pressure sensor would always be less than about 1.5 meters away. Considering the velocity of propagation of high explosives to be in the range of 670 to 1,170 meters per second, it can be estimated that the elapsed time from an explosive detonation until the blast wave is detected by a pressure transducer would be in the range of 0.0 milliseconds (for an explosive detonation in direct proximity to a pressure sensor) to 1.3 - 2.2 milliseconds.

Once the pressure wave has contacted a sensor, a small amount of time is needed for the sensor to respond and create an output signal. This time is less than 1.0 microseconds for the sensors which were previously described. The output signals from the pressure sensors would then be processed via an electronic control unit. The time required for a microprocessor to process the input signals includes the time for conversion of pressure signals from analog to digital format and the time needed for the processor to loop through an instruction set of programmed code. Although the exact processing time will depend on the type of processor and specific algorithm used, a reasonable estimation can still be obtained. First, by examining the previously reported pressure profile of a typical explosive blast (Figure 5), a total pressure pulse duration of 0.4 to 1.1 milliseconds is observed. It is likely that the explosive detection system will be monitoring only the initial rapid increase in pressure with a time duration range of 0.2 to 0.5 milliseconds. In order for the electronic processing unit to detect this rapid pressure rise, sampling rates of 8 to 20 Kilohertz would be needed to

ensure a minimum of 3-4 data points over this time interval. The actual time required for analog to digital conversion for each data point is on the order of 50 microseconds. Once digitized, the incoming pressure data and calculated derivative of the pressure signal would then be compared to prior measured values and to stored reference values. These operations would be carried out via an appropriate algorithm operating on a microprocessor at speeds on the order of 1 microsecond per instruction. Finally, in the event that of explosive blast confirmation, an appropriate actuation signal would be sent to the panel actuation unit. Thus an additional 50-100 microseconds would be required for the digital to analog conversion of the output signal. In summary, the total time required for detection of an explosive pressure pulse and for the subsequent electronic processing of the data is conservatively estimated to be in the range of 0.5 to 1.0 milliseconds. The final step involved in the processing system is the sending of an output activation signal to the vent panel actuation system. This process would be much faster than the processing time as it relies on the speed of data transmission through an electrical wire.

By summing the time duration of the individual events involved in sensing and processing, an estimate of the overall processing system response time can be determined. For the example process as described, the total amount of time required from the instant of the explosive detonation to the sending of an activation signal to the vent panel actuation system is estimated to be less than 3.2 milliseconds (Table 5).

Table 5

Summary of Estimated Total System Response Time for Sensing and Processing

Event	Conservatively Estimated Time Duration	Fastest Possible Estimated Time Duration
Propagation Time of Explosion to Contact Closest Sensor	1.3 – 2.2 Milliseconds	0.0 Milliseconds
Sensor Rise Time	<5 Microseconds	<5 Microseconds
Processing Time (Including Output of Activation Signal for Panel Actuation System)	<1.0 Milliseconds	<0.5 Milliseconds
Total Response Time of Sensing and Processing	**<3.2 Milliseconds**	**<0.5 Milliseconds**

CHAPTER IV

PANEL ACTUATION SYSTEMS AND RESPONSE TIME ESTIMATION

Panel Actuation Response Time

Once an explosive event has been detected and confirmed on-board an aircraft by the detection processing unit, an activation signal is sent to a panel actuation system. There are numerous vent panel designs and actuation methods which could be employed for the active venting system. For the purpose of this study, however, three different panel actuation systems will be evaluated for response time: 1) Hinged Vent Panel, 2) Edge Perforated Vent Panel, and 3) Fractured Vent Panel.

Background on Pyrotechnic Actuators

Before evaluating the response times of the individual panel designs it is first important to introduce a family of actuators known as pyrotechnics. Pyrotechnic actuators are a logical choice for applications which require a fast response with typical functional times on the order of a few milliseconds. The pyrotechnic family of actuators utilizes explosive and propellant chemical compositions to accomplish tasks such as actuation, severance, fracture, and valving. Pyrotechnic devices have been widely used on space and military aerospace programs. Literally hundreds of

pyrotechnic devices are installed on modern military aircraft. Some of these are designed for functional use such as release of armaments while others are used only in emergencies such as canopy release for pilot ejection. As an additional example, the United States Space Shuttle is equipped with over 400 pyrotechnic devices (Bement, 1995). The reason pyrotechnic actuators are used so extensively is due to their high efficiency. Pyrotechnics deliver high energy per unit of weight and are generally small volume devices. Pyrotechnics are also stable for long periods of time which is an important consideration for applications in which a system is required to perform reliably even after long installation periods. Although service life varies by application, installation durations of 10-20 years have been reported for pyrotechnic devices on military aircraft (Bement, 1995).

All the previously described attributes of pyrotechnic actuators make them ideal candidates for use in an aircraft active venting system. In fact, all three of the vent panel designs evaluated in this study will utilize some form of a pyrotechnic actuator.

Hinged Vent Panel

The first vent panel design to be evaluated utilizes a hinged construction which would be securely affixed to the aircraft. In the event of an on-board explosion, a linear pyrotechnic actuator would fracture a holding pin, and force the forward edge of the vent panel away from the aircraft. The force of internal cabin pressurization

acting on the face of the vent panel would assist in rapidly rotating the panel free of the aircraft in order to create a vent opening (Figure 10).

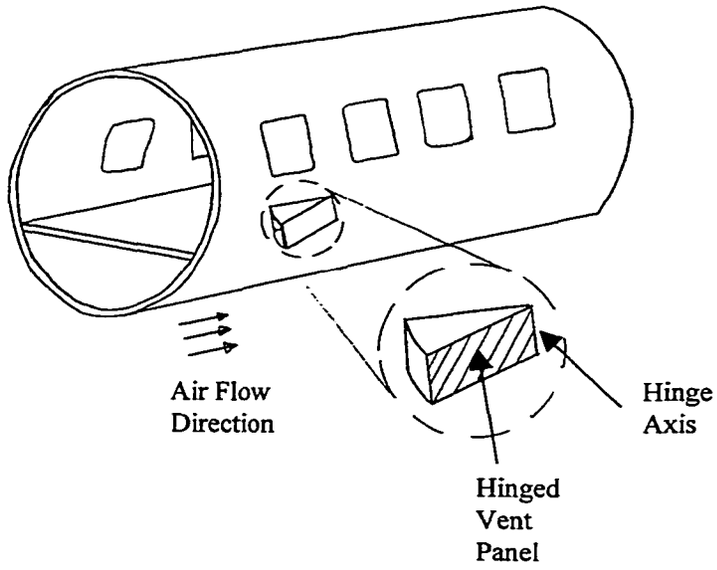

Figure 10. Conceptual Illustration of a Hinged Vent Panel.

It is envisioned that the hinged panel would be designed to break free of the aircraft after reaching a given angle of rotation. The jettisoning of the panel is intended to prevent the panel from striking and damaging the plane after rotating through an angle of 180 degrees.

In order to estimate the typical actuation response time of a rotating vent panel, Newton's second law for rotational motion was assumed (Equation 4.1).

$$\sum T = J\alpha \tag{4.1}$$

Where: ΣT = The Sum of All Torques Acting About the Hinged Axis
α = Angular Acceleration of the Panel
J = Moment of Inertia of the Panel About the Hinge

For a hinged vent panel on a pressurized vessel, the applied torque results from the internal cabin pressurization acting across the surface area of the vent opening. Considering the simple case of a hinged vent panel being released from rest at time zero, equation 4.2 can be solved for the panel position as a function of time (Equation 4.2).

$$\theta(t) = \left(\frac{T}{J}\right) \cdot \left(t^2\right) \cdot \left(\frac{180}{2\Pi}\right) \tag{4.2}$$

Where: $\theta(t)$ = Panel angle as a function of time (in degrees)

It should be noted that this analysis assumes that the torque applied to the hinged vent panel is constant. In reality, the torque due to internal pressurization would not be constant but rather would decrease as the panel opens and vent air stream contacts the panel at an increasingly shallower angle. For the purposes of this analysis, however, it will be assumed that the torque applied to the vent panel will be constant over the initial small range of panel motion (say from zero to 45 degrees of rotation).

Scale-Model Testing of Hinged Vent Panel

In order to validate the simplified model of panel motion (equation 2), scale-model testing of a hinged vent panel was conducted. A compressed air storage tank was used in scale model testing of decompression times (Figure 11).

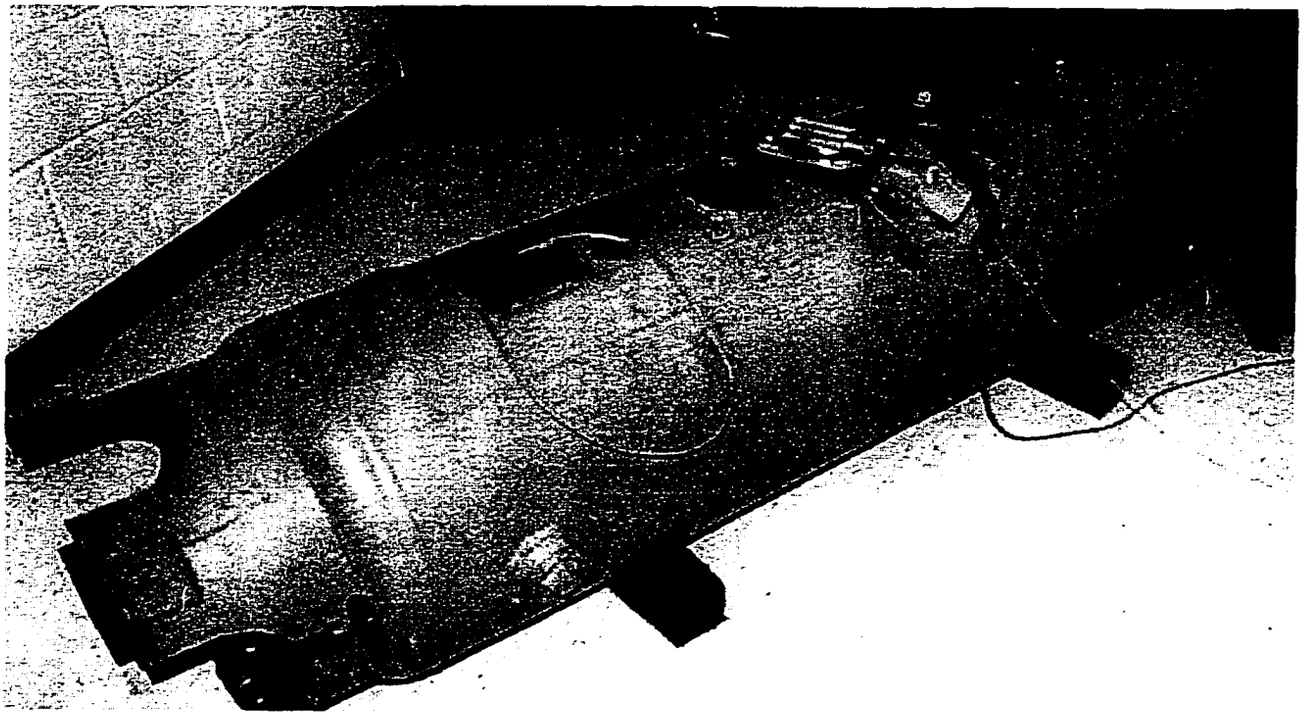

Figure 11. Photo of the Compressed Air Storage Tank Used in the Analysis of the Motion of a Scale-Model Hinged Panel.

The tank diameter was 0.521 meters (20.5 inches) and the nominal tank length was 1.80 meters (71 inches). The compressed air tank was fitted with an aluminum hinged panel which seals a vent opening on the tank (Figure 12). The hinged panel was designed to be manually released by a latch attached to a string.

The compressed air tank was pressurized with air to a gage pressure of 51.7 KPa (7.5 psig). This pressurization in a laboratory atmosphere is equivalent to the maximum pressure differential experienced by a Boeing 737 for flights above 5640 meters (18,500 feet) (Greenwald, 1967). When the scale-model panel latch is released by pulling on the string, the internal air pressure forces the panel away from the tank

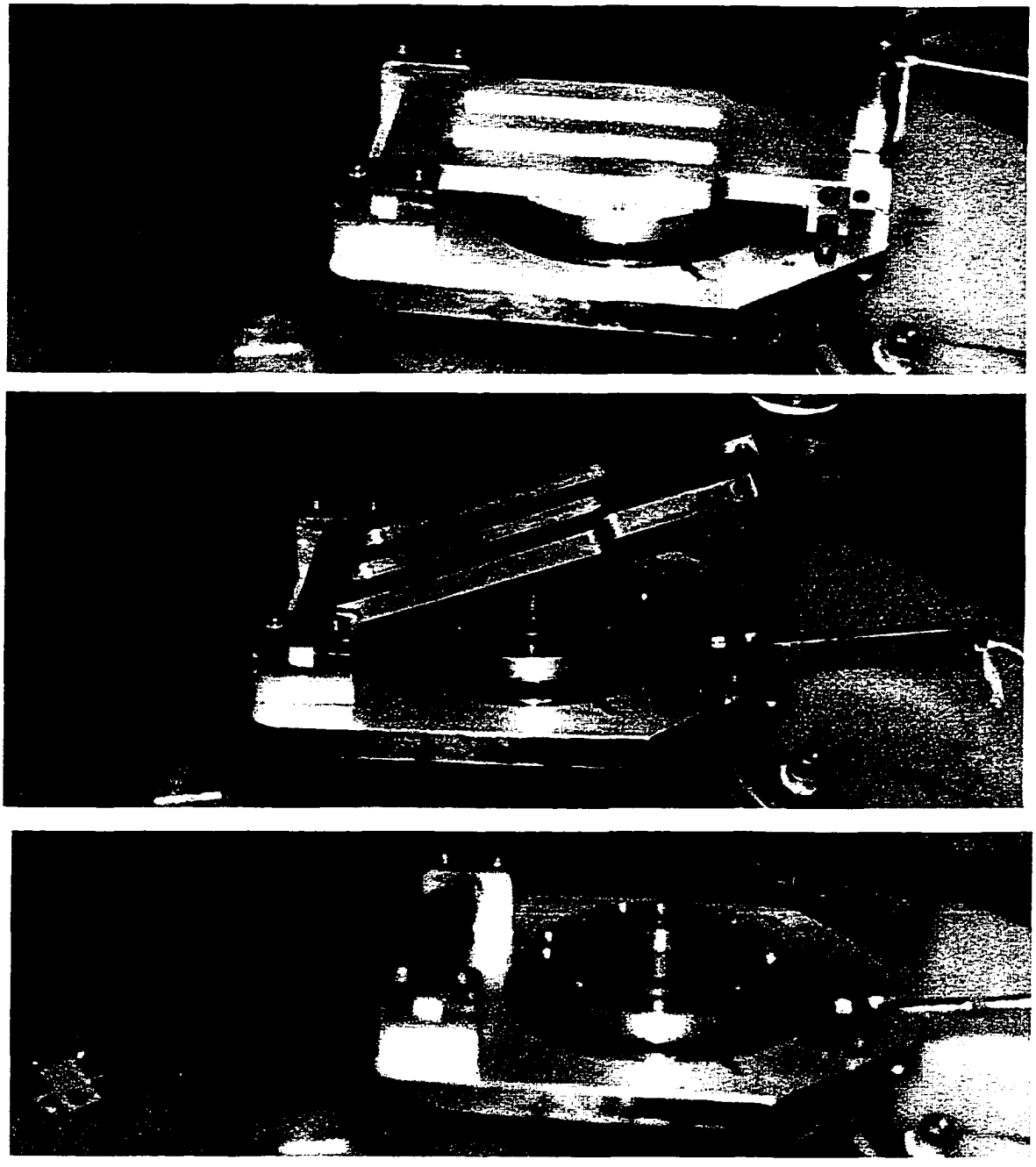

Figure 12. Photos Showing the Scale-Model Hinged Panel on the Compressed Air Tank in the Fully Closed (Top), Partially Open (Middle), and Fully Open (Bottom) Condition.

vent opening. A ball of clay was placed on the tank to catch and trap the hinged panel in the fully open position.

The scale-model hinged panel was irregularly-shaped with approximate overall dimensions of 65 x 155 x 9.5 millimeters. It was formed from aluminum and had a mass of 0.207 kilograms and a moment of inertia about the hinged axis of 0.001587 $kg \cdot m^2$. The hinged flap was used to seal a 37.3 millimeter diameter vent opening on the compressed air tank. Assuming that the internal pressurization of 51.7 KPa acts as a resultant force at the center of the vent opening (69 millimeters from the hinged axis), the initial applied torque on the hinged panel from the internal pressurization is 3.90 N·m.

Using the specific moment of inertia and applied torque due to internal pressurization in Equation 4.2, the predicted position of the scale model vent panel after release at time zero can be calculated (Figure 13).

In order to experimentally verify the predicted scale-model panel response, stroboscopic photography was used. A Polaroid camera with 3000 speed film was used in a dark room to capture the position of the hinged flap as illuminated by a strobe light pulsing at 10 millisecond intervals (Figure 14). The panel position at 10 millisecond intervals was manually measured from the resulting photographs (Table 6). Note from the data that the first recorded flash which resulted in a non-zero panel angle occurred at some time interval after the instant of panel release. This indicates a limitation in the experimental method which does not allow a direct measurement of

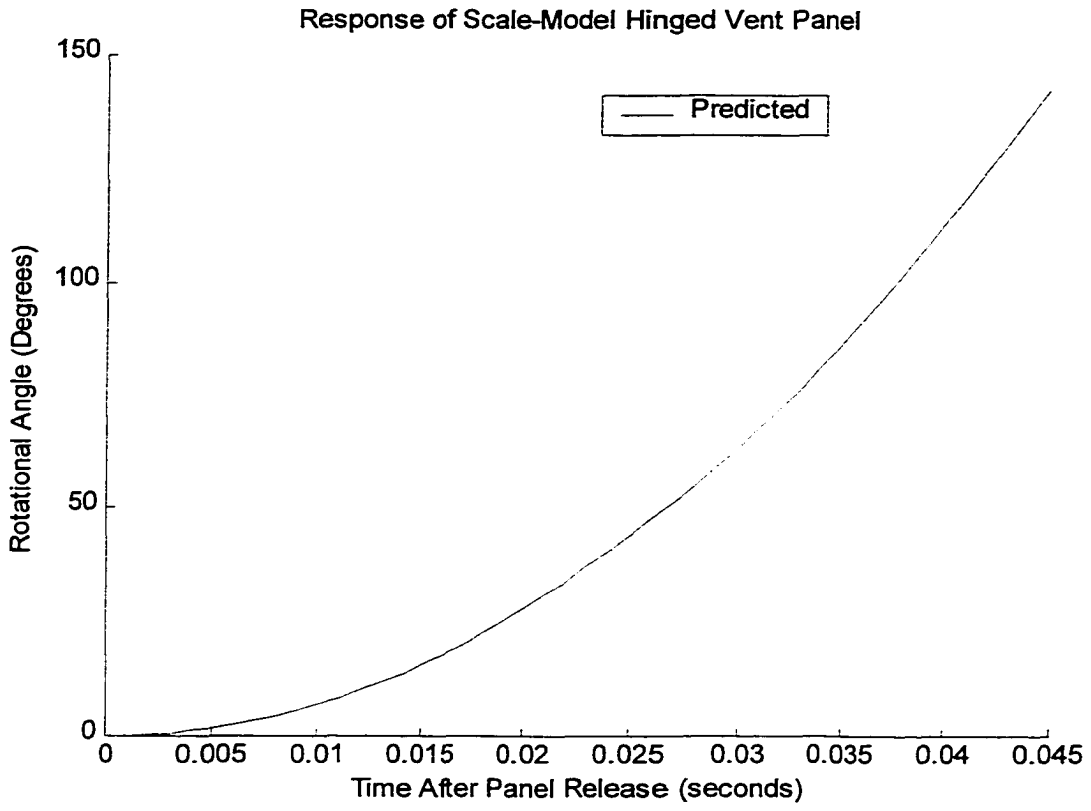

Figure 13. A Plot of the Predicted Position of the Scale-Model Hinged Vent Panel After Being Released at Time Zero.

the exact instant of initial panel motion. This problem was overcome by plotting a polynomial fit to the experimental data points to determine the time at which the panel first began to move. Once this initial time was determined, the remaining data points were time corrected to give absolute time values for each strobe flash. The time corrected vent panel position then compares quite favorably with the predicted position from Equation 4.2 (Figure 15).

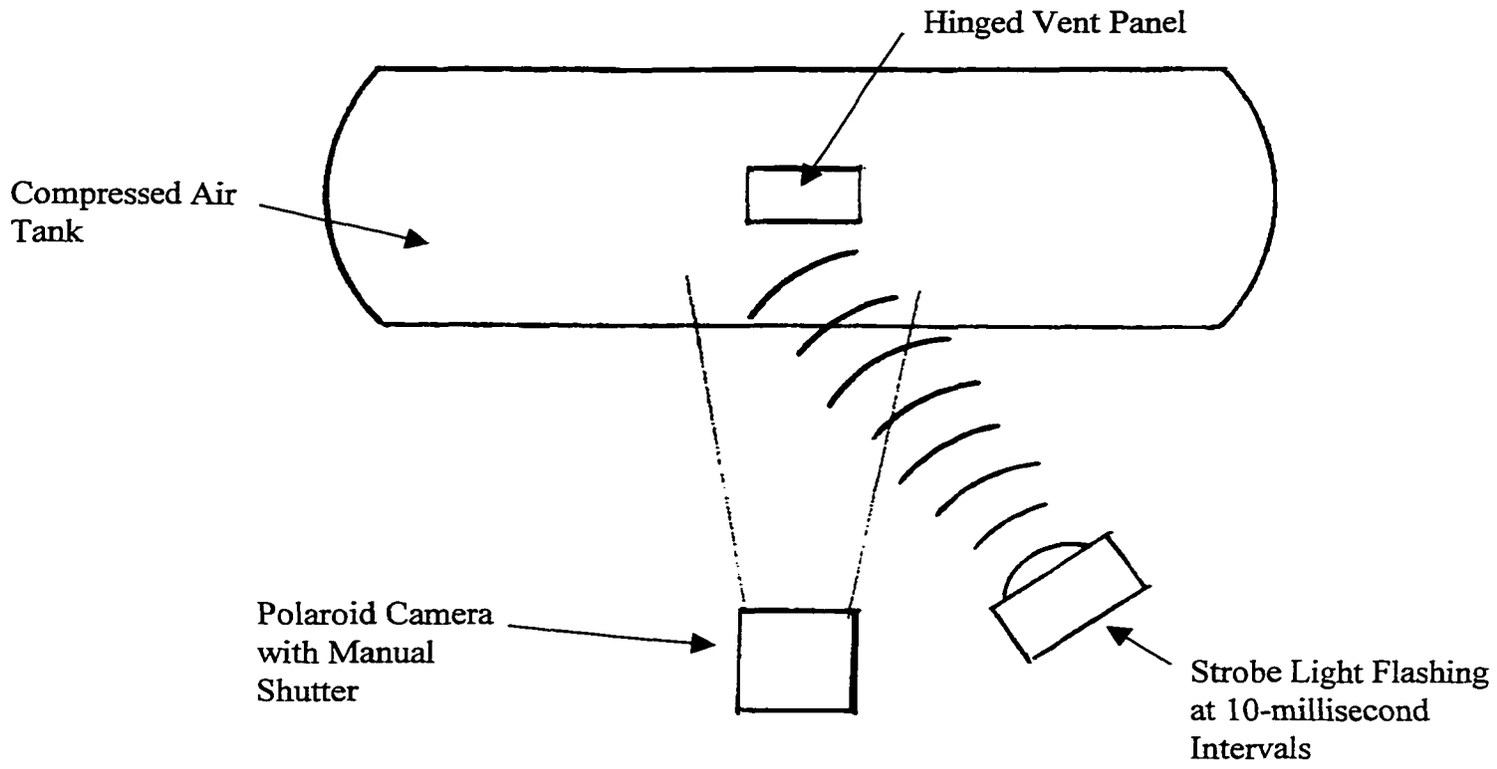

Figure 14. The Experimental Configuration Used to Photograph and Quantify the Motion of a Scale-Model Hinged Vent Panel.

Table 6

Time Response of a Scale-Model Hinged Vent Panel

Flash #	Angle of Panel (Degrees)	Corrected Time (Milliseconds)
1	6.9	4.48
2	19.6	14.48
3	48.9	24.48
4	88.5	34.48
5	127.2	44.48

The close correlation of the scale-model hinged panel motion to the prediction gives confidence that this method can be used to establish a general response time of a full-sized vent panel.

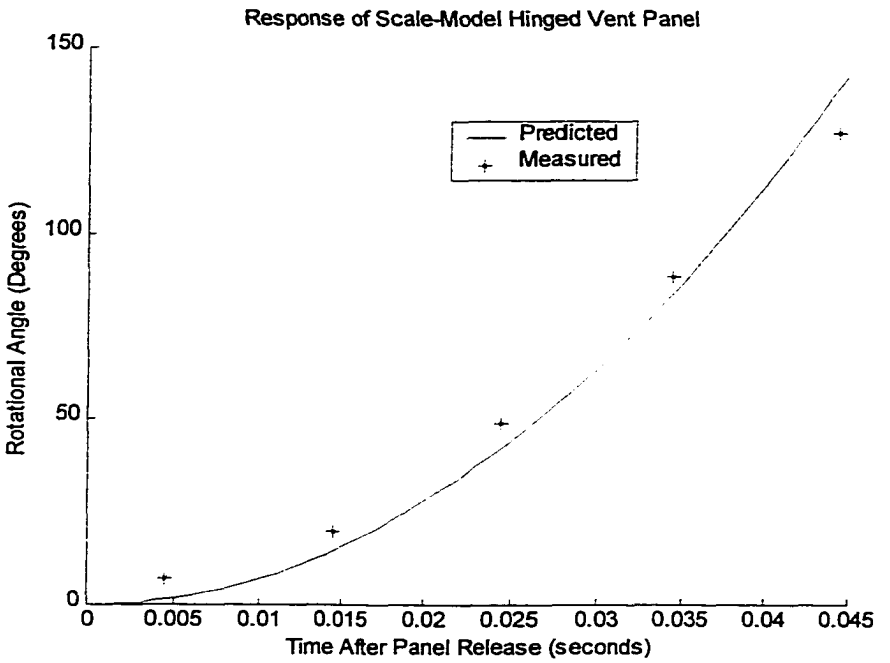

Figure 15. A Plot of the Measured and Predicted Position of the Scale-Model Hinged Vent Panel After Being Released at Time Zero.

Predicted Response Time of a Full Size Hinged Vent Panel

As described previously, the actuation of a hinged panel on an aircraft would likely employ a pyrotechnic linear actuator. Such a device would serve to sever a holding pin which would release the panel from the aircraft. The released panel would be rapidly forced away from the aircraft by the internal cabin pressurization acting across the face of the panel. It is also conceivable that the force produced by a pyrotechnic linear actuator would aid in forcing the panel away from the plane. For the purpose of determining the typical actuation response time of a vent panel, a reasonably sized panel has been selected (Figure 16).

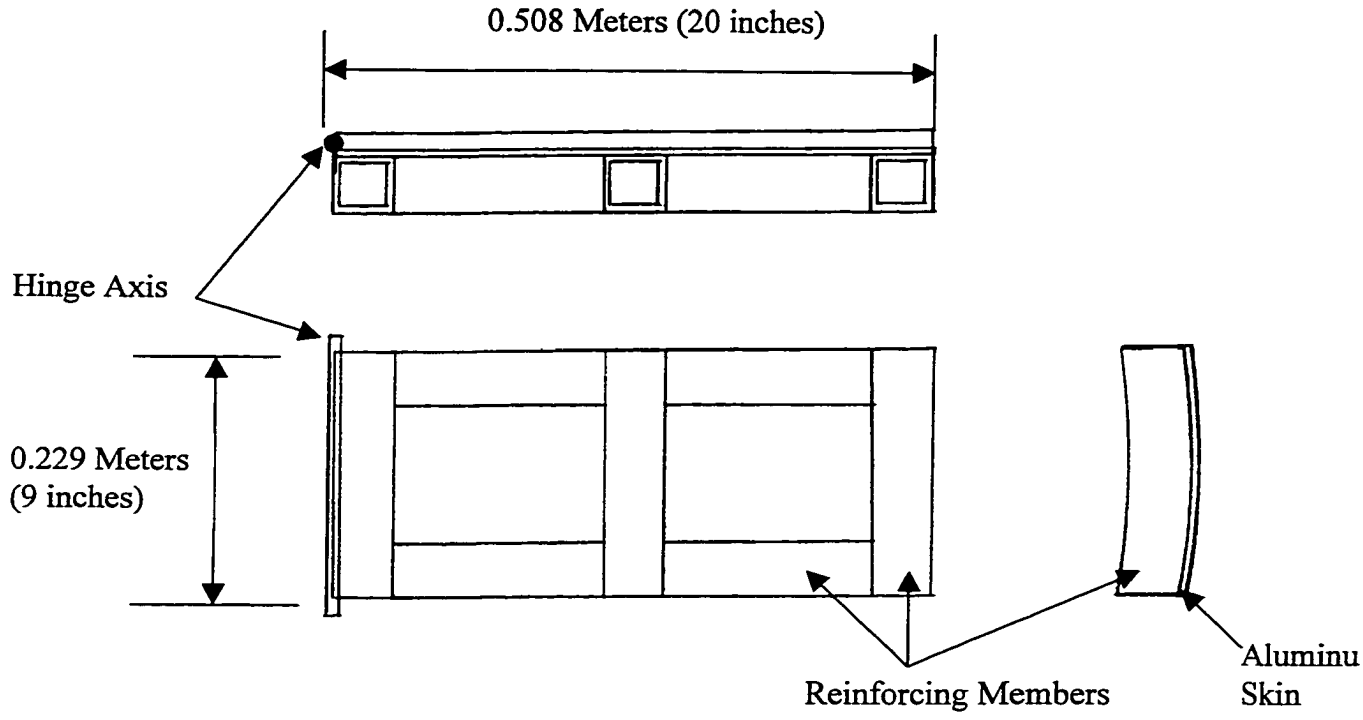

Figure 16. A Depiction of a Suitable Hinged Vent Panel Selected for Use on a Commercial Aircraft Active Venting System.

The dimensions of the selected vent panel were selected so as to fit between adjacent frame and stringer members of a typical commercial aircraft. The vent panel used in this analysis consists of a thin skin of aluminum reinforced with aluminum rectangular box-beam reinforcing members around the perimeter and circumferentially through the center of the panel. A solid model of the panel assembly was created using computer-aided design software and the panel mass (1.45 Kg) and moment of inertia about the hinged axis (0.1476 Kg·m^2) were determined. For this panel, an internal cabin pressurization of 51.7 KPa acting across the entire inner panel surface would result in an applied torque of 1528 N·m about the hinge axis. Before estimating the time response of the released panel, it is first necessary

to determine the actuation response time of the pyrotechnic actuator. Although the ideal actuator would be no doubt designed specifically to suit an active venting application, the response time and force output of a standard device can be used as a representative data for this analysis. For this purpose, the NASA pin-puller family of pyrotechnic actuators which have been used extensively on space flights have been selected (Bement, 1995) The time duration from the instant an actuation signal has been received until peak actuation force is delivered is on the order of 0.05 to 0.1 milliseconds. A typical force output curve of a NASA pin-puller (Model – Hi-Shear NGGC, 450 inch-pound) acting on a ¼-inch diameter pin is given in Figure 17 (Bement, 1995).

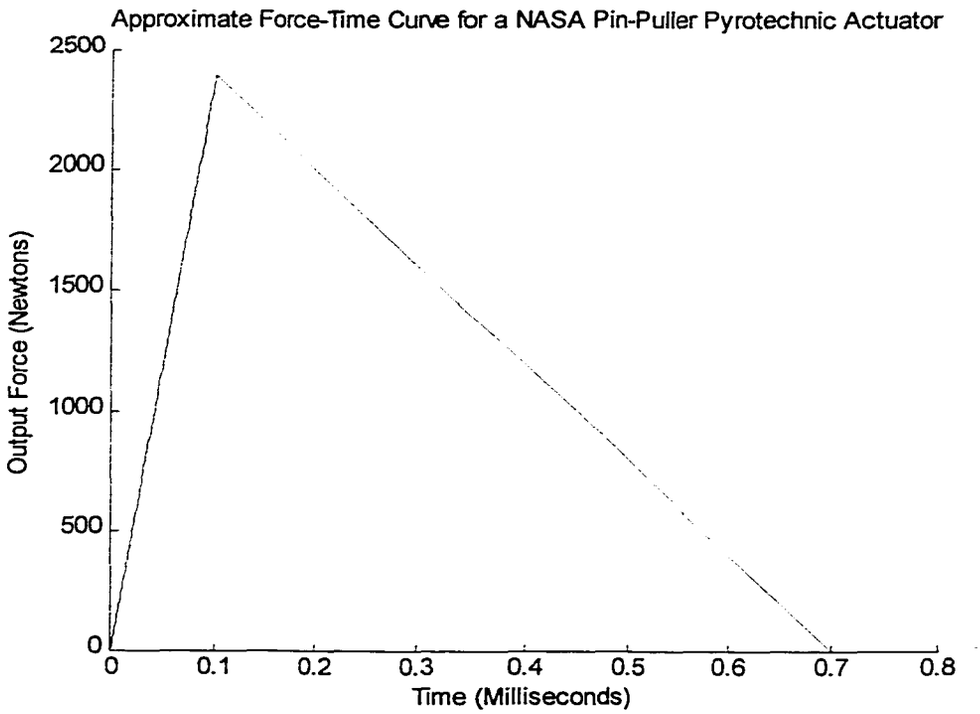

Figure 17. Approximate Force-Time Curve for a NASA Pin-Puller Pyrotechnic Actuator. (Model – Hi-Shear NGGC, 450 inch-pound) (Adapted from Bement, 1995).

It is envisioned that the pyrotechnic actuator would be positioned near the edge of the vent panel opposite the hinged end. Although the energy generated by the pyrotechnic actuator would be largely dissipated in fracturing the panel retaining structure, some of the force produced may provide additional torque to rotate the panel away from the aircraft.

Once the pyrotechnic actuator has severed the panel retaining member, the panel is free to rotate due to the torque created from the internal pressurization acting on the panel face. Using the specific geometric properties of the full-size vent panels the previously derived equation of rotation (Equation 4.2) now becomes:

$$\theta(t) = \left(\frac{1528\,\mathrm{N}\cdot\mathrm{m}}{0.1476 Kg\cdot m^2}\right)\cdot\left(t^2\right)\cdot\left(\frac{180}{2\pi}\right) \tag{4.3}$$

For this simple analysis, only the torque on the panel due to internal cabin pressurization (51.7 KPa) is considered. The resulting panel motion after release at time zero is plotted in Figure 18. From this figure it can be seen that the panel will rotate to a fully open position (90 degrees from its initial position) in about 17.4 milliseconds. It is clear that some amount of pressure venting will begin before the panel rotates to a fully open position. For the purposes of this analysis, it will be conservatively estimated that venting begins when the panel has rotated to an angle of 15 degrees from its initial position. Thus, for the full size vent panel opening under internal pressurization alone, it is projected that venting would begin at approximately 7.1 milliseconds after the panel is severed.

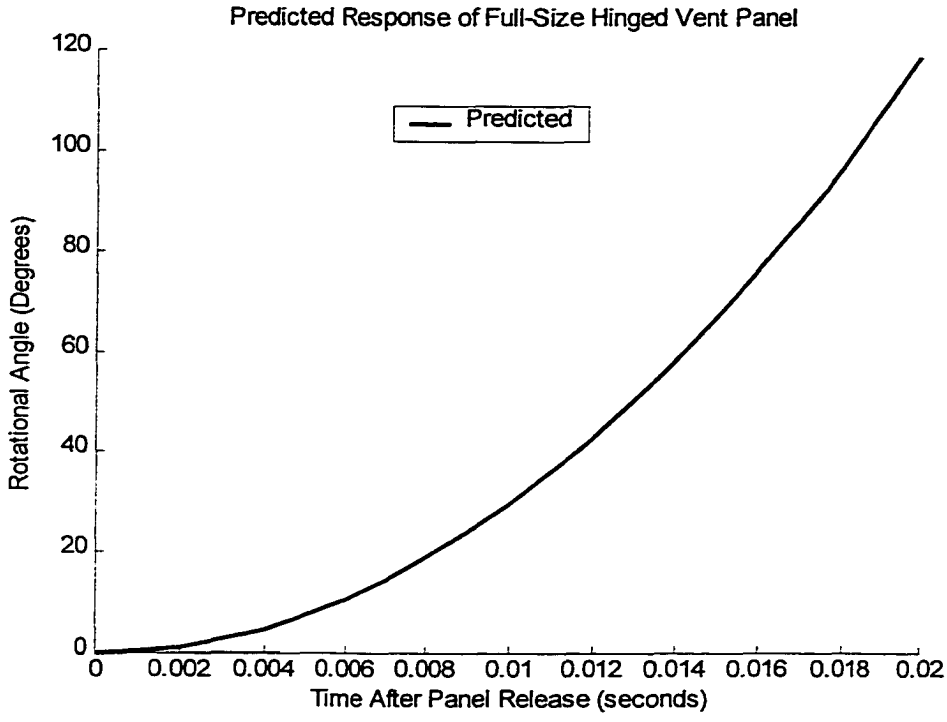

Figure 18. A Plot of the Predicted Position of a Full-Size Hinged Vent Panel After Being Released at Time Zero.

At this point, it is important to mention that an actual vent panel which deploys while an aircraft is in flight would also experience some additional torque due to the on-coming air-stream. Considering the force on a flat plate from an impinging air flow normal to the face of the plate (simulating a vent panel having rotated through an angle of 90 degrees) as: (Fox, 1985)

$$F = \left(-u \cdot \left|\rho \cdot V \cdot A\right|\right) \tag{4.4}$$

Where:
F = Force on plate in direction of on-coming airflow
u = Velocity of on-coming airflow
ρ = Density of on-coming airflow
V = Velocity of airflow leaving plate
A = Area of on-coming air jet

Given the cruising speed of a Boeing 737 as 237 meters/second (530 miles per hour), the area of the vent panel assumed to be 0.116 square meters, and the density of air at 10,000 meters as 0.4135 kg/m^3, the net force on the panel from the on-coming airflow when the panel is in the fully open position is calculated to be 2694 Newtons. This equates to a torque about the panel hinge axis of 684 Newton-meters. This torque is significant when compared to the initial torque on the panel due to cabin pressurization of 1528 Newton-meters. However, in the initial range of panel motion (between zero and fifteen degrees of rotation), the torque on the panel from the on-coming airflow is much less since the panel is generally aligned with the airflow direction. For these small angles, the force on the panel in the airflow direction can be approximated by using Equation (4.4) and by using the cross-sectional area of the panel which projects into the air stream. For a panel rotational angle of 15 degrees, this equates to a projected surface area of 0.030 square meters and a resulting force of 697 Newtons. Considering only the portion of this force which is perpendicular to the panel face, the resulting torque about the hinge axis is 45.8 Newton-meters. Since for small angles, the added torque on the panel is small with respect to that caused by internal pressurization (about 3%), the airflow effects will be neglected for this analysis. It is important to note, however, that neglecting the torque contributions of the on-coming air-stream and the linear pyrotechnic actuator makes the response time estimation conservative and actual panel response times may be faster.

Potential Disadvantages of Hinged Vent Panels

Before leaving this analysis, it must be noted that major barriers exist to the implementation of hinged vent panels on actual aircraft. This stems from the fact that hinged fuselage panels may require significant redesign of the aircraft structure since each of these panels would require pressure seals and perimeter structural strengthening of the aircraft structure similar to that required for windows and cargo doors. As it is a primary goal of aircraft designers to minimize the number of required fuselage openings, the incorporation of several additional vent panels around the fuselage may prove to be a challenging prospect. Another concern with hinged vent panels is the potential danger that the jettisoned panels may re-impact the aircraft and damage critical flight components of wings, control surfaces, and engines.

Edge Perforated Vent Panel

In order to overcome the drawbacks of a vent panel which requires a perimeter door-type seal, it may be desirable to utilize a pyrotechnic actuator which can create a vent opening by cutting through the fuselage wall in a circular or rectangular shape. Once a portion of the fuselage has been severed, the internal cabin pressurization would force the panel away from the aircraft (Figure 19). This process could be implemented through the use of a pyrotechnic actuator which features a cord filled with explosive material. This flexible cord can then be shaped as desired to create a cutting force along its entire length. Such a device is known as a flexible linear-shaped charge (FLSC).

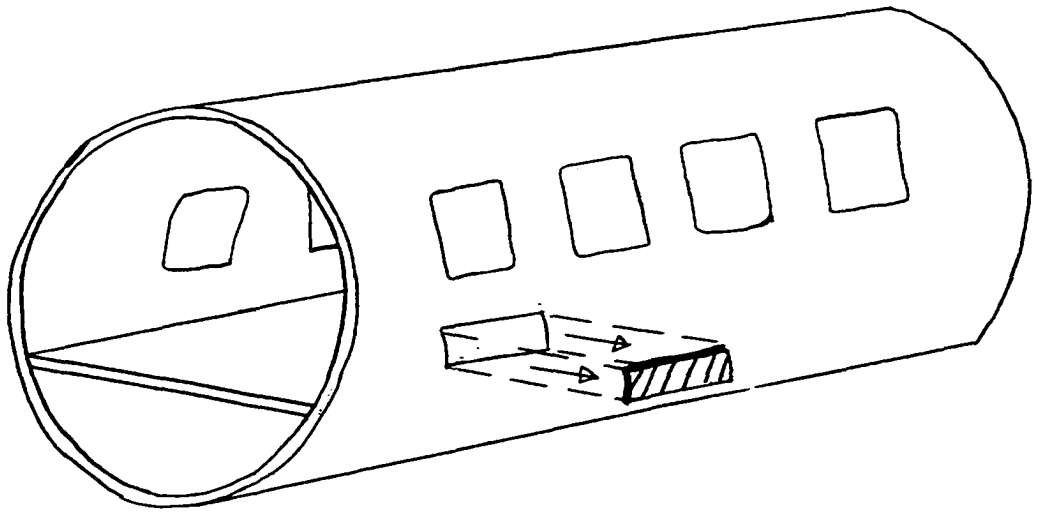

Figure 19. An Illustration of the Deployment of an Edge-Perforated Vent Panel.

Background on Flexible Linear-Shaped Charge Actuators

FLSCs are composed of a column of explosive material housed in a cladding of a metallic material such as aluminum, copper, lead, or silver. These devices have been used extensively in space and aerospace applications for efficient severing of metallic structures. Typically a length of FLSC is applied to a structure along a span to induce a fracture or separation of the contact area. Such a system is currently installed as an ejection mechanism on the United States military F-111 aircraft crew module. In the event of a emergency, the F-111 flight crew activates an escape system which utilizes a perimeter placement of FLSC to blast away the crew module from the surrounding aircraft structure. This crew module is then forced away from the plane and returns to earth by means of a parachute system.

FLSC has also been placed along the outside portion of propellant tanks on

numerous rocket programs to allow emergency jettisoning of fuel in the event of loss of vehicle controllability. In this application, the FLSC is designed to detonate and cut longitudinal fractures in the steel propellant tanks to provide rapid loss of pressurized fuel.

Another interesting use of FLSC has been proposed as a safety system for providing an emergency in-flight exit for light aviation aircraft (Bement, 1980). This system is intended to be activated during an irrecoverable spin or stall condition. In such an instance, the pilot activates an emergency handle which initiates the detonation of a square shaped arrangement of FLSC. This explosive device which is placed on the interior of the aircraft structure adjacent to the pilot severs a 30 by 30 inch (0.76 by 0.76 meter) hole in the aircraft fuselage (skin and stringer) to provide an escape opening for the parachute-clad pilot. Without this system, a pilot in a spin or stall must cross the aircraft from a seat on the left side to a doorway on the right, and force open the airplane door. This can be a very difficult and time-consuming task, especially when heavy centrifugal loads are present.

Bement's proposed in-flight egress system was thoroughly tested and qualified for use on light aviation aircraft. A total of 68 explosive tests on samples, full-sized flat panels, and actual aircraft fuselage structures were conducted. In the actual aircraft tests, the skin (0.063 inches or 1.6 millimeters thick) and stringer were cleanly severed. For cutting the stringer, an additional section of FLSC was wrapped around the stringer itself. This doubling of FLSC proved necessary to simultaneously cut through the skin and stringer.

On the inside of the aircraft, the FLSC material was surrounded by a containment channel of 0.063 inch (1.6 mm) thick cold-rolled steel. This containment channel prevents explosive pressures from directly entering the passenger cabin of the aircraft. Instead, the explosive pressures generated by the FLSC are contained within the channel and provide the jettison force which pushes the severed panel away from the fuselage. Full-scale explosive fuselage testing resulted in the ejection of a 14.6 pound (6.62 kg) panel with a velocity of 45 feet/second (13.7 meters/second). This velocity will move the panel a distance of 1.1 inches (27.4 mm) in 2 milliseconds.

Bement's egress system has some key similarities to the actuation system needed for active venting. First, FLSC can be used in both systems as an "add-on" system of rapidly severing panels from a fuselage. This approach requires little structural modifications to existing aircraft. The FLSC can also be formed in a variety of configurations to cut openings of desired shape on a variety of aircraft. The use of containment channels to surround a FLSC greatly speeds the exit velocity of a severed panel and increases the effectiveness of the venting system in relieving fuselage pressure.

One of the primary challenges of using flexible linear-shaped charges for active venting is the need for a high explosive input initiator. The external energy required to activate a pyrotechnic device is called an initiation input. Common initiation inputs are mechanical, electrical, pneumatic, explosive transfer and laser. Selecting the proper initiation input and energy level is critical to ensure proper

system function and to avoid inadvertent initiation. For FLSCs the primary detonation of an initiator is used to start the explosive reaction of the shaped charge.

One common initiator used with FLSCs can be generally classified as blasting caps. These often take the form of small metallic cups filled with an explosive composition. By activating a low energy mechanical input, such as by pulling a handle, or by using a low energy electrical input (1 Amp of electrical current) these blasting cap initiators will detonate. This energy release of the initiator then fires the FLSC device. Although blasting caps are commonly used and are very low cost devices, they do not produce a sufficiently fast reaction for use in an active venting application. Typical functional response times of a cap initiated FLSC are well in excess of the required 2-4 millisecond range.

Another commonly used initiation mechanism for FLSCs is an explosive transfer line. Two common types of explosive transfer lines are flexible confined detonating cord (FCDC) and shielded mild detonating cord (SMDC). These devices consist of an extrusion of an explosive composition housed inside a metallic or strong plastic tubing. This construction allows a flexible explosive member which is capable of confining the products of detonation within its housing. Explosive transfer lines allow the transfer of explosive energy across a distance in a rapid fashion. Typical velocities for explosive transfer lines are of 40-50 microseconds per foot. Although this is quite rapid for many applications, it may not be sufficient for active venting. Consider, for example, the case of a control unit which detonates the explosive transfer line which is located at a distance of 15 feet (4.6 meters) from the FLSC

device. In this case, the signal transfer time from control unit to FLSC is 0.6 to 0.75 milliseconds. The time required for signal transmission using explosive transfer lines may be longer than desired for an active venting system. Most likely, a better solution involves the use of electronic signals to communicate with initiator devices located close to the FLSCs.

Another initiator which has been widely used on space and aerospace applications is an exploding bridgewire initiator (EBW). EBWs use a low-resistance material such as gold to form a bridgewire. An internal spark gap is utilized to prevent conduction of low voltage and current levels. Detonation is initiated through the discharge of a large capacitor which has been pre-charged to a voltage of several thousand volts. When this voltage is applied across the spark gap, the bridgewire explodes and vaporizes, which then provides impulse energy to initiate the secondary explosive. EBW detonations are very fast with typical detonation times of 10 microseconds after receipt of firing signal. This time response appears compatible with the requirements of active venting.

One major drawback of the EBW initiation system for the active venting application is the need for bulky power supplies, cabling, and capacitors in order to produce large discharge voltages. Additionally, the capacitors must be fully charged at all times to allow instantaneous discharge in the event of an on-board bomb detonation.

Several other variations of EBWs have been proposed which can reduce the need for high voltage activation. Grubelich (1992) has reported a semiconductor

bridge initiator designed to be a low energy, fast response device which is compatible with digital signal technology. This approach intends to use "smart processing" to replace large voltage generating devices. The primary caution with this attempt to decrease initiation energy is the increased potential for inadvertent firing due to electronic noise, static discharge, lightning, and the like. Assuming these concerns are adequately addressed, these low-energy EBWs could become a viable candidate for active venting initiation.

Estimation of Response Time for Edge Perforated Vent Panels

For this analysis, it was assumed that a flexible linear-shaped charge is configured to an exploding bridgewire initiator to create a fuselage vent opening. For comparison purposes, the same panel size and geometry as used in the hinged panel analysis will be used (Figure 16). In the case of the FLSC, it has been established that the EBW will initiate a detonation of the explosive cord within 10 microseconds after receiving an input signal. Once initiated, a detonation will propagate through the FLSC at a speed of approximately 8500 meters per second. Thus, the entire length to the FLSC around the vent opening perimeter (approximately 1.5 meter length) will detonate within about 0.18 milliseconds. Using these estimates, it will be assumed that the edge perforated vent panel will be completely severed within 0.20 milliseconds after having received an input signal.

Once the panel has been severed, the subsequent panel motion can be modeled. Assuming the panel to be a uniform sheet which is initially restrained at the

edges and released at some point in time, the theoretical panel position can be calculated using an equation for one-dimensional motion under constant acceleration:

$$x = x_0 + v_{x0} \cdot t + \frac{1}{2} \cdot a_x t^2 \tag{4.5}$$

Where:
x = Position of the panel in the direction normal to the panel face
x_0 = Initial position of the panel
v_{xo} = Initial velocity of the panel
a_x = Initial panel acceleration (assumed to be constant for small displacements)
t = time (where panel is released at t=0)

Defining the initial position of the panel to be zero and considering no initial velocity for this case, Equation 4.5 becomes:

$$x = \frac{1}{2} \cdot a_x t^2 \tag{4.6}$$

The initial panel acceleration can be approximated as:

$$a_x = \frac{P}{\rho \cdot h} \tag{4.7}$$

Where:
a_x = initial panel acceleration
P = Initial Pressure Differential on the Panel
ρ = Mass Density of the Panel
h = Thickness of the Panel

For the case of the severed panel structure, an effective panel thickness can be calculated as:

$$\text{h} = \text{Effective Thickness} = \frac{\text{Panel Mass}}{\rho \cdot (\text{Panel Length}) \cdot (\text{Panel Width})} \tag{4.8}$$

Substituting the appropriate values for the panel under consideration yields:

$$\text{h} = \frac{1.45\ \text{Kg}}{(2923\text{Kg/m}^3) \cdot (0.508\ \text{meters}) \cdot (0.229\ \text{meters})} = 0.00426\text{meters} \tag{4.9}$$

Thus the initial panel acceleration becomes:

$$\text{a} = \frac{(51{,}700\ \text{Pa})}{\left(2923\frac{kg}{m^3}\right) \cdot (0.00426m)} = 4152.0\frac{m}{s^2} \tag{4.10}$$

Using this initial acceleration with Equation 4.6, an expression can be found for panel position (distance from aircraft in normal direction to panel face) as a function of time after being released.

$$x = \frac{1}{2} \cdot a_x t^2 = \left(2076.0\frac{m}{s^2}\right) \cdot t^2 \tag{4.11}$$

Using this equation, the panel position after being severed is plotted in Figure 20. From this analysis, it can be seen that the panel moves to a distance of 50 millimeters away from the aircraft in approximately 4.9 milliseconds, and to a distance of 100 millimeters in approximately 6.9 milliseconds. For the purposes of this analysis, it will be conservatively estimated that an unobstructed vent opening has

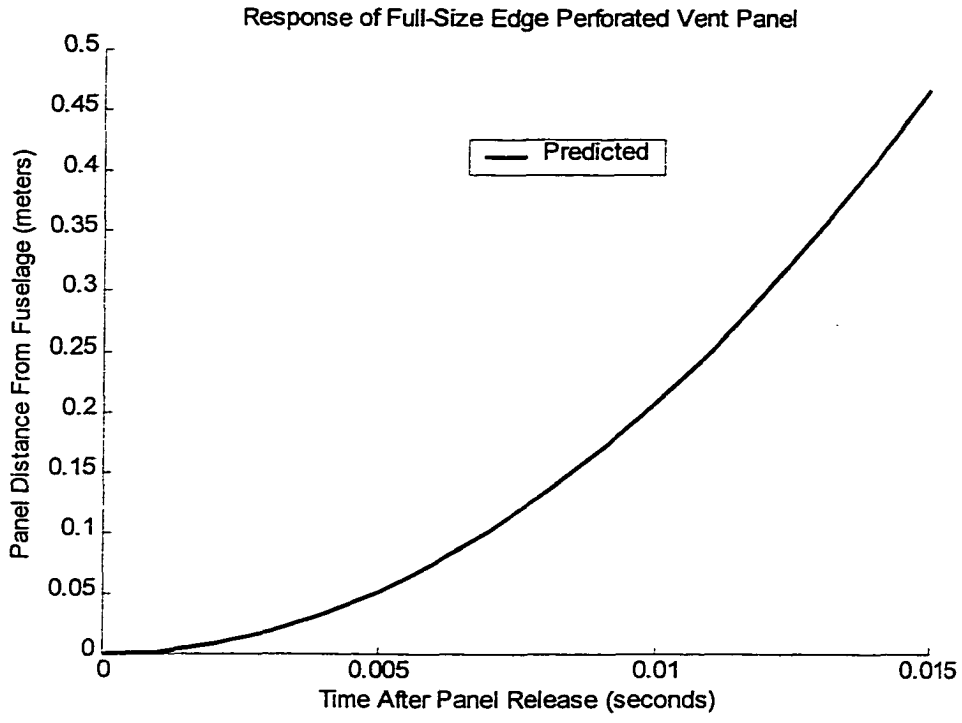

Figure 20. A Plot of the Predicted Position of a Full-Size Edge-Perforated Vent Panel After Being Severed at Time Zero.

been created when the panel reaches a distance of 100 millimeters (about twice the panel thickness including reinforcing members) from the fuselage.

At this point it is important to consider briefly the implementation of an edge perforated vent panel on an existing aircraft. The edge perforated vent panel using flexible linear-shaped charge actuators presents benefits over the hinged panel design. Most of all, the use of a metal cutting actuator eliminates the need for the pressure seals around the vent openings. In some sense, this design allows the vent panels to be fitted onto existing aircraft structures by merely affixing the device to the aircraft interior. Although this is an attractive option, it is speculated that additional fuselage reinforcement would be needed around the vent opening locations. Without additional

structural support, the perforated vent openings may not be able to withstand the stresses caused by flight loading and by the pressure of escaping air from the aircraft interior. Thus, initiating a small vent opening may lead to an unwanted larger opening which could jeopardize the aircraft structure. Additionally, as was the case for hinged panels, ejected edge perforated panels may re-impact the plane and cause unacceptable damage to flight critical components such as wings, engines, or control surfaces.

Fracturable Vent Panel

One additional method of introducing a rapid vent opening in an aircraft fuselage is initiate a fracture in a structural panel member. This could be most readily accomplished in commercial aircraft which utilize tempered glass panes for passenger windows. Tempered glass is manufactured by the process which raises the temperature of the glass close to the softening point. The glass is then removed from the heat source and chilled rapidly. This process is used to greatly enhance the mechanical properties of sheet glass by creating residual compressive stresses near the glass surface and residual tensile stresses on the interior of the glass sheets (Shand, 1958). Although tempering does increase mechanical properties of glass, the residual stresses which are present in the glass create a unique fracture pattern in the event that the glass does fail. When a sheet of tempered glass experiences the initiation of even a very small crack, the internal stresses relieve rapidly as the glass instantly shatters into many small fragments. Thus, it is conceivable that a vent panel could be designed

which relies on the initiation of a crack in a portion of a tempered glass window assembly in order to create a rapid vent opening.

A typical window assembly for a commercial aircraft contains three transparent panes; 1) An outer pressure pane, 2) An inner safety pane, and 3) A thin inner dust cover typically constructed of clear plastic (Figure 21) (Niu, 1988).

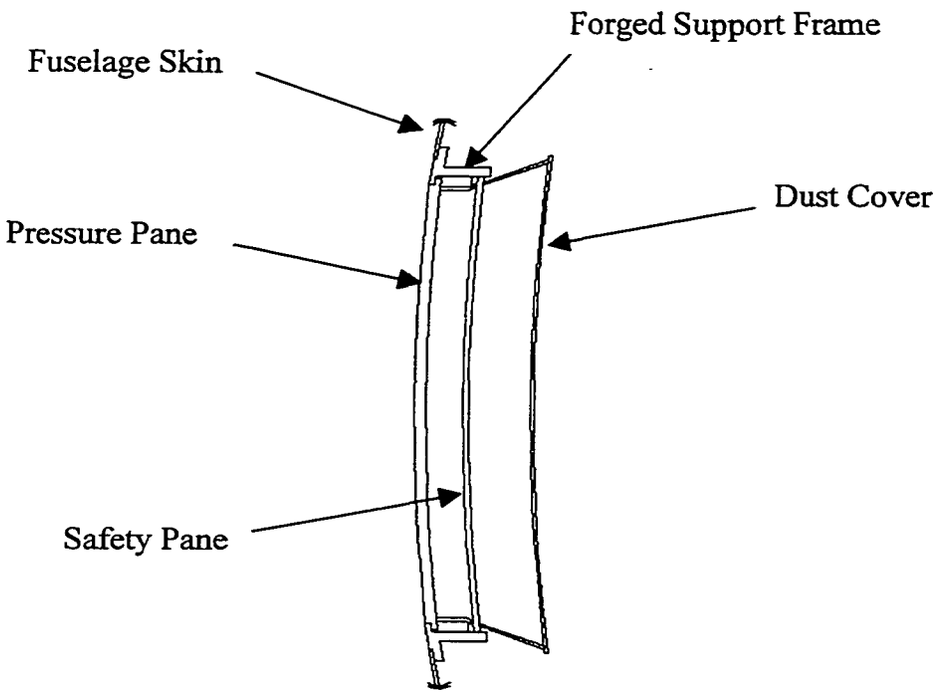

Approximate window dimensions = 25.4 x 35.5 centimeters (10 x 14 inches)
Window surface area = 901.7 cm^2 (140 $inches^2$)
Outer Pressure Pane Thickness = 10.2 mm (0.40 inches)
Inner Safety Pane Thickness = 6.35 mm (0.25 inches)
Dust Cover Thickness = 2.03 mm (0.080 inches)

Figure 21. Assumed Dimensions of a Boeing 737-700 Window Assembly. (Adapted from typical aircraft window construction (Niu, 1988)).

To achieve a rapid vent opening for an active venting system using a fractured

panel, the outer two pressure rated panes of glass would need to be fractured simultaneously. In order to achieve this glass fracture rapidly, it would likely be desired to use a small pyrotechnic device affixed to a portion of the outer perimeter of the glass panes. Once the tempered glass panes have been shattered, the resulting glass fragments will be forced away from the aircraft by the internal cabin pressurization. Before attempting to predict the actuation response time of a fracturable window assembly, a scale-model panel was first analyzed.

Scale-Model Testing of Fractured Glass Vent Panel

Scale-model testing was conducted in order to determine the time of the shattering response of a tempered glass panel affixed to a compressed air tank. The glass panel was configured with a mechanical crack initiation mechanism to fracture the glass and thus create a rapid vent opening of the pressurized air tank. As the resulting shattered glass pieces were forced away from the tank rapidly, the pressure drop in the air tank was recorded with an oscilloscope. The positions of the glass pieces at various time intervals after fracture were determined through the use of an adjustable time-delay photoflash and a 35 millimeter camera with a mechanical shutter. The scale-model testing data will be used later to validate an analytical method for predicting the behavior of a fractured glass panel.

For this test, a compressed air tank was used as a pressure vessel with a 37.3 millimeter vent opening positioned at the mid-length of the tank. A single vent opening was used for this test since the motion of the fractured panel directly in front

of the vent opening (equations 4.6 and 4.7) does not depend on the vent surface area, but rather on internal tank pressure, glass density, and panel thickness. The effect of vent size on the time needed to vent the tank will be addressed in Chapter 5 of this report. The perimeter of the vent opening was machined with a groove to accept an O-ring which forms a pressure seal for a piece of tempered soda lime glass (6.35 centimeters square and 4.63 mm thick). The glass member was retained with small holding brackets which forced the glass against the O-ring seal to allow pressurization of the compressed air tank (Figure 22).

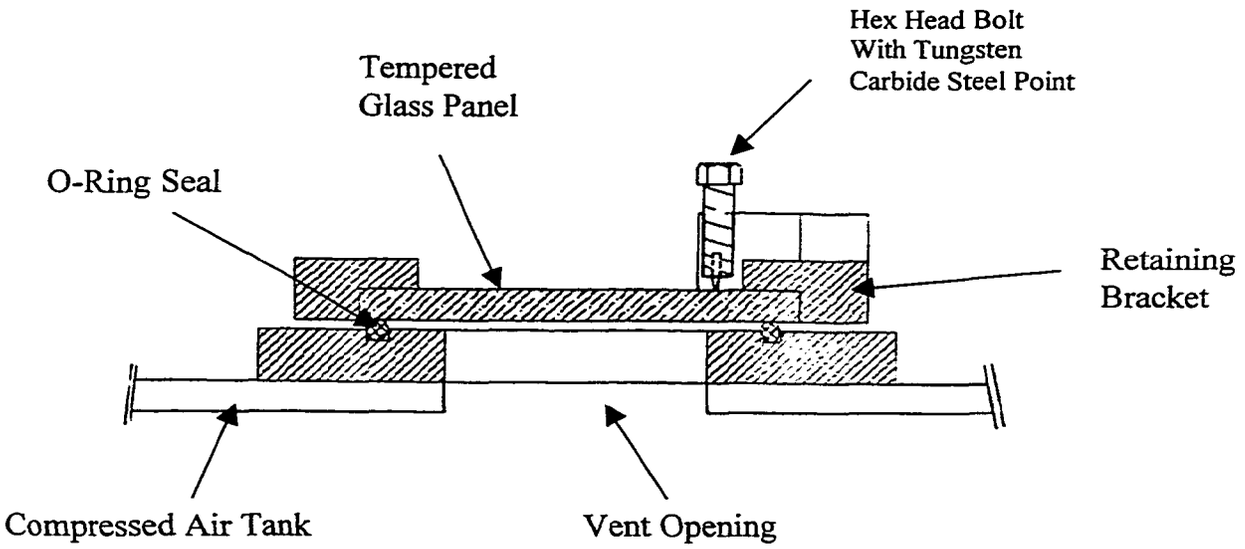

Figure 22. A Section View of the Experimental Configuration Used to Initiate Fracture in a Scale-Model Tempered Glass Vent Panel.

In order to initiate a fracture in the tempered glass piece, a tungsten carbide probe was fitted into the tip of a machine screw. The machine screw was placed into a threaded aluminum block which allowed the tungsten carbide tip of the screw was

then tightened until it made light contact with the tempered glass face. Since a fine threaded machine screw was used, only a small further rotation (about 120 degrees) of the screw head would be needed to drive the sharp tip into the glass and initiate a fracture.

Since this experiment would involve flying shards of glass, for safety reasons it was necessary to initiate the glass fracture at some distance from the tank. For this reason, a small wrench was attached to the head of the machine screw and a string was tied to the opposite end of the wrench. The string was fed through a series of guides and pulleys to allow an operator to pull on the string and initiate a glass fracture while standing safely behind a protective curtain.

With a glass fracture mechanism in place, it became necessary to determine a method for recording the precise instant at which the glass broke. For this purpose, a thin strip of electrically conductive paint was applied to the glass face. Each end of the conductive paint strip was connected to a simple electronic circuit which was monitored by an oscilloscope (Figure 23). When the glass fractures, the electrical continuity is lost and a low to high voltage transition is recorded by the oscilloscope.

For this experiment it was also desired to determine the position of the broken glass pieces at various times after the initial fracture. To accomplish this task, a conventional 35 millimeter camera with a manual shutter was used in conjunction with a variable delay electronic timing circuit (Figure 24). When the glass fractures

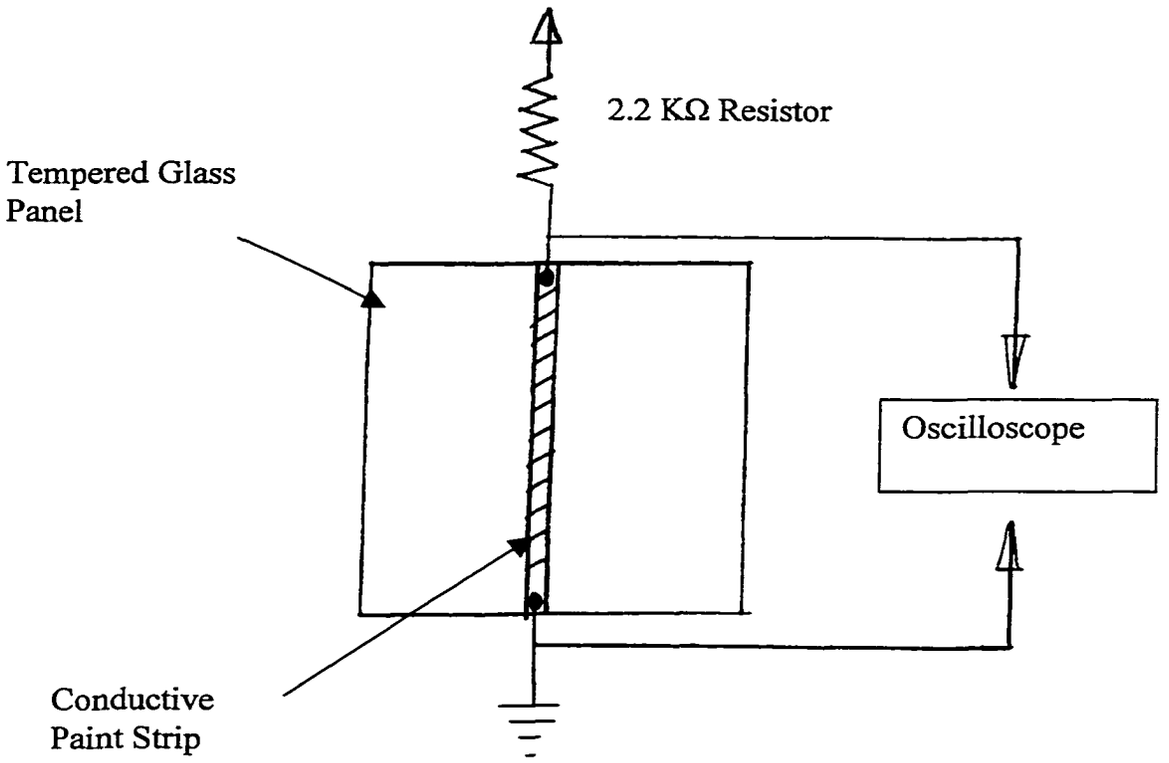

Figure 23. The Experimental Configuration Used for Determining the Instant of Glass Fracture.

and the conductive paint path is broken, the low to high electrical transition signal is fed to a 7474 inverter which inverts the signal to a high to low transition. This falling edge then triggers a 555 timer to begin outputting a time-delay pulse. The duration of this output pulse can be set through the selection of appropriate values of a resistor and capacitor. After completion of the timing pulse of desired duration, a falling edge pulse was fed to a second 555 timer which immediately triggered a silicon controlled rectifier (SCR) to fire a photo flash. For this experiment, a Vivitar 283 photo flash

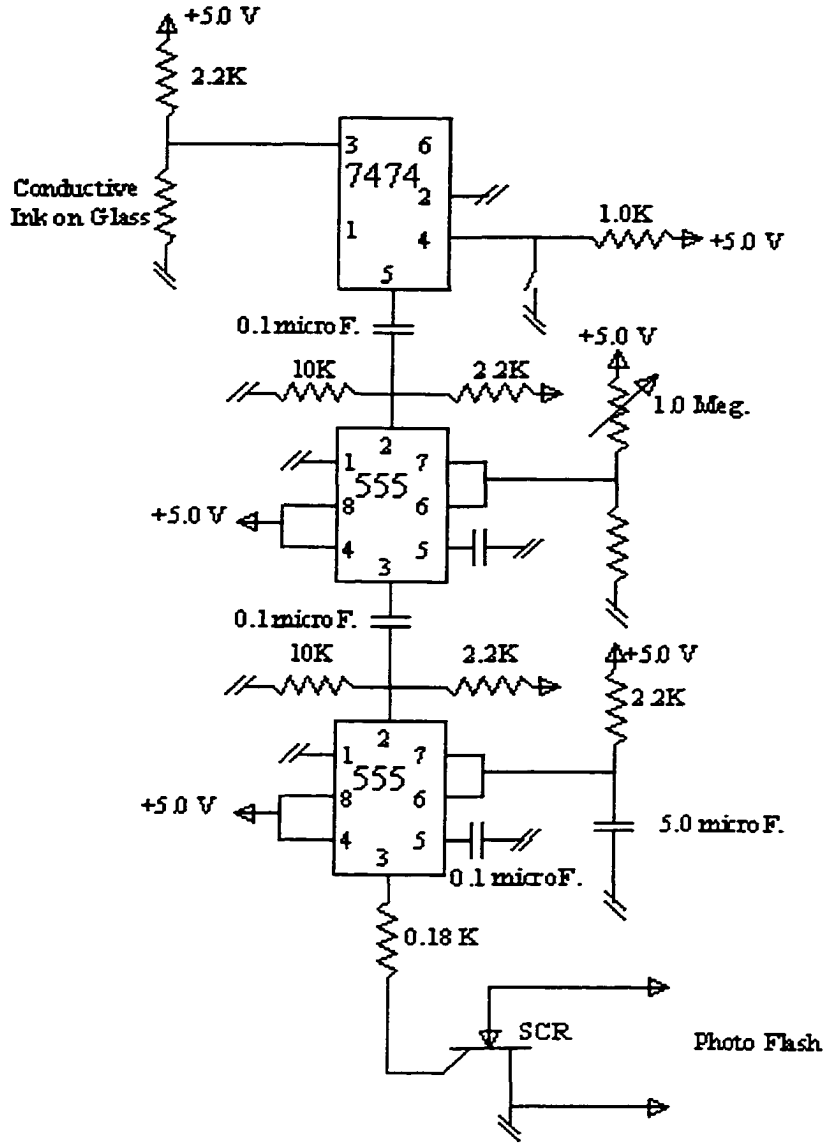

Figure 24. A Schematic Diagram of the Circuitry Used to Produce a Variable Time-Delay Photo Flash for Determining Glass Position After Fracture Initiation.

was used with a jumper wire inserted across the thyristor contacts to minimize the duration of the photo flash (Winters, 1990). Using this method, a flash duration on the order of 60 microseconds was achieved.

One important measure of the effectiveness of a panel actuation method is the time required for a vent opening to be created on a structure. For the fractured glass window assembly it is important to predict the time needed for the glass pieces to move away from the window opening to allow unobstructed airflow from the aircraft. It is also necessary to determine the time needed for the pressure inside the fuselage to drop after an activation signal has been sent to the actuation system, which can be defined as the total system delay time (Figure 25).

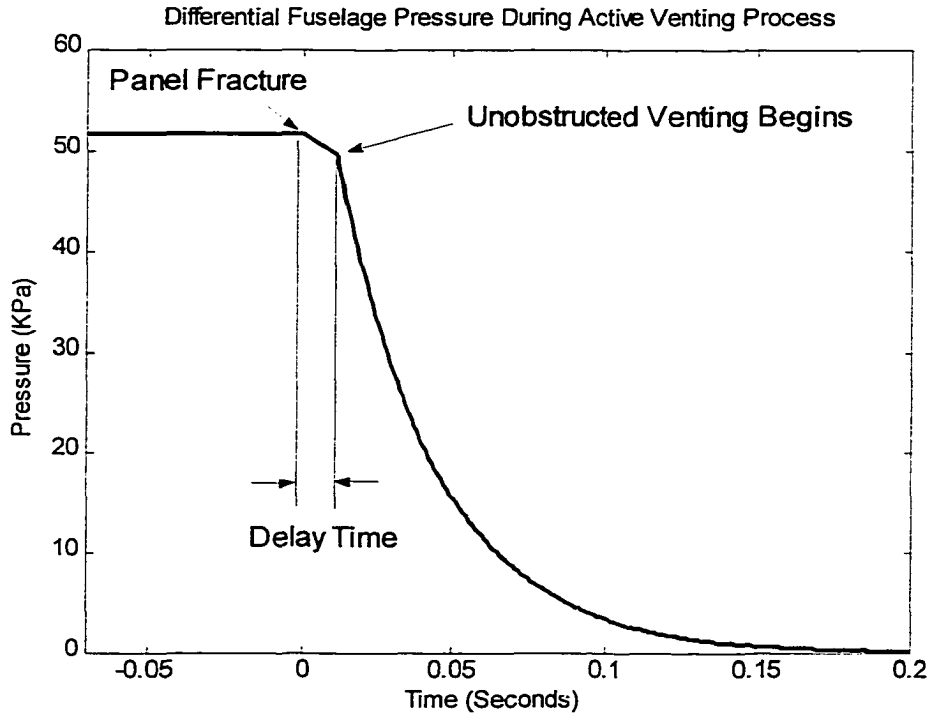

Figure 25. Plot of the Pressure Response of an Aircraft Cabin to Illustrate the Time Delay of an Active Venting System.

The total delay time includes the time required for an actuation system to create an unobstructed vent opening in the fuselage. Once a vent opening has been

established, however, the pressure inside the aircraft will not drop instantaneously. The pressure drop inside the aircraft will be delayed depending on the distance from the vent opening. This time lag can be defined as propagation delay and can be approximated as the time is takes for a sound wave to travel in air from the vent opening to the point of pressure measurement.

Determining Delay Time for the Scale Model Glass Fracture Vent Opening

For this testing, the compressed air storage tank was pressurized to 51.7 KPa. This pressurization in a laboratory atmosphere is equivalent to the maximum pressure differential experienced by a Boeing 737 in flight above 5640 meters (18,500 feet) (Greenwald, 1967).

The compressed air tank was equipped with a pressure transducer manufactured by Sensym, Inc. of Milpitas California (part number STIV 20015G2A). This transducer utilizes a silicon piezoresistive sensing element and is rated for a pressure range of 0 to 15 psig (0 to 103.4 Kpa). The Sensym pressure transducer requires an excitation of 10 to 30 Volts DC and produces an output signal of 0.333 Volts per psig with a 1.0 Volt zero pressure offset.

The output signal from the pressure transducer was connected to a Tektronix TDS300 Oscilloscope (Figure 26). The oscilloscope was set to trigger on the falling edge of the pressure profile and transient tank pressure data were captured. The data was then exported to a personal computer using software (Wavestar Version 1.1) available from Tektronix Inc. of Beaverton, Oregon. The data were then analyzed

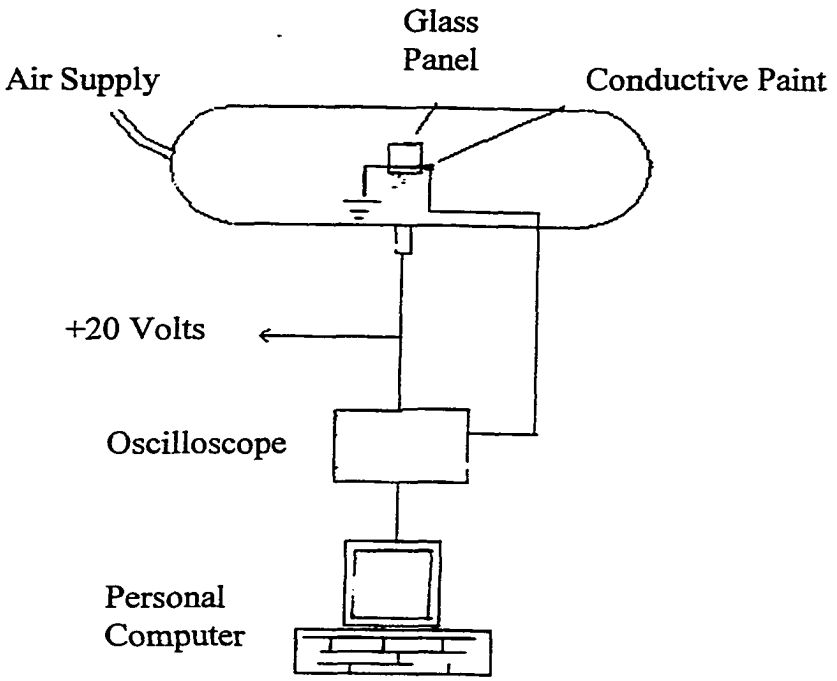

Figure 26. Schematic of the Test Configuration for Measuring the Decompression Time of the Compressed Air Tank.

using the software numerical analysis tools in MATLAB version 5.2. A typical transient pressure curve for rapid decompression of the compressed air tank is shown in figure 27.

The total measured system delay time for the scale model compressed air tank for a series of trials for a pressure transducer located at a distance of 0.368 meters (14.5 inches) from the vent opening are given in Table 7. Assuming the propagation delay in the scale model testing can be approximated as the time required for a sound wave to travel in air from the vent opening to the point of pressure measurement, we

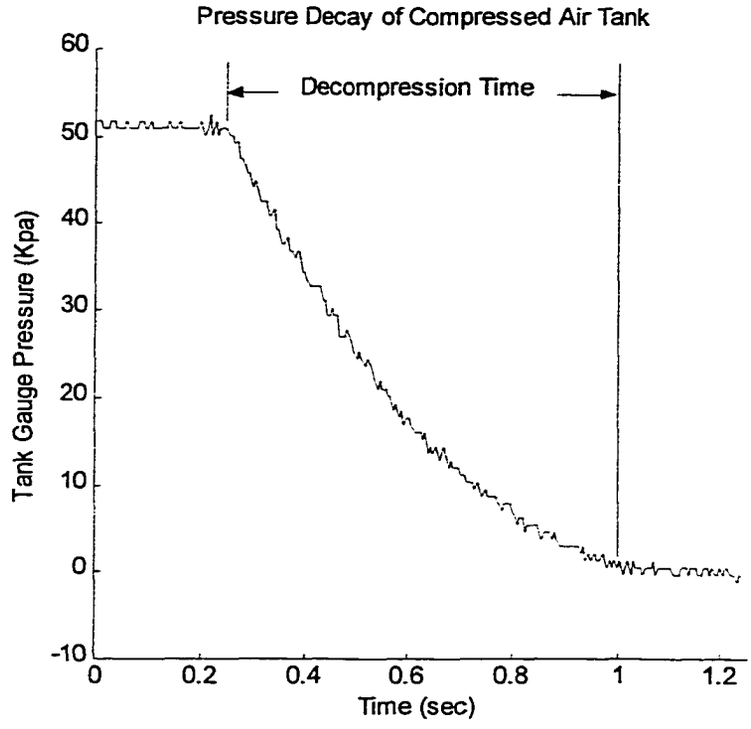

Figure 27. Transient Pressure Decay Recorded for a Decompression of the Compressed Air Tank.

Table 7

Measured Delay Times for Fractured Glass Vent Opening on Compressed Air Tank

Experimental Trial	Total Delay Time (milliseconds)
1	1.89
2	2.21
3	1.78
4	2.09
5	2.76
6	1.82
7	2.41
Average	**2.14**
Standard Deviation	**0.356**

can calculate the propagation delay for the compressed air tank testing (equation 4.12).

$$T_p = \frac{d}{c} \tag{4.12}$$

Where: T_p = Propagation Delay (s)
d = Linear distance from pressure transducer to vent opening
c = Speed of sound in air inside air tank

Assuming the speed of sound of air in the tank to be that of standard atmosphere and the linear distance from sensor to vent opening of 0.368 meters, the propagation delay for the air tank is:

$$T_p = \frac{0.368\text{m}}{340.3\ \text{m/s}} = 1.08\text{x}10^{-3}\ \text{seconds} \tag{4.13}$$

Thus, subtracting the propagation delay time from the average total measured delay time for the compressed air tank gives an actuation system delay time of 1.06 milliseconds. This actuation system delay time can be considered the time needed from the instant of glass fracture to create an effectively unobstructed vent opening.

It would be useful to relate the actuation delay time to the position of the broken glass pieces at that time. Photographs of the flying glass fragments taken at various time delays after the initiation of glass fracture are shown in Figure 28. From these photographs it is apparent that venting begins almost immediately after the glass panel is shattered.

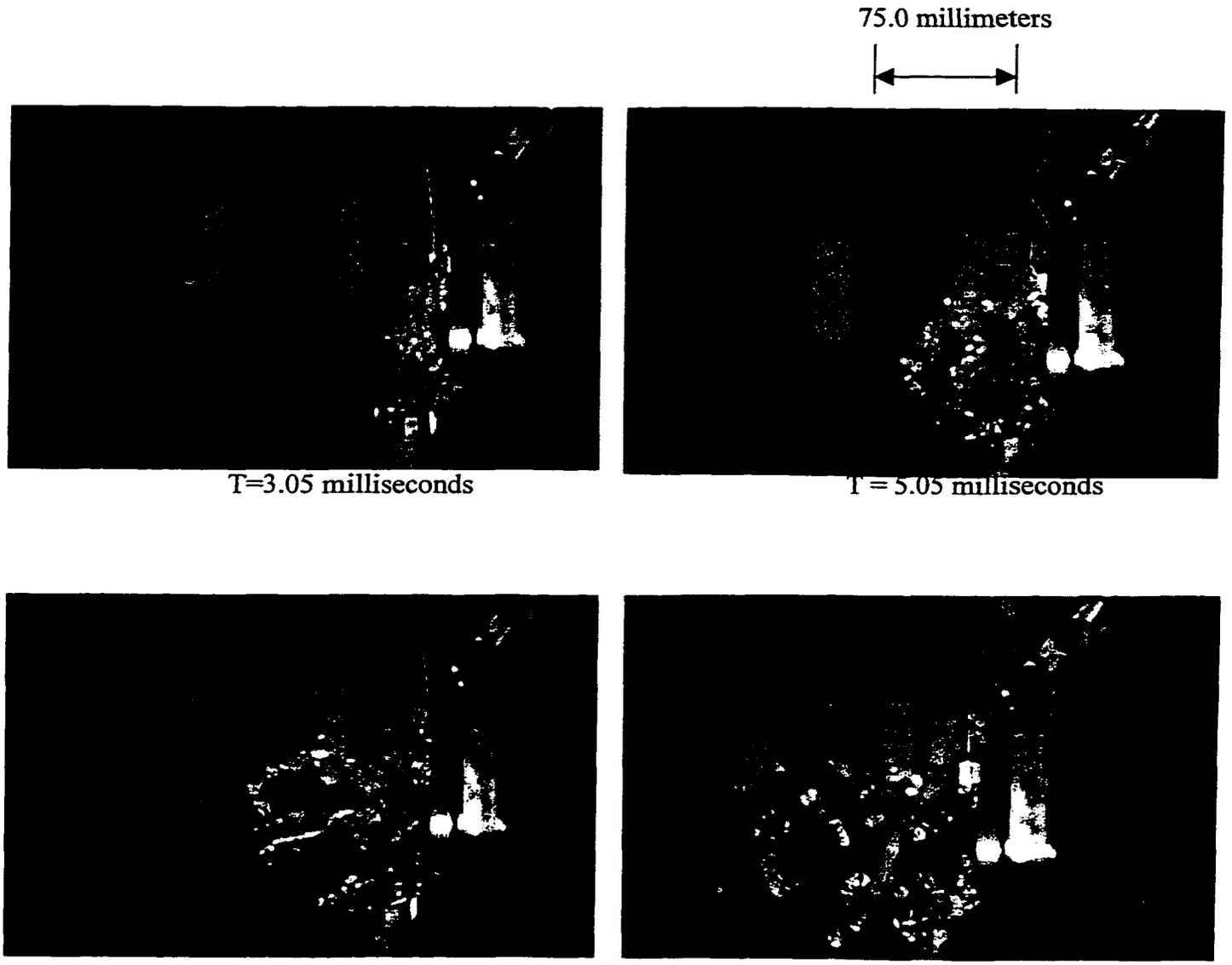

Figure 28. Photographs Showing Tempered Glass Fragments at Various Time Delays After Fracture Initiation.

Predicting Glass Position for Scale-Model Testing

If we make the assumption that the glass pane is a uniform sheet initially restrained at the edges and then released at some time, the theoretical position of the

panel can then be calculated as for the previously described edge-perforated panel analysis. The equation for one-dimensional motion under constant acceleration from an initial rest position can then be used:

$$x = \frac{1}{2} \cdot a_x t^2 \tag{4.14}$$

Where: x = Position of the glass panel in the direction normal to the glass face
a_x = Initial panel acceleration (assumed to be constant for small displacements)
t = time (panel is released at t=0)

Again, the following expression will be used for initial panel acceleration:

$$a_x = \frac{P}{\rho \cdot h} \tag{4.15}$$

Where: a_x = initial panel acceleration
P = Initial Pressure Differential on the Glass Panel
ρ = Mass Density of the Glass Panel
h = Thickness of the Glass Panel

Substituting the appropriate values for our scale model tank gives:

$$a = \frac{(51{,}700\ \text{Pa})}{\left(2474 \frac{kg}{m^3}\right) \cdot (0.00461 m)} = 4533.0 \frac{m}{s^2} \tag{4.16}$$

Using this initial acceleration with Equation (4.15), an expression can be found for glass panel position as a function of time after being released.

$$x = \frac{1}{2} \cdot a_x t^2 = \frac{1}{2} \cdot \left(4533.0 \frac{m}{s^2} \right) \cdot t^2 \tag{4.17}$$

$$x = \left(2266.5 \frac{m}{s^2} \right) \cdot t^2 \tag{4.18}$$

In reality, the glass fragments do not all behave in the same fashion as a flat panel of uniform thickness. This is especially true of fragments which are small with respect to the original thickness of the glass plate. Neglecting these small fragments, the average position of the approximate center of mass of the glass pieces at given times can be determined from the stop-action photographs, and the results plotted along with the predicted values from Equation (4.18) (Figure 29).

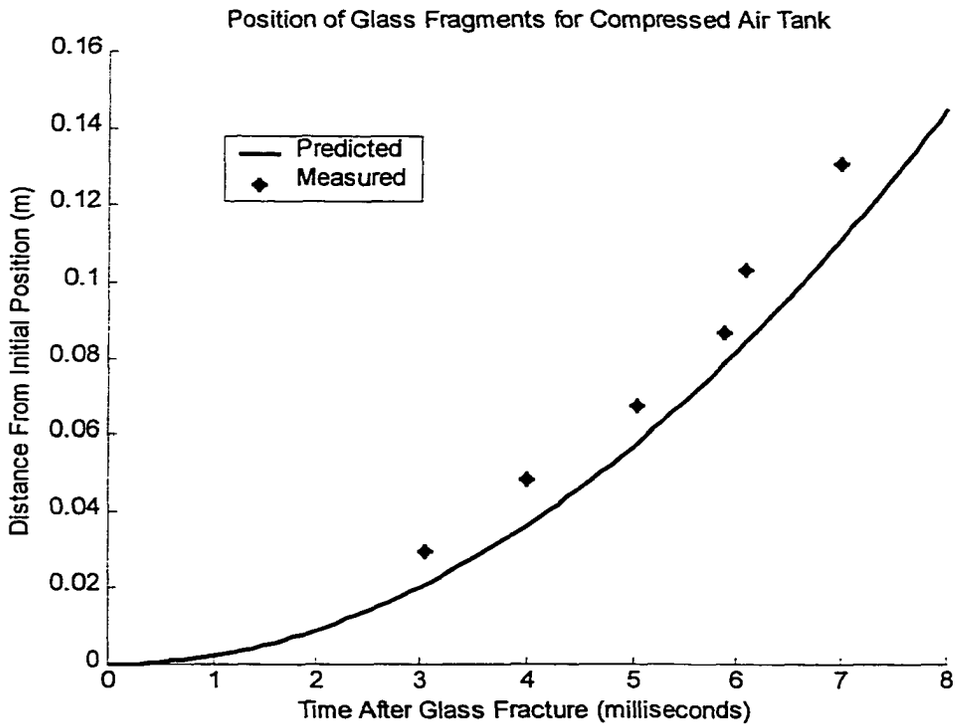

Figure 29. Plot of Average Position of Glass Fragments as a Function of Time after Glass Panel Fracture. Solid Line Indicates Predicted Behavior Using Model of a Uniform Flat Panel Under Constant Acceleration.

This plot indicated that the flat panel assumption works quite well in predicting the glass panel position for distances close to the initial glass position. The average deviation of measured glass position from the theoretical values is 18.5%. In all cases, the measured glass positions were further away from the tank than predicted. This discrepancy is probably caused by the small amount of time needed after glass fracture for the glass to displace enough to break the electrical continuity of the conductive paint strip. It is important to note from Figure 29 that the glass has moved to a distance of 0.5 centimeters (0.20 inches) at the actuation system delay time of 1.06 milliseconds. This distance is quite comparable to the original glass thickness of 0.46 centimeters. This result indicates that the glass moves only a very short distance before an effectively unobstructed vent opening has been established.

Predicting Response Time of a Fractured Window Assembly of a Boeing 737-700

Considering the adequacy of Equation 13 in predicting the position of fractured glass pieces for the scale-model experiments, this method will be applied to a full-scale window of a Boeing 737-700 aircraft. It will be assumed that the window glass will be fractured by a small pyrotechnic initiator located at a point on the window perimeter. Based on pyrotechnic actuator response times as discussed previously in this chapter, it will be assumed that the time required for this actuator to initiate a glass fracture will be on the order of 0.1 milliseconds.

In the case of an active venting system deploying while an aircraft is flying at altitude, the fractured pieces of the tempered glass panes will then be forced away

from the aircraft by the pressure differential experienced by the unrestrained glass. For this analysis, it will be assumed that the thin plastic inner window pane, which is not designed to carry pressure loading, will be immediately forced out of the aircraft once outer two load-bearing glass panels have been fractured. The response time of the fracture panel venting system will thus depend on the time needed for the outer two glass members to move away from the aircraft to a distance at which an effectively unobstructed vent opening has been created.

Neglecting the thin plastic inner pane, the behavior of the two outer window panes will be considered. For simplicity, it will be assumed that once the outer panes have been simultaneously shattered, the glass fragments from both panes will behave as a single window with the combined thickness of both panels. In this case, the initial acceleration of the panel is calculated as:

$$a_x = \frac{P}{\rho \cdot h} \tag{4.19}$$

$$a = \frac{(51{,}700\,\text{Pa})}{\left(2470\frac{kg}{m^3}\right)\cdot(0.01655m)} = 1264.7\frac{m}{s^2} \tag{4.20}$$

The position of the fractured glass pieces after fracture initiation can then be calculated as follows:

$$x = \frac{1}{2}\cdot a_x t^2 = \frac{1}{2}\cdot\left(1264.7\frac{m}{s^2}\right)\cdot t^2 \tag{4.21}$$

$$x = \left(632.4\frac{m}{s^2}\right) \cdot t^2 \tag{4.22}$$

Using this method, the predicted window glass position of the outer glass panes can then be plotted (Figure 30).

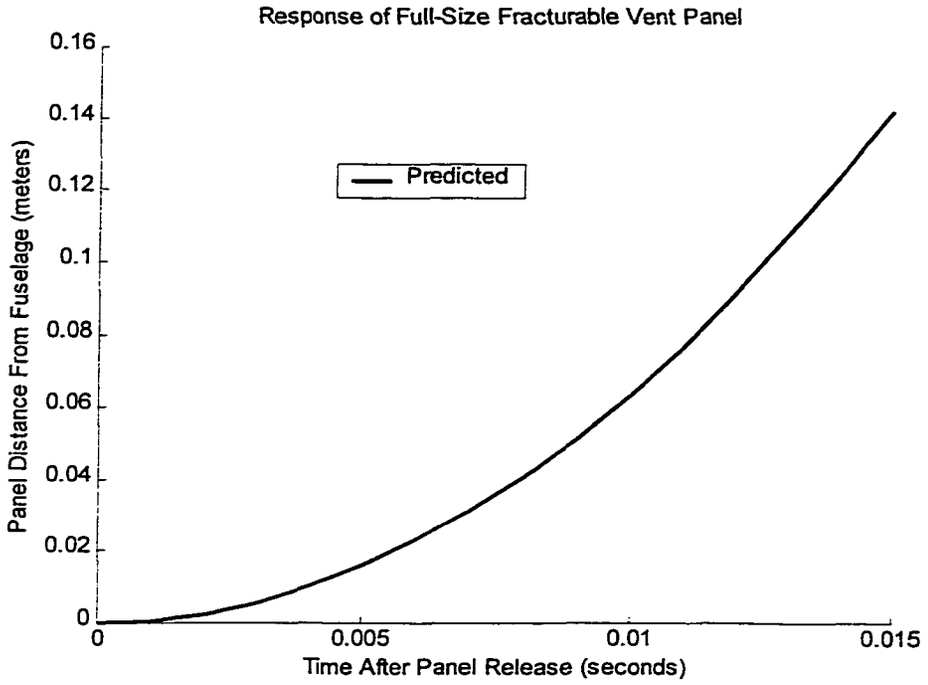

Figure 30. Predicted Position of Glass Fragments After Fracture Initiation.

For the full-size fracturable panel, it will be conservatively estimated that venting will begin when the glass fragments reach a distance of 15 millimeters (approximately three times further than that measured for the scale model panel) from their initial position. Thus, the time required from the instant of panel fracture to the point at which venting begins is estimated to be 4.9 milliseconds.

Summary of Estimated Response Times of Panel Actuation Systems

In summary, the estimated response times of each of the three panel actuation systems have been determined (Table 8).

Table 8

Summary of Estimated Response Times of Panel Actuation Systems

	Type of Panel		
	Hinged	Edge Perforated	Fracturable
Pyrotechnic Actuator Response Time	<0.1 milliseconds	<0.2 milliseconds	<0.1 milliseconds
Panel Response Time	7.1 milliseconds	6.9 milliseconds	4.9 millisecond
Estimated Total Response Time of Panel Actuation System	7.2 milliseconds	7.1 milliseconds	5.0 milliseconds

From these preliminary analyses, it seems that it is reasonable to assume that a total panel actuation response time of 5 to 7 milliseconds would be typical for the selected vent panel used in this study. At this point it should be noted that the accuracy of these predictions depends to a large degree on size and construction of the actual panel assemblies. It is possible that in actual practice vent panel actuation times may be significantly shorter than predicted (on the order of 1.5 milliseconds) due to

the contribution of explosive pressure (assumed magnitude of 500 KPa) acting against the inner surface of the vent panel. It must also be noted that in each case, an estimate was made as to the point at which the venting process actually begins. Although these two factors pose important topics for further study, the determined time estimate for panel response times (Table 8) will be used as representative data for the current analysis.

CHAPTER V

PREDICTING AIRCRAFT DECOMPRESSION TIMES

Background on Aircraft Pressurization

Aircraft cabin pressurization is the process of maintaining a cabin atmosphere of an altitude lower than the actual flight altitude. Pressurization is achieved through on-board compressors which create a positive pressure inside the aircraft (De Remer, 1992). Cabin pressurization was attempted in the United States as early as 1921, but the first successful test flight of a pressurized aircraft, a Lockheed XC-35, did not occur until 1939 (Greenwald, 1967). Cabin pressurization allows aircraft flight at higher altitudes without the need for supplemental oxygen. Cabin pressurization also prevents or minimizes the effects of decompression sickness caused by exposure of the human body to extremely low barometric pressures (Table 9).

Table 9

Atmospheric Pressure as a Function of Altitude (Thompson, 1972)

Height Above Sea Level – m (ft)	Ambient Pressure Atm – (KPa)	Temperature °C
0 (0)	1.00 (101.3)	15.0
2,000 (6,562)	0.7846 (79.5)	2.0
4,000 (13,120)	0.6085 (61.7)	-11.0
6,000 (19,680)	0.466 (47.2)	-24.0
8,000 (26,250)	0.3519 (35.7)	-36.9
10,000 (32,810)	0.2615 (26.5)	-49.9
12,000 (39,370)	0.1915 (19.4)	-56.5
14,000 (45,930)	0.1399 (14.2)	-56.5

Typical aircraft compression systems are designed to maintain atmospheric pressure inside the fuselage up to a given altitude at which a maximum pressure differential is reached. A Boeing 737, for example, can maintain atmospheric pressure, 101.3 KPa (14.7 psi), up to an altitude of 5,640 meters (18,500 feet). For flights at higher altitudes, a maximum pressure differential of 51.7 KPa (7.5 psi) between the aircraft cabin and the ambient atmosphere is maintained (Greenwald,1967). Plots of pressure levels for various flight altitudes of a typical Boeing 737 aircraft are given in Figure 31.

Aircraft Decompression

The use of cabin pressurization in aircraft gives rise to the possibility of an in-flight loss of pressurization, or decompression, due to a structural failure of the aircraft. In the event that a breech occurs in an aircraft fuselage, the pressurized cabin air will flow through the opening to the lower pressure ambient atmosphere. The rate at which aircraft decompresses from a higher pressure to a lower pressure, known as decompression time, is determined primarily by the volume of the pressurized cabin, the altitude-dependent pressure differential, and the size of the opening in the aircraft.

Physiological Effects of Decompression

Two types of aircraft decompression are often cited in the literature: explosive decompression and rapid decompression. Although often used interchangeably, these terms describe two unique types of physical events. Explosive decompression is defined as a change in aircraft cabin pressure faster than the rate at which human

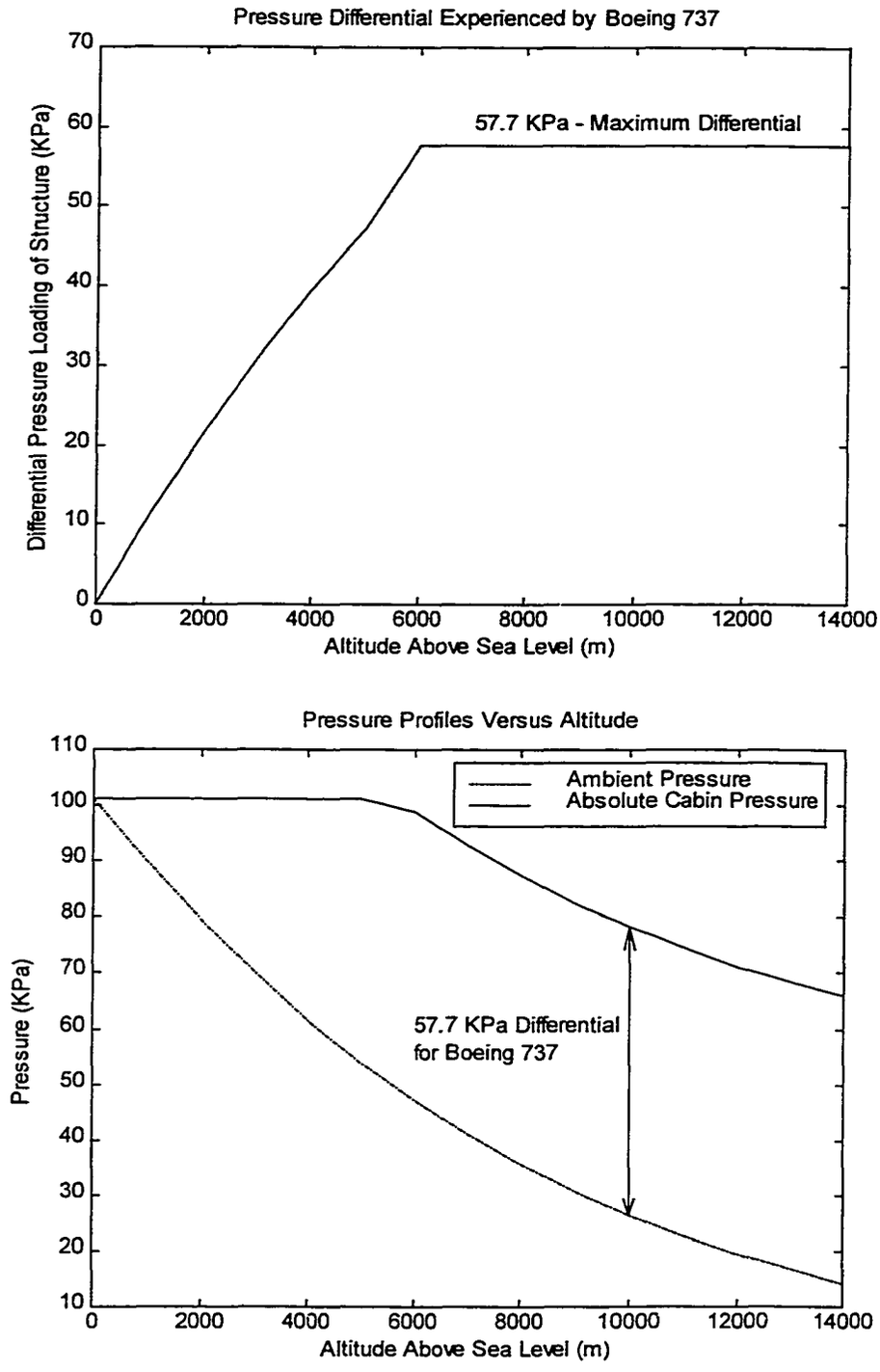

Figure 31. Pressure Profiles for Boeing 737 Aircraft (Thompson, 1972).

lungs can decompress or exhale. Since the typical time required to release air from the lungs is 0.2 seconds, it has been proposed that a decompression occurring faster than 0.5 seconds is classified as explosive and potentially harmful to the human lungs (De Remer, 1992). A rapid decompression, on the other hand, is defined as the change in cabin pressure which occurs slower than the lungs can decompress. For this reason, a rapid decompression reduces the likelihood of permanent damage to passengers and crew when compared to an explosive decompression. In the absence of more concrete data regarding physiological damage caused by a rapid decompression event, the proposed decompression time limits (0.2 to 0.5 seconds) were considered as conservative estimates for the purposes of this study.

Predicting Aircraft Decompression Time

Since the earliest usage of pressurized aircraft, it has been important to develop a generalized method for predicting aircraft decompression times. One of the most comprehensive studies of aircraft decompression was carried out by Fritz Haber and Hans Clamman, at the United States Air Force School of Aviation Medicine. In 1953, Haber and Clamman published a general method of predicting aircraft decompression times in which they proposed the following relationship:

$$T_d = \frac{(V \cdot P_1)}{(A \cdot c)} \tag{5.1}$$

Where:
T_d = Total time of fuselage decompression (s)
V = Volume of the fuselage compartment (m^3)
A = Area of fuselage orifice (m^2)
P_1 = A non-linear function of the fuselage and ambient pressures
c = Speed of sound in air (m/s)

Scale Model Testing

In order to better understand the rapid decompression phenomenon and to test the Haber and Clamman decompression model, scale model testing was carried out in the present study using two different size pressure vessels. The first vessel was a compressed air storage tank and the second was constructed from a section of PVC pipe. Various decompression experiments were conducted on each vessel as described in the following sections.

Compressed Air Tank Testing

A compressed air storage tank was used in scale model testing of decompression times (Figure 32). The tank diameter was 0.521 meters (20.5 inches) and the nominal tank length was 1.80 meters (71 inches). The compressed air tank was fitted with a hinged panel (Figure 33) which seals interchangeable vent openings of various sizes (Figure 34). The hinged panel was designed to be released remotely by a latch attached to a string. The compressed air tank was pressurized with air to a gage pressure of 51.7 KPa (7.5 psig). This pressurization in a laboratory atmosphere is equivalent to the maximum pressure differential experienced by a Boeing 737 in flight above 5640 meters (18,500 feet) (Greenwald, 1967). This pressure value has been selected for use in all decompression experiments described in this report. When the panel latch is released by pulling on the string, the internal air pressure forces the hinged panel away from the tank vent opening. A ball of clay was placed on the tank to catch and trap the hinged panel in the fully open position (Figure 33).

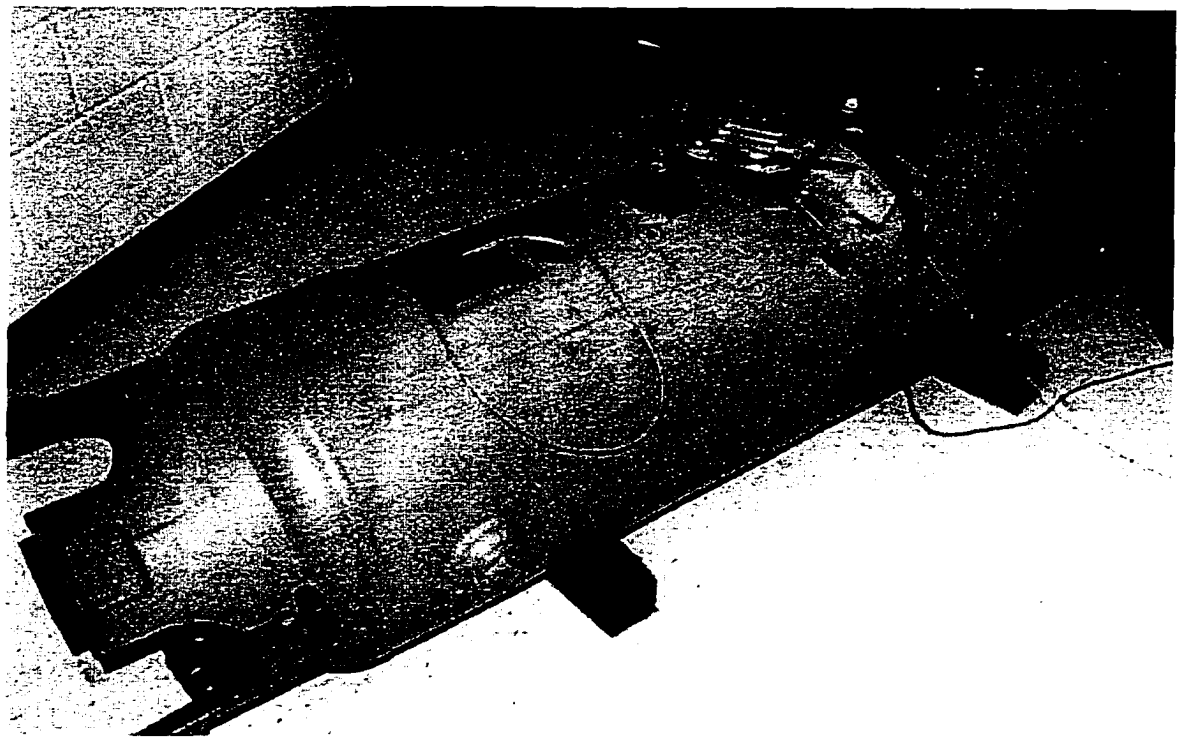

Figure 32. Photo of Compressed Air Tank Equipped With Hinged Panel (Located at the Center of Tank Facing Upward).

In this configuration, the hinged panel opens rather quickly. Once the panel latch has been released, the panel rotates from a fully closed position through an angle of 90 degrees in about 30 milliseconds as described in the panel actuation section of this report. The hinged panel arrangement worked well in providing a repeatable method of creating a rapid opening in the compressed air tank.

The compressed air tank was equipped with a pressure transducer manufactured by Sensym, Inc. of Milpitas California (part number STIV 20015G2A). This transducer utilizes a silicon piezoresistive sensing element and is rated for a pressure range of 0 to 15 psig (0 to 103.4 Kpa). The Sensym pressure transducer

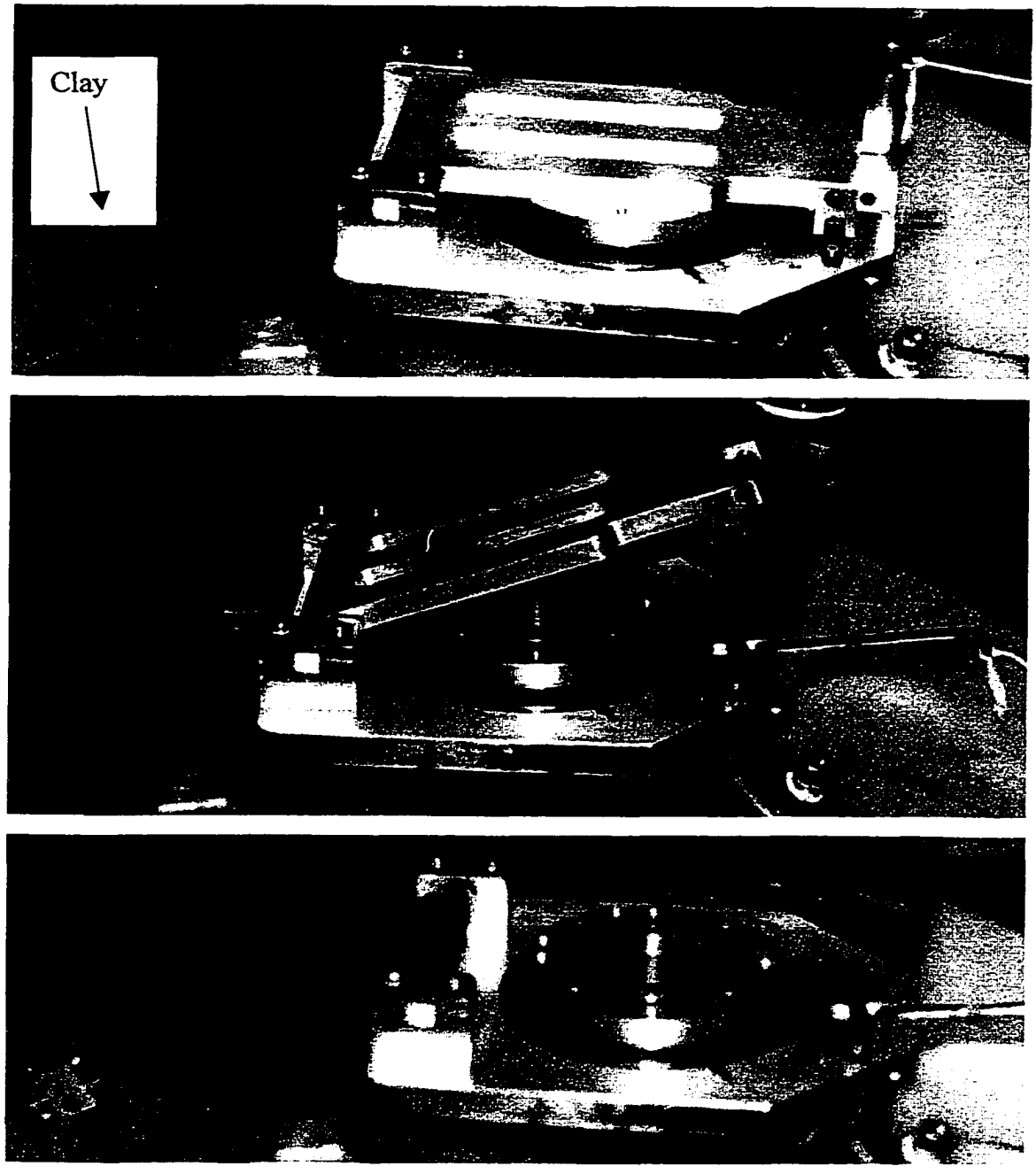

Figure 33. Photos Showing the Hinged Panel on the Compressed Air Tank in the Fully Closed (Top), Partially Open (Middle), and Fully Open (Bottom) Condition.

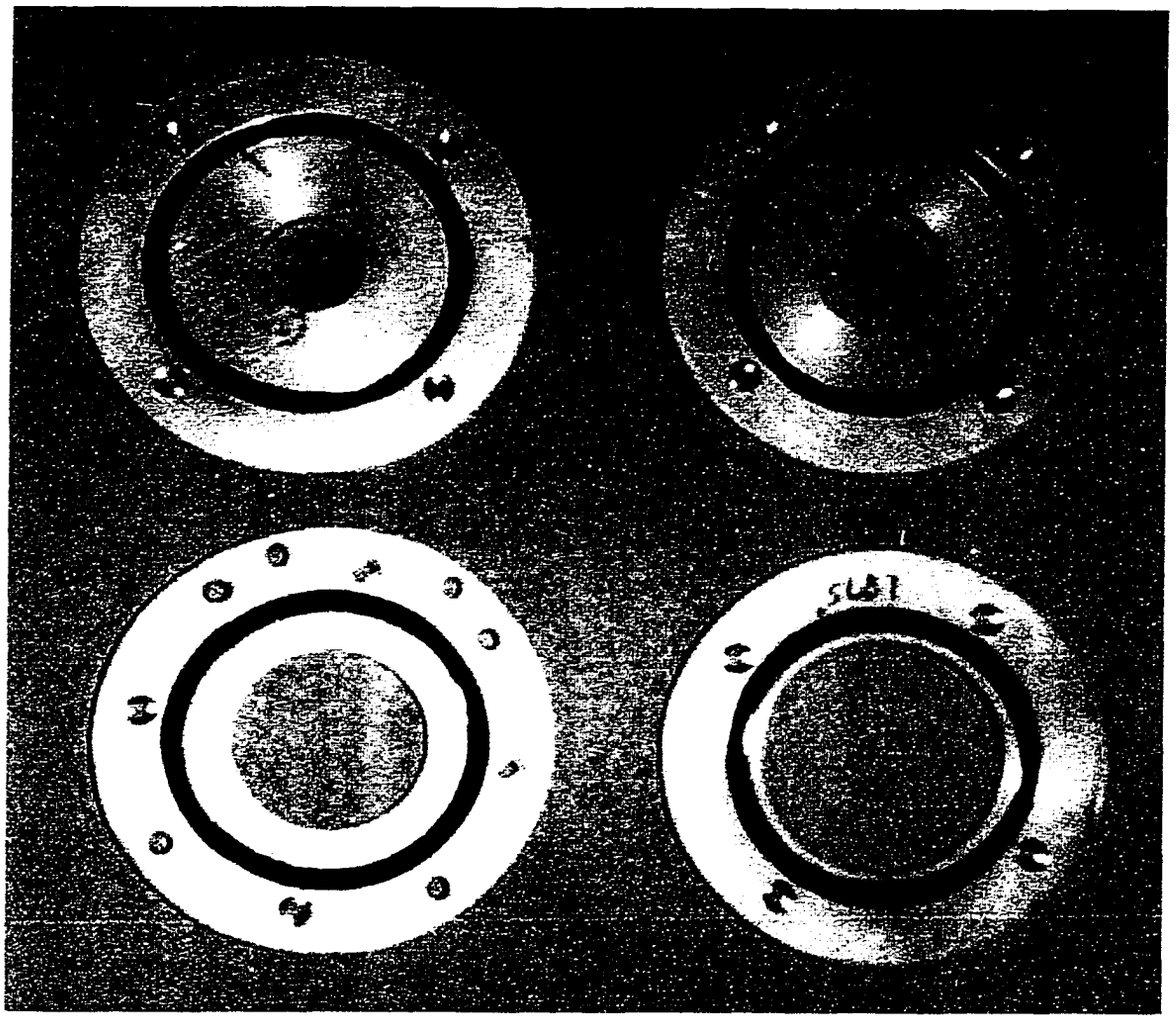

Figure 34. Photo of Orifice Plates Used on Compressed Air Tank. Orifice Diameters are (Clockwise From Upper Left) 1.91 cm, 2.54 cm, 4.76 cm, and 3.73 cm.

requires an excitation of 10 to 30 Volts DC and produces an output signal of 0.333 Volts per psig with a 1.0 Volt zero pressure offset.

Calibration of Pressure Transducer

The Sensym pressure transducer was calibrated by simultaneously pressurizing it and an absolute pressure transducer manufactured by MKS Instuments of Andover Massachesetts (Model #750B23TFE2GA). The Sensym transducer pressure readings agreed with those of the MKS transducer within 2%. The repeatability of the Sensym pressure transducer was also examined by performing the calibration procedure twice. Both calibration trials produced a linear relationship between the the output signal and applied pressure level. The two slopes of best-fit lines through the calibration data agreed to within 0.03 %. Based on these calibration measurements, it was determined that to achieve a tank pressure of 7.5 psig (51.7 Kpa gage), a calibrated sensor output voltage of 3.475 Volts is required.

Measuring Decompression Times

The output signal from the pressure transducer was connected to a Tektronix TDS300 Oscilloscope (Figure 35). The oscilloscope was set to trigger on the falling edge of the pressure profile and the transient tank pressure data were captured. The data were then exported to a personal computer using software (Wavestar Version 1.1) available from Tektronix Inc. of Beaverton, Oregon. The data were analyzed using the software numerical analysis tools in MATLAB version 5.2. A typical transient pressure curve for rapid decompression of the compressed air tank is shown in Figure 36.

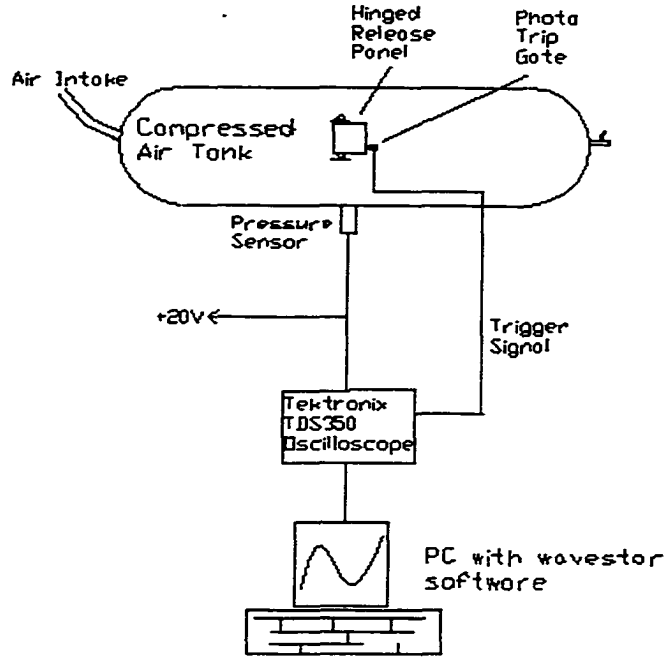

Figure 35. Schematic of the Test Configuration for Measuring the Decompression Time of the Compressed Air Tank.

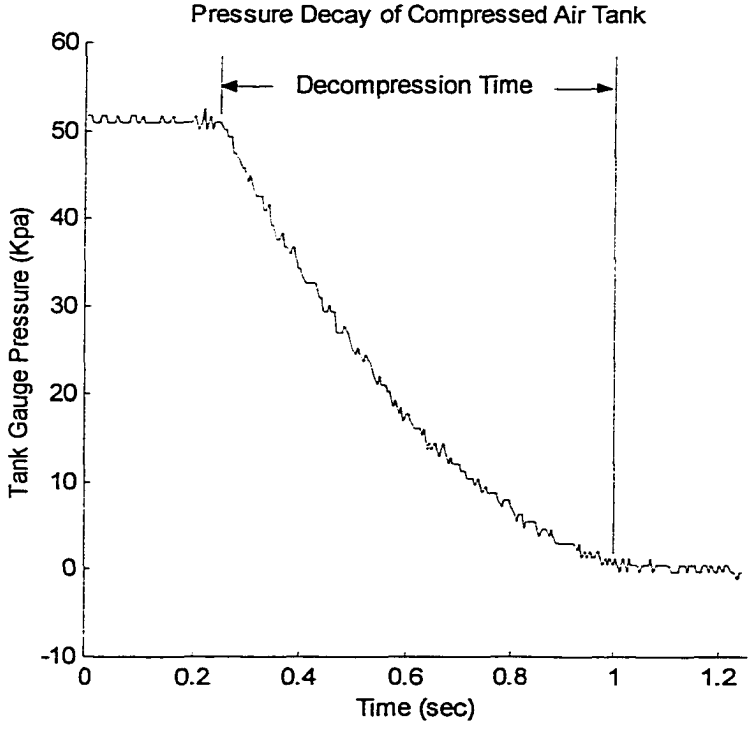

Figure 36. Transient Pressure Decay Recorded for a Decompression of the Compressed Air Tank.

Effect of Pressure Transducer Location

Inherent in the method of predicting decompression times proposed by Haber and Clamman is the assumption that transient pressure behavior of an aircraft is uniform throughout the vessel. In order to determine the validity of this assumption for the compressed air tank, a series of venting trials were conducted. Total tank decompression times were recorded with the pressure transducer located in various locations on the tank (Figure 37).

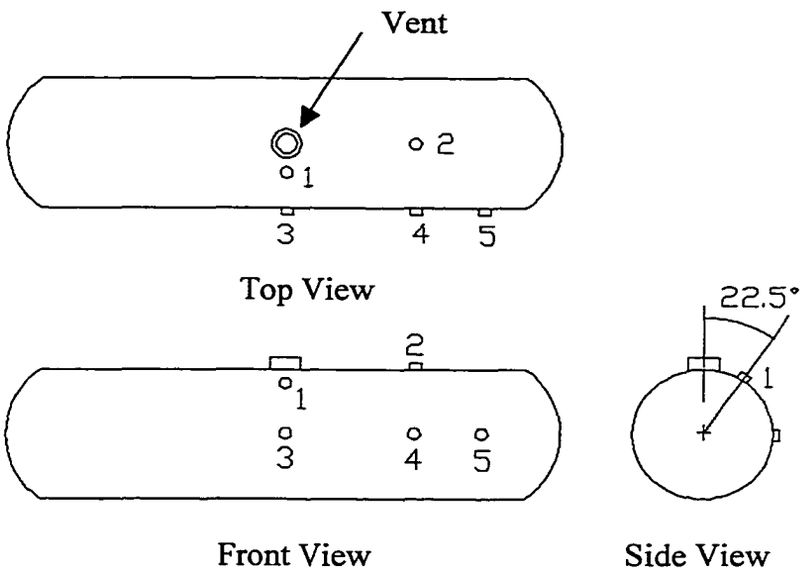

Figure 37. Pressure Transducer Locations Used to Measure the Decompression Time of the Compressed Air Tank

The results indicate that the average tank decompression times were not significantly affected by the placement of the pressure transducer (Table 10). It is noted from the data, however, that the consistency in measured decompression times varied depending on transducer sensor. Decompression time measurements were the

Table 10

Mean Decompression Times for Compressed Air Tank
With Varying Pressure Transducer Locations

Pressure Transducer Location	Mean Tank Decompression Time (SD)
1	0.7365 sec. (0.0203)
3	0.7355 sec. (0.00599)
5	0.7425 sec. (0.00791)

least consistent (larger standard deviation) for the sensor location closest to the vent opening (location 1). This inconsistency is thought to be due to flow instabilities in the proximity of the vent opening. For this reason, it was decided not to use pressure transducer location 1. Instead pressure transducer location 3, located at a 90-degree angle from the vent opening, was selected for measurements in the remainder of this study (Figure 37).

Effect of Vent Opening Size – Compressed Air Tank

Four different size vent openings were used with the hinged panel on the compressed air tank to measure decompression times (Figure 33). The mean decompression times of 10 trials and standard deviations are given in Table 11. The average decompression time for each vent opening size was plotted against the calculated V/A ratio, where V is the volume of the compressed air tank, and A is the area of the vent opening. These experimental results were plotted (Figure 38) against the predicted decompression times for the compressed air tank using the Haber and Clamman (1953) method as described below: (Equation 5.2)

Table 11

Mean Decompression Times for Compressed Air Tank
With Vent Openings of Various Sizes

Vent Opening Diameter	Vent Opening Area	Volume to Area Ratio (V/A)	Mean Tank Decompression Time (SD)
1.905 cm	2.85 cm^2	1109.8 m	3.46 sec. (0.108)
2.54 cm	5.07 cm^2	623.9 m	2.04 sec. (0.048)
3.73 cm	10.93 cm^2	289.4 m	0.736 sec. (0.00599)
4.76 cm	17.80 cm^2	177.7 m	0.486 sec. (0.0161)

$$T_d = \frac{(V \cdot P_1)}{(A \cdot c)} = \frac{(V) \cdot (1.01)}{(A) \cdot (340.3\ m/s)} \tag{5.2}$$

Which reduces to:

$$T_d = \frac{(V)}{(A)} \cdot (0.00297) \cdot m^{-1} \cdot s \tag{5.3}$$

Where: T_d = Total time of decompression of compressed air tank (s)
V = Volume of the compressed air tank (m^3)
A = Area of vent opening in compressed air tank (m^2)
P_1 = 1.01 (From Haber and Clamman for a tank pressurization of 51.7 KPa gage in standard ambient atmosphere)
c = Speed of sound in air in standard atmosphere (m/s)

Effect of Vent Opening Size – PVC Pipe Vessel

A second pressure vessel used in scale-model testing was constructed from a section of PVC pipe. The PVC pipe vessel had an inside diameter of 0.203 meters (8 inches) and a nominal length of 1.63 meters (64 inches). Plastic pipe end caps were

compressed onto the PVC pipe using four 12.7 millimeter (½-inch) diameter threaded rods and 1.27 cm (0.5 inch) thick aluminum end plates (Figure 39).

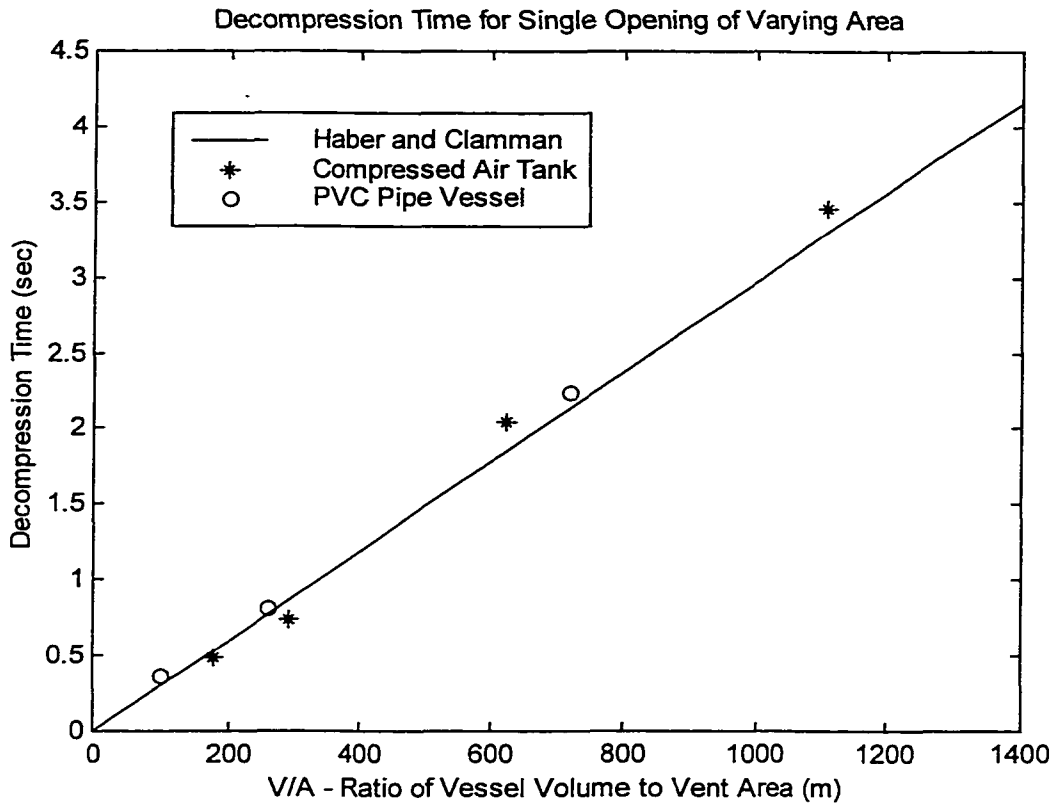

Figure 38. Plot of Measured Decompression Times of Two Pressure Vessels with Varying Vent Opening Areas. The solid line indicates the predicted results from the Haber and Clamman method.

The pipe was assembled in this fashion in order to allow the pipe to be opened as would not be possible if the end caps were secured with permanent PVC cement. In order to create a pressure tight seal, a compressible rubber O-Ring was placed between the cut ends of the PVC pipe and an internal flange in the end caps. In order to test the decompression times of the PVC pipe vessel, the Sensym pressure transducer was screwed into a drilled and tapped hole in the PVC wall at the mid-

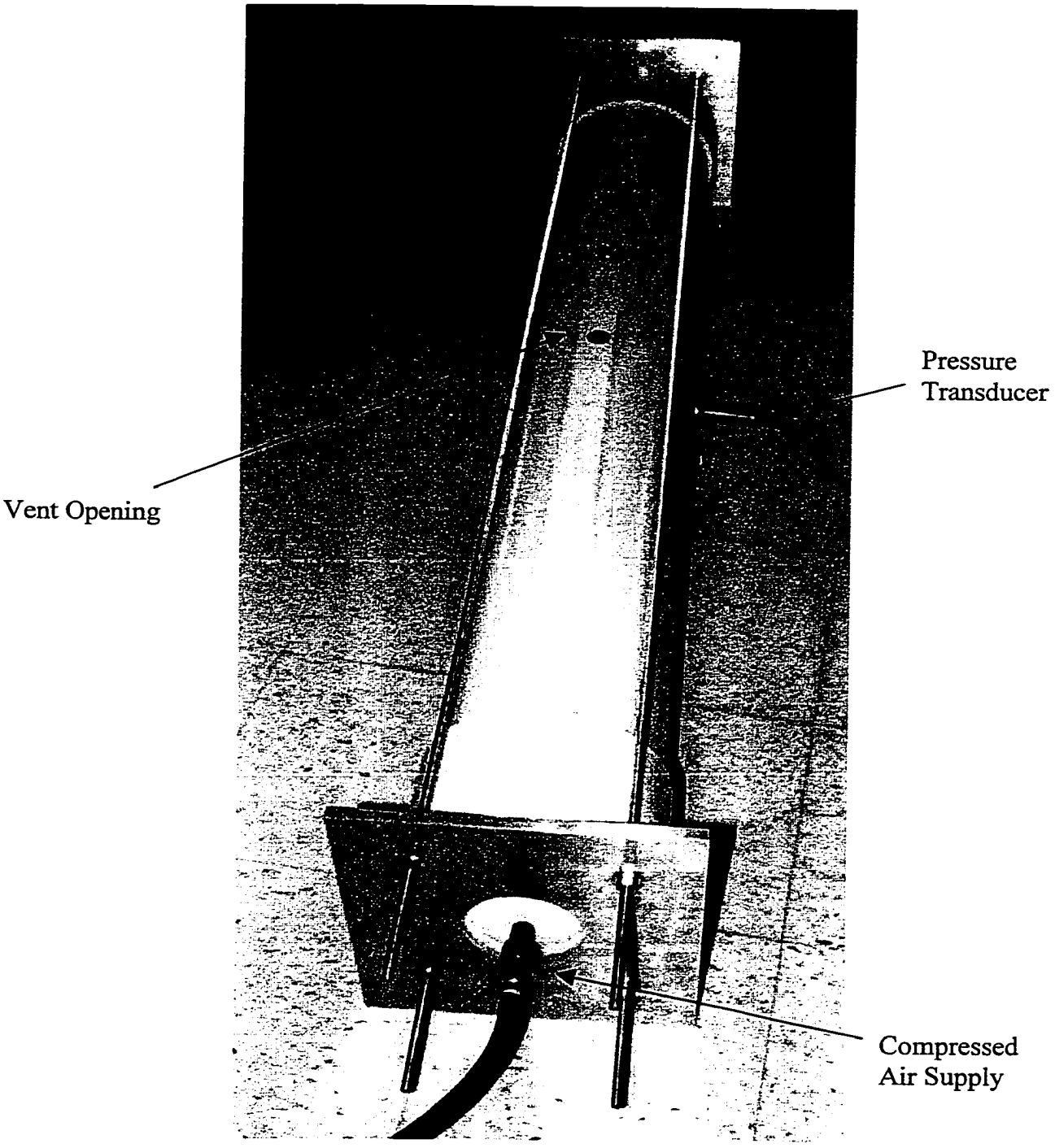

Figure 39. Photo Showing the PVC Pipe Vessel.

length of the pipe. One pipe end cap was also fitted with a quick-disconnect type compressed air fitting for connection to a compressed air supply.

In order to measure the decompression time for various size vent openings, a small hole (0.953 cm diameter) was drilled in the PVC pipe wall at its mid-length. This hole was located at a 90-degree angle to the pressure transducer location. A rubber stopper was pushed into the hole and the PVC pipe vessel was pressurized to 51.7 Kpa gage pressure (7.5 psig). The rubber stopper was then pulled from the hole with a string to create a rapid opening in the PVC pipe vessel. The corresponding transient pressure decay in the PVC pipe vessel was recorded with an oscilloscope in the same manner as described for the compressed air tank. After the data for a series if 10 trials were recorded, the vent hole was drilled into a slightly larger hole and the process was repeated. The average decompression time for three hole sizes is recorded in Table 12.

The decompression results of both the compressed air tank and PVC pipe vessel are plotted along with the Haber and Clamman prediction in Figure 38, showing excellent correlation.

Effect of Vent Opening Distribution on a Single Side of a PVC Pipe Vessel

Another scale model decompression test was conducted to determine the effect of distributing multiple vent openings along the longitudinal axis of a cylindrical pressure vessel. To accomplish this test, a series of 0.437 cm diameter holes were drilled at intervals of 3.5 centimeters (1.38 inches) along one side of the PVC pipe vessel (Figure 40). The hole size was selected to create a ratio of vessel

Table 12

Mean Decompression Times for PVC Pipe Vessel
With Vent Openings of Various Sizes

Vent Opening Diameter	Vent Opening Area	Volume to Area Ratio (V/A)	Mean Tank Decompression Time (SD)
0.953 cm	0.713 cm^2	716.7 m	2.25 sec. (0.056)
1.59 cm	1.99 cm^2	257.3 m	0.816 sec. (0.0213)
2.54 cm	5.07 cm^2	100.8 m	0.372 sec. (0.0135)

volume to vent area similar to the volume of the passenger cabin of a commercial aircraft divided by the area of an aircraft window. The hole spacing was scaled to the diameter of the vessel to simulate the spacing of windows along a commercial aircraft fuselage. The holes were covered with a long channel of aluminum covered with a rubber gasket. The channel was manually forced against the holes in the PVC pipe in order to create a pressure seal and the vessel was again pressurized to 51.7 Kpa gage pressure (7.5 psig). The aluminum channel was then manually pulled away from the tank and the resulting pressure decay was recorded using the previously described method. This test was repeated for a varying number of 0.437 cm diameter vent holes. The mean decompression times for 10 trials are given in Table 13.

Effect of Vent Opening Distribution on Two Opposing Sides of a PVC Pipe Vessel

One final scale model test was conducted to determine the effect of vent openings on opposing sides of a cylindrical vessel. For this test, the previously

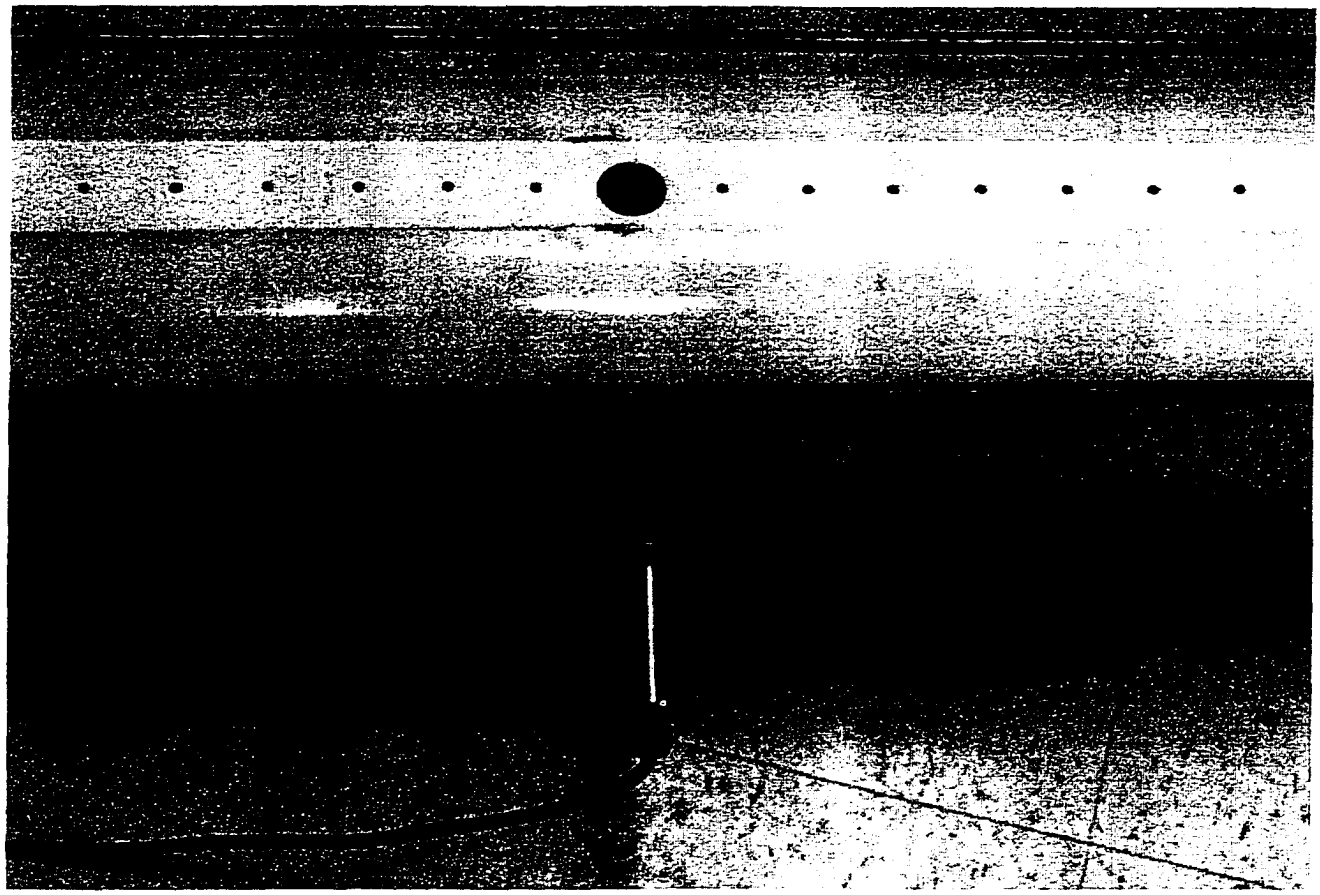

Figure 40. Photo Showing the PVC Pipe Vessel With 13 Vent Holes Along One Side of the Pipe. (The Black Circle in Center is a Solid Plug Used to Seal a Prior Opening).

Table 13

Mean Decompression Times for PVC Pipe Vessel With Varying Numbers of Vent Openings on a Single Side

Number of Vent Openings	Diameter of Each Vent Opening	Total Area of All Vent Opening	Volume to Area Ratio (V/A)	Mean Tank Decompression Time (SD)
1	0.437 cm	0.15 cm^2	3406.7 m	12.1 sec. (0.282)
5	0.437 cm	0.75 cm^2	681.3 m	2.09 sec. (0.0623)
13	0.437 cm	1.95 cm^2	262.1 m	0.766 sec. (0.0266)

described PVC pipe configuration was used with a new center pipe section. A series of decompression times were initially measured for a pair of small holes (0.437 cm diameter each) drilled on opposing sides of the pipe. Additional tests were conducted for two pairs and four pairs of holes. Two pieces of aluminum channel, fitted with a resilient gasket material, were manually forced against the pipe on opposite sides to seal the vent openings. The PVC pipe vessel was pressurized to 51.7 KPa gage pressure (7.5 psig) and the aluminum channel sealing members were then manually pulled away from the vent openings. The resulting decompression time was recorded and the mean times of 10 experimental trials are recorded in Table 14.

Table 14

Mean Decompression Times for PVC Pipe Vessel With Varying Numbers of Vent Openings on Opposite Sides

Number of Vent Openings	Number of Vent Openings Per Side	Total Area of All Vent Opening	Volume to Area Ratio (V/A)	Mean Tank Decompression Time (SD)
2	1	0.30 cm^2	1703.3 m	5.84 sec. (0.454)
4	2	0.60 cm^2	851.7 m	2.62 sec. (0.087)
8	4	1.20 cm^2	425.8 m	1.26 sec. (0.043)

The measured decompression times for the PVC pipe vessel with multiple distributed vent openings are shown in Figure 41. A summary of all decompression time results is also included in Figure 41.

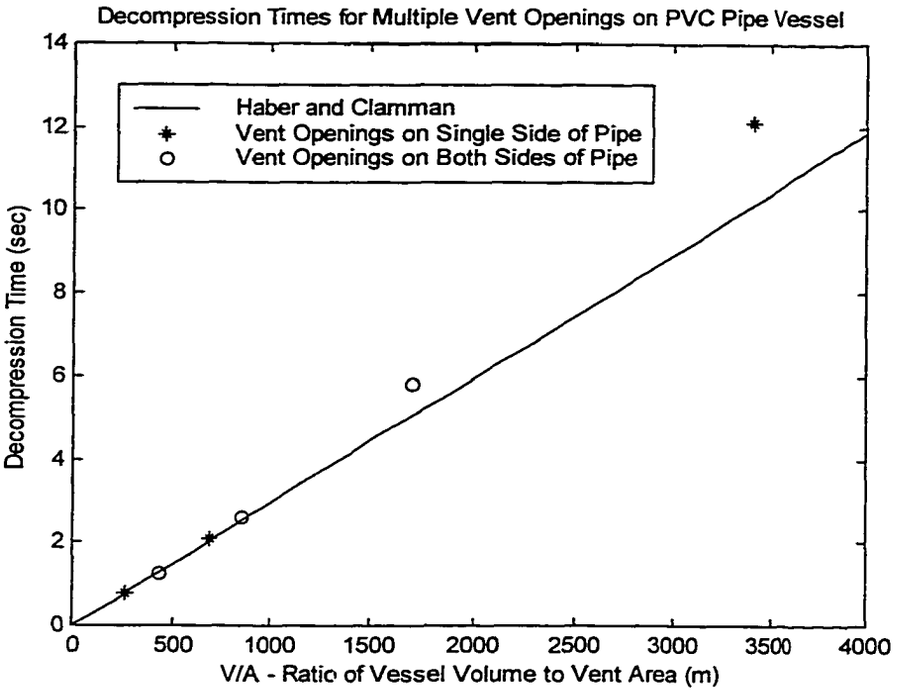

a)

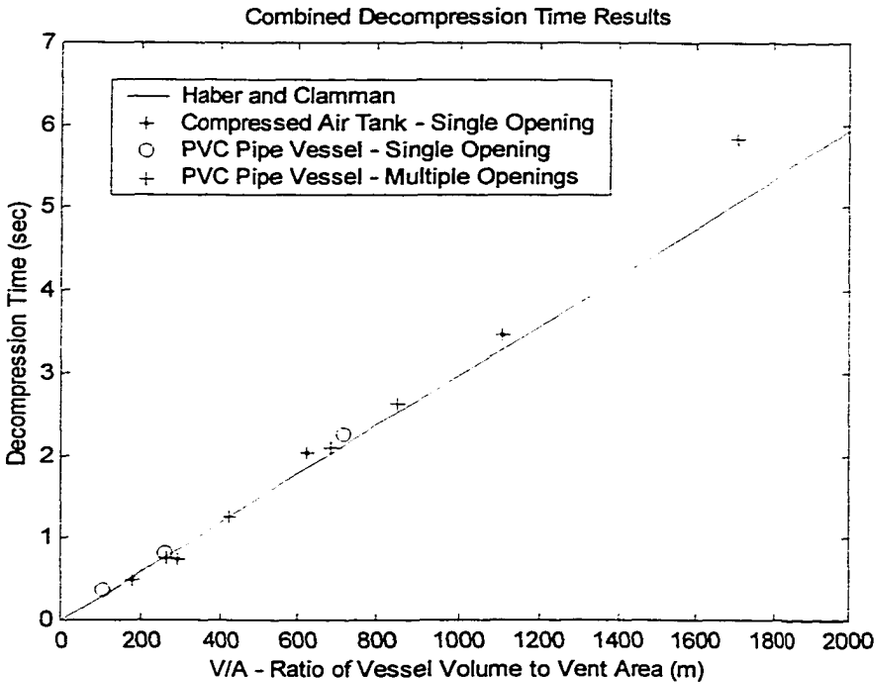

b)

Figure 41. Plot of Measured Decompression Times of the PVC Pipe Vessel with Multiple Distributed Vent Openings and Summary Plot Including All Decompression Time Results.

Selection of Aircraft for Prediction of Decompression Time

In order to extend the prior methods of predicting pressure vessel decompression times to an actual commercial aircraft fuselage, a specific model of aircraft will be chosen. For this analysis an aircraft from the Boeing 737 family would be selected due to the widespread usage of the aircraft in commercial fleets around the world. The 737 is also a good choice for an active venting system since the aircraft does not typically employ luggage containers for baggage handling and are thus not amenable to explosion protection from hardened luggage containers.

Background on the Boeing 737 Family of Aircraft

The Boeing 737 family of aircraft has been termed the most popular jetliner in the world (Anon., 2000). The first member of the Boeing 737 family, the 737-100 first entered commercial service in February 1968 and was followed quickly by the slightly longer 737-200 in April 1968. The initial 737-200 aircraft was replaced by the Advanced 737-200 which entered service in 1971. The 737-200 proved to be a highly versatile and dependable aircraft and was a popular choice of commercial carriers in the 1970s and 1980s. The first successor to the 737-200 was the 737-300 which first came into service in 1984. The 737-300 allowed increased passenger seating due to an increased fuselage length. In 1986, Boeing introduced a further extended fuselage aircraft, the 737-400. In 1990, Boeing placed a new aircraft, the 737-500 into service. The 737-500 featured a smaller fuselage on the order of the

popular 737-200 aircraft, but which utilized the latest technologies found on the 737-300 and 737-400.

In 1993, Boeing began work on the next generation of aircraft in the 737 family. These new planes, the 737-600, -700, -800, and –900 are intended to fly higher, faster, and farther than the predecessor 737 aircraft. Although these aircraft bring the total of members of the 737 family to nine, all of these planes utilize a similar fuselage radius and similar structural details including window size and spacing. For this reason, a typical mid-length aircraft (Table 15), the Boeing 737-700, has been chosen for decompression analysis (Anon., 2000).

Table 15

Summary Data on Boeing 737 Family of Aircraft
(Anon., 2000)

Aircraft	Aircraft Length	Maximum Number of Passengers	Entered Commercial Service
737-100	28.7 m (94.0 ft)	99	1968
737-200	30.53 m (100 ft)	124	1968
737-300	33.4 m (109.6 ft)	149	1984
737-400	36.4 m (119.6 ft)	168	1988
737-500	31.0 m (107.8 ft)	132	1990
737-600	31.2 m (102.5 ft)	132	1998
*737-700	33.6 m (110.3 ft)	149	1997
737-800	39.5 m (129.5 ft)	189	1998
737-900	42.1 m (138.2 ft)	189	2001

*Note: The 737-700 has been chosen for venting analysis in this study.

Prediction of Decompression Times for Boeing 737-700

Using the method of Haber and Clamman (1953) one can predict the decompression time of a Boeing 737-700 fuselage for a variety of venting scenarios.

It should be noted that the method of Haber and Clamman will provide only an approximation of the decompression time of an actual aircraft fuselage in the lack of actual measured data. The proposed method relies on certain assumptions including zero impediment to air flow inside the cabin (such as due to seats, passengers, and overhead bins), disregarding temperature changes in the gaseous air during the process, ignoring the correction factor for the pattern of airflow through the panel (sometimes called the flow coefficient) and other factors. With these limitations in mind, the Haber and Clamman method can be used to gain a general understanding of the decompression behavior of portions of an aircraft fuselage.

The Boeing 737-700 is composed of two primary major pressurized spaces, the passenger cabin and the cargo area, separated by the cabin floor. Since a sudden decompression in either of these spaces could create a significant pressure differential on the cabin floor, a series of air vents maintain an equilibrium of pressure between the passenger cabin and cargo area. These side wall vents are located beneath the windows of commercial aircraft in the passenger cabin and are distributed along the length of the fuselage (Niu, 1988). Estimating the cross sectional area of each of these vents to be 0.020 square meters, and considering the approximately 68 side wall vents on a Boeing 737-700, the total vent area between passenger cabin and cargo hold is estimated to be 1.36 square meters.

The volume of air in the passenger cabin of a Boeing 737-700 can be estimated through the use of scale drawings of key aircraft dimensions. Assuming the cross-sectional area of the 737-700 passenger cabin to be 5.68 square meters and using a nominal fuselage length of 24.5 meters, the total passenger cabin volume is

estimated to be 139 cubic meters. Subtracting the interior volume occupied by the aircraft seats, estimated at 11 m^3, and further subtracting the volume occupied by the overhead storage bins, estimated at 6 m^3, the internal cabin volume of a Boeing 737-700 is approximately 122 m^3. The volume of air in the cargo hold (59.3 meters) is found by multiplying the cross sectional area of the cargo hold (3.26 square meters) by the nominal fuselage length (18.2 meters) (Niu, 1988; Anon. 2000). Assuming that one half of the total cargo hold volume would be typically filled with luggage, the air volume in the hold will be assumed to be 29.7 cubic meters.

In addition to determining the appropriate volumes of air inside the aircraft, the pressure function, P_1, of Equation 22 must also be determined for a variety of altitudes. Interpolating data from Haber and Clamman yields a non-linear relationship between the pressure function, P_1, and the differential pressure ratio (Figure 42). The resulting pressure function values, P_1, for a variety of flight altitudes of a Boeing 737 are given in Table 16.

Example of Predicting Decompression Times for Boeing 737-700

In order to determine the estimated decompression time for a 737-700 at a given flight altitude, the vent passages between the passenger cabin and cargo hold must be considered. Given the large surface area (1.36 square meters) of the vent passages involved, it is likely that any attempt to induce a rapid venting of cabin pressurization in the event of an on-board explosion must include the entire air volume inside the aircraft. To illustrate this point, consider the time needed to vent

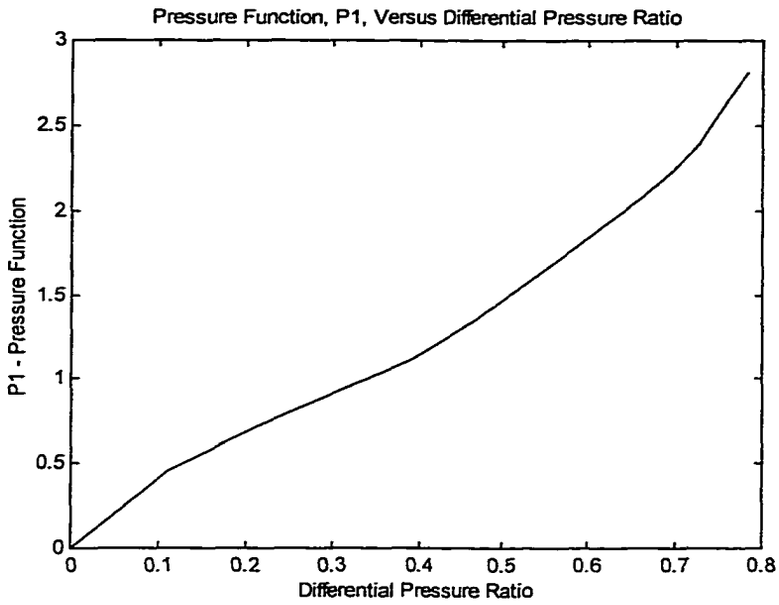

Figure 42. Plot of Pressure Function Versus Differential Pressure Ratio. (Haber and Clamman, 1953).

Table 16

Pressure Functions for Various Flight Altitudes of a Boeing 737 Aircraft (Thompson, 1972)

Height Above Sea Level (m)	P_{AO} - Ambient Pressure (KPa)	P_{CO} – Absolute Cabin Pressure (KPa)	Differential Pressure Ratio $(P_{CO} - P_{AO})/(P_{CO})$	P_I - Pressure Function*
0	101.3	101.3	0	0
1,000	89.9	101.3	0.110	0.46
2,000	79.5	101.3	0.215	0.72
3,000	70.1	101.3	0.308	0.93
4,000	61.7	101.3	0.391	1.12
5,000	54.0	101.3	0.467	1.35
6,000	47.2	98.9	0.523	1.55
7,000	41.1	92.8	0.557	1.67
8,000	35.7	87.4	0.592	1.80
9,000	30.8	82.5	0.627	1.94
10,000	26.5	78.2	0.661	2.08
11,000	22.7	74.4	0.695	2.23
12,000	19.4	71.1	0.727	2.38
13,000	16.6	68.3	0.757	2.63
14,000	14.2	65.9	0.784	2.81

*Note: Pressure Function Data Approximated From Haber and Clamman Plot (1953).

the air in the cargo hold into the passenger cabin through the side wall vents. If we examine the possibility of a Boeing 737-700 flying at 10,000 meters and suffering a rapid decompression in the passenger cabin. Assuming for a moment that this decompression is extremely fast, a pressure differential of 51.7 KPa would develop between the passenger cabin and cargo hold.

Using Equation 22, the time (T_d) required for the 29.7 cubic meters of air in the cargo hold to pass through the sidewall vents (with a total cross section area of 1.36 square meters) into the passenger cabin can be determined.

$$T_d = \frac{(V \cdot P_I)}{(A \cdot c)} = \frac{(122\,m^3)\cdot(2.08)}{(1.36m^2)\cdot(340.3\,m/s)} = 0.13 seconds \tag{5.4}$$

Thus, it appears that in the event of a decompression of the passenger cabin, the cargo area will vent rather quickly (0.13 seconds) through the side wall vents. For this reason, in this analysis it will be assumed that any attempt to vent a portion of the aircraft fuselage must include all of the air volume (168.7 cubic meters) inside the fuselage.

The next consideration in determining the decompression time of a pressurized Boeing 737-700 flying at a given altitude is the surface area of the vent opening which opens to the ambient atmosphere. Again, using Equation 22, the decompression time (T_d) for the case of a 737-700 flying at an altitude of 10,000 meters can be determined as follows:

$$T_d = \frac{(V \cdot P_1)}{(A \cdot c)} = \frac{(168.7\ m^3) \cdot (2.08)}{(A) \cdot (340.3\ m/s)} \tag{5.5}$$

Which reduces to:

$$T_d = \frac{(1.03)}{(A)} m^{-1} \cdot s \tag{5.6}$$

This procedure can be repeated for decompressions at other altitudes. A plot of the estimated decompression time for the passenger cabin of a Boeing 737-700 flying at selected altitudes versus vent opening area is given in Figure 43(a). If one were to consider an active venting system which simultaneously releases multiple aircraft windows, it is important to relate decompression time to the number of windows used as vents. Considering the area of a single passenger window of a 737 aircraft is 0.0903 square meters (McFadden, 1979), the predicted decompression times for a 737-700 flying at various altitudes are plotted as a function of the number of aircraft windows used as vent openings (Figure 43(b)).

Conclusions

An active venting system requires the rapid initiation of pressure release from an aircraft fuselage. In order to reduce the structural loading on the aircraft to a minimum, this venting should occur as fast as possible. In order to avoid the physiological problems associated with an extremely fast pressure drop, known as explosive decompression, care must be taken to limit the decompression rate of the passenger cabin. The design of an active venting system must therefore provide the

fastest possible pressure release of an aircraft fuselage which will not by itself cause serious injuries to the passengers on-board the aircraft. As mentioned previously, it has been stated that decompressions which occur slower than 0.5 seconds will not cause serious lung damage to humans (De Remer, 1992).

The scale-model testing using two different pressure vessels was quite successful in validating the decompression time model of Haber and Clamman (1953). It was also determined that their model was valid for predicting decompression times for a single vent opening or for a series of vent openings distributed along a cylindrical pressure vessel. This finding allows confidence in using the Haber and Clamman model to estimate the decompression time of an actual aircraft fuselage with various vent openings.

The Haber and Clamman model was subsequently applied to the passenger cabin of a Boeing 737-700 which undergoes decompression at various flight altitudes. With this method it was estimated that a total vent surface area of 1.1 to 2.3 square meters would be sufficient to completely vent the pressurized cabin in 0.5 seconds for flight altitudes from 4,000 to 12,000 meters. For a Boeing 737-700, this corresponds to the area of approximately 12 to 26 out of 68 total windows. As a point of reference, if all 68 windows (surface area of 6.14 square meters) on the Boeing 737-700 were used as vents, the predicted decompression time of the fuselage would be in the range of 0.09 to 0.19 seconds for the altitudes of 4,000 to 12,000 meters.

With such a small area (1.1 to 2.3 square meters) of vent openings required to achieve the fastest decompression time allowed by human factors, the use of aircraft

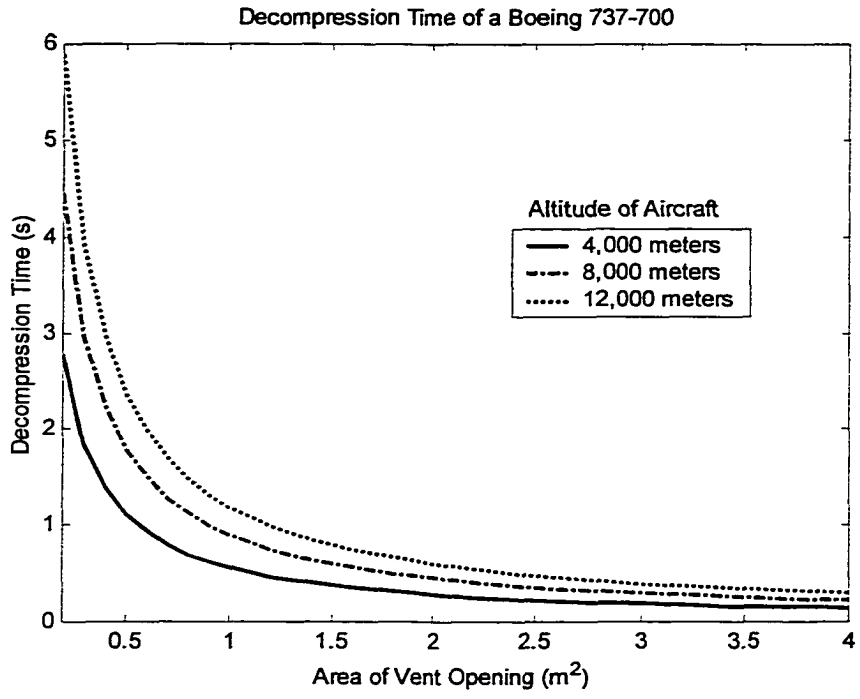

a)

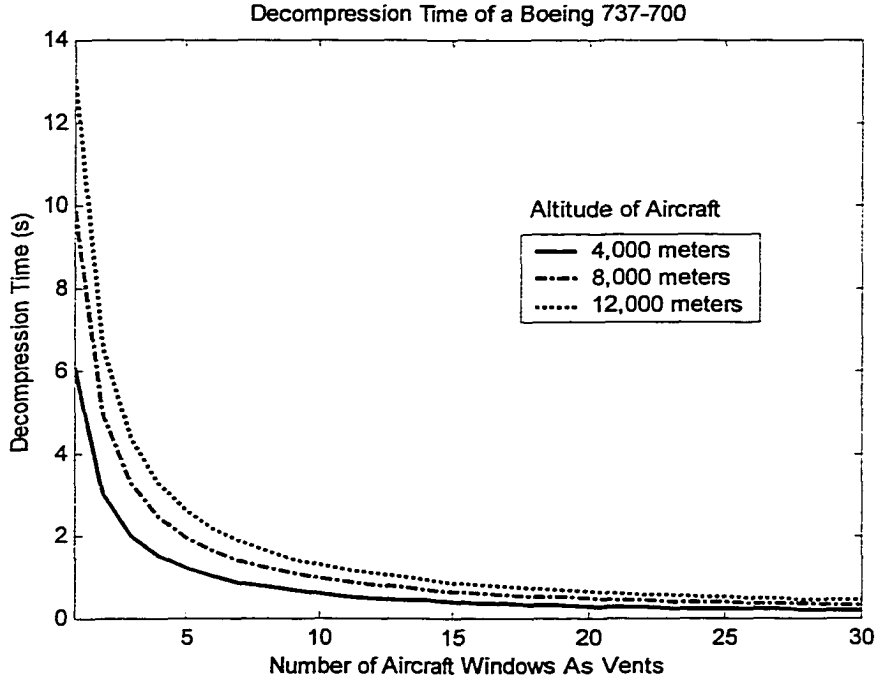

b)

Figure 43. Estimated Decompression Times of the Passenger Cabin of a Boeing 737-700 Aircraft as a Function of Vent Area.

windows as vents becomes advantageous for several reasons. First, aircraft windows are present on most all commercial aircraft. Windows represent existing openings in the fuselage structure and are surrounded by reinforcing members. As such, aircraft windows are not designed to be load-bearing structural members of the aircraft (with the exception of the cabin pressurization loading). For this reason, the in-flight loss of aircraft windows does not introduce a significant weakening of the fuselage structure. Another advantage of using fractured aircraft windows as vent openings is that only a small pyrotechnic actuator is needed to shatter the glass panes and initiate a rapid vent opening. A small pyrotechnic actuator could be used in one location on the periphery of the glass panel. This would require very little added weight to the aircraft and would also require only a small section of pressure shielding around the pyrotechnic actuator to prevent actuation pressures from entering the passenger cabin. One final advantage of using fractured glass panels as vents is that the small fragments of glass pose much less of a threat to re-impacting other parts of the aircraft such as engines, wings, and control surfaces than for a reinforced aluminum panel member.

For the actual selection of window locations for use as active vents, it would probably be wise to choose windows in pairs on opposite sides of the aircraft (6 to 13 windows per side). This will ensure that the lateral thrust caused by the escaping cabin air pressure will be generally balanced by a thrust in the opposing direction. Most likely the vent windows would be distributed along the entire length of the aircraft. Since the danger of passenger ejection from or sealing against fractured window openings exists, it might be possible to select some vent windows not directly adjacent to passenger seating areas. It may also be possible to select

windows located between rows of passenger seats such that the seat back adjacent to the window would serve to prevent passenger expulsion.

CHAPTER VI

STRUCTURAL RESPONSE AND VENTING EFFECTIVENESS

Background on Modeling of Fuselage Blast Response

The task of predicting the structural response of an aircraft fuselage to an internal explosive detonation is extremely formidable. The uncertainties of the interaction between explosive pressures and complex fuselage geometry, coupled with the erratic propagation of damage through the structure render attempts at predictive modeling nearly impossible.

Although the prospects are daunting, several attempts at modeling the simplified response of a fuselage structure have been made. These efforts can generally be classified in three ways: 1) Computational Fluid Dynamics (CFD) of dynamic explosive pressures, 2) structural response and/or fracture mechanics of initial blast damage, and 3) coupled fluid/structure interaction of the damage initiation and damage propagation processes. A brief review of these prior modeling efforts follows.

There have been several attempts to use CFD to predict the transient pressures generated by an explosive detonation inside a confined fuselage structure (e.g. Chan, 1992; Strang, 1992). The CFD approach treats the fuselage as a sealed vessel to

calculate the transient pressures as an explosive shock wave propagates through the aircraft, makes contact with its structure, and reflects from it. The results of CFD analysis are useful to gain an understanding of the initial loading pressures on the structure in the early time range before structural damage occurs.

The second research approach uses dynamic finite element analysis to predict the incipient local failure of the aircraft structure in the vicinity of the explosion (Kanninen, Marchand, and O'Donoghue, 1992; Moyer, McNaight, and Miller, 1992; Gefken, Simons, and Sanai 1993). These previous efforts have utilized models of small portions of the fuselage in order to predict damage patterns caused by explosives of varying size and at various distances from the structure. In general, this approach does not consider the behavior of the fuselage in the subsequent time interval after damage initiation has occurred. The dynamic finite element models of localized damage also do not adequately account for the transient pressure loading of the structure as the internal pressures vent from the fuselage through damage sites.

A third, and rather complex, analysis method that has been used to model fuselage blast response combines CFD capability with a structural response code (Chen, 1997; Kamoulakos, Chen, Mestreau, Lohner, 1996; Moon, 1995, 1996). This approach simultaneously uses a fluids finite element code and a structural finite element code in an iterative process to model the explosive pressure propagation and impact with the fuselage, the subsequent structural damage initiation and propagation,

and the venting of pressures through the resulting damage sites. This complicated analysis method is extremely computationally intensive.

Analysis Method for Determining Venting Effectiveness

For the purposes of this study, the dynamic finite element method was used to gain an understanding of the time-response of a typical commercial aircraft fuselage to an internal explosion. The results of this analysis were used as a general means of predicting fuselage damage under various load cases.

The analysis approach employed in this study used the previously determined time sequence of explosive events (Chapters 1 through 5) to compare the structural response of a fuselage under several loading conditions. Specifically, a finite element model of a portion of a commercial aircraft structure was used with five applied load cases: 1) Explosive loading on unpressurized fuselage (baseline damage case), 2) explosive loading on a pressurized structure without pressure venting, 3) explosive loading on a pressurized structure with pressure venting initiated at 7.3 milliseconds after blast detonation, 4) explosive loading on a pressurized structure with pressure venting initiated at instant of blast contact with structure (1.6 milliseconds after blast detonation), and 5) explosive loading on a pressurized structure with pressure venting with blast loading of structure delayed by 50 milliseconds after venting initiation. In order to reduce the model complexity, only the detonation of an explosive device located at the center of the fuselage radius was considered for this study. It was also

assumed that, in a worst case scenario, the nearest pressure sensor was located at a maximum possible distance of 1.5 meters away from the initial position of the explosive. With these simplifying assumptions, a simultaneous consideration of the time sequences of both the explosive shock wave propagation and the active venting system deployment (Table 17) can be established (Figure 44).

Table 17

Summary of Time Durations of Active Venting Process Events

Event	Conservatively Estimated Time Duration	Fastest Possible Estimated Time Duration
Explosive Propagation to contact sensor (0-1.5 meter travel)	1.3 milliseconds	0.0 milliseconds
Electronic Signal Processing	1.0 milliseconds	0.1 milliseconds
Actuation and Response of Panel to Create Unobstructed Vent Opening	5.0 milliseconds	1.5 milliseconds
Total Elapsed Time From Instant of Detonation to Vent Initiation	**7.3 milliseconds**	**1.6 milliseconds**

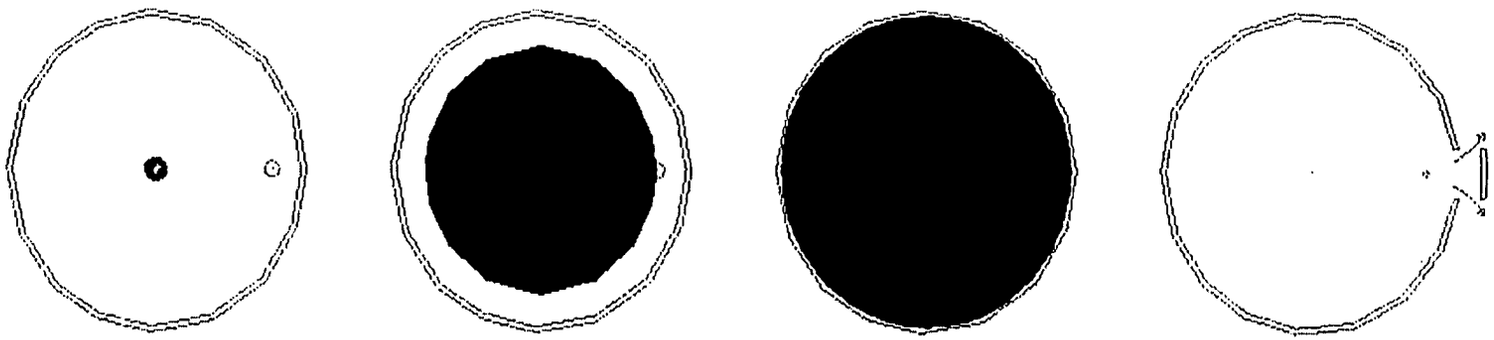

Time = 0.0 milliseconds	Time = 1.3 milliseconds	Time = 1.6 milliseconds	Time = 7.3 milliseconds
Explosive Detonation	Pressure Wave Contacts Sensor (1.5 meters away)	Pressure Wave Contacts Structure (1.88 meters away)	Unobstructed Vent Opening Established – Venting Begins

Figure 44. Assumed Time Sequence of Events for Explosive Detonation at Center of Fuselage (Radius = 1.88 meters) for Conservative Time Estimates.

Under the simplified blast scenario used for this study, the transient differential pressures experienced by the structure for all five loading cases (cases A, B, C, D, and E) under consideration can be specified (Figure 45). Specific details of the three load cases have been summarized in Table 18.

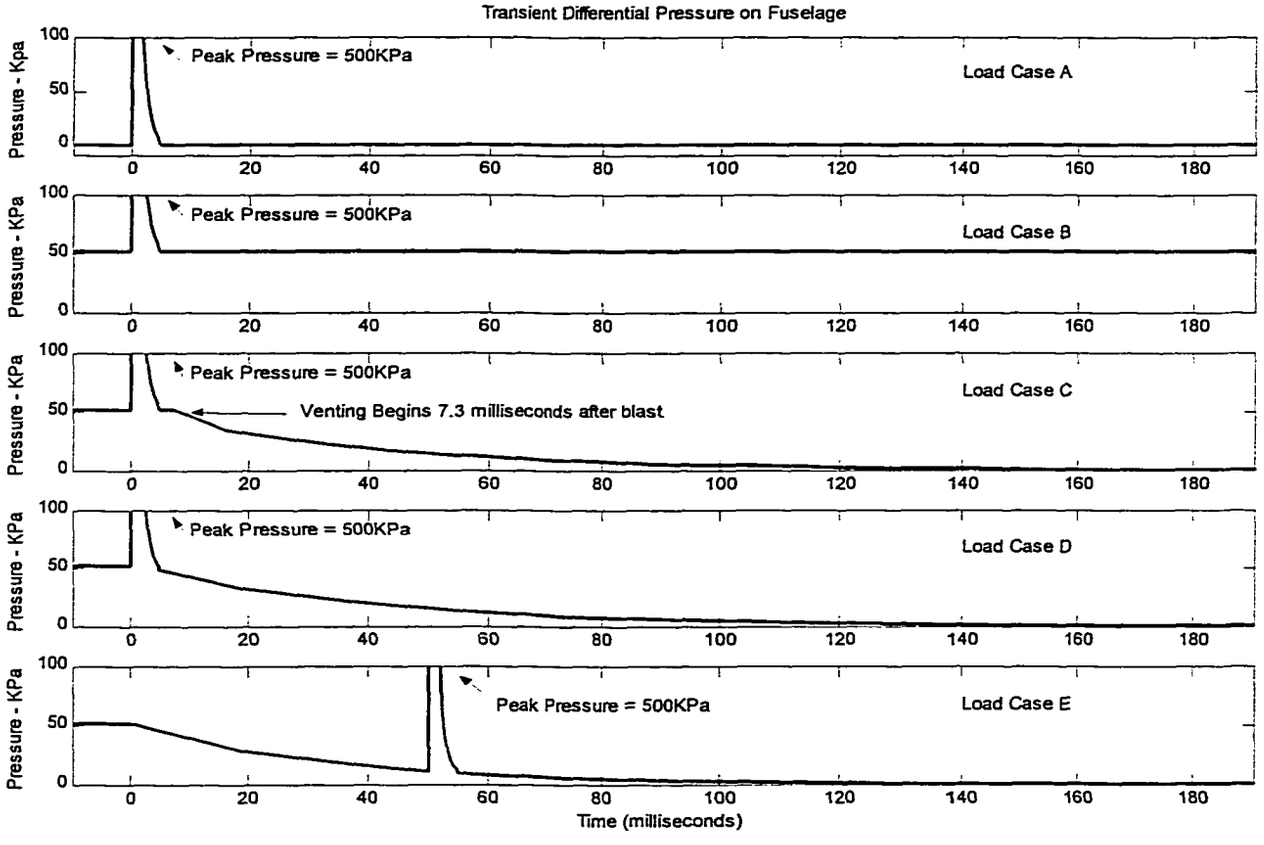

Figure 45. Graphical Representations of the Five Transient Pressure Load Cases Which Will be Applied to the Fuselage Model.

Table 18

Summary of Pressure Data Used for the Five Load Cases

Load Case	Description	Comments
A	Pressure Pulse on Unpressurized Fuselage	Cabin Differential Pressurization Set to Zero for Entire Analysis
B	Pressure Pulse on Pressurized Fuselage Without Venting	Cabin Differential Pressurization Remains Constant at 51.7 KPa for Entire Analysis
C	Pressure Pulse on Pressurized Fuselage With Venting	Cabin Differential Pressurization Initially at 51.7 KPa, Then Follows Exponential Decay Starting at 7.3 Milliseconds After Detonation
D	Pressure Pulse on Pressurized Fuselage With Venting	Cabin Differential Pressurization Initially at 51.7 KPa, then Follows Exponential Decay Starting at Instant of Blast Contact With Fuselage (1.6 Milliseconds After Detonation)
E	Pressure Pulse on Pressurized Fuselage With Venting	Cabin Differential Pressurization Initially at 51.7 KPa. Blast Loading of Structure Delayed by 50 Milliseconds After Venting Initiation.

Finite Element Model of a Commercial Aircraft Fuselage

Geometry, Materials, Elements and Boundary Conditions

In order to determine the structural response of the aircraft structure under the three established loading conditions, a finite element model of an aircraft structure was constructed. Owing to the difficulty in obtaining design data for the Boeing 737-

700 aircraft, it was decided to use the dimensions, materials, and construction of a generally similar structure, the Boeing 707-300 aircraft. For this purpose, the prior work of Moon, Bharatram, Schimmels, and Venkayya (1995; 1996) provided valuable design information on the Boeing 707-300 aircraft structure obtained from the tear-down and measurement of an actual fuselage and from a four-volume stress report originally published by Boeing Aircraft Corporation (Anon, 1958).

The Boeing 707-300 aircraft is a basic monocoque construction consisting of an outer aluminum skin supported by longitudinal stringers and circumferential frame members. A typical cross-section of a Boeing 707-300 is shown in Figure 46. For the present analysis, a portion of the fuselage in the passenger cabin was modeled. The selected structure ranges from the floor of the passenger cabin to the top center-line of the aircraft (approximately 3.6 meters in the circumferential direction). The longitudinal section of the modeled structure spans a distance of 4.6 meters (Figure 47). The selected portion of the aircraft fuselage was modeled using the finite element package ANSYS (Release 5.4) available from ANSYS Inc. of Canonsburg, PA.. The structure was modeled to include the outer aluminum skin, reinforcing stringers and frames, window panels and window support frame members. The specific details of each of these elements are discussed next.

Fuselage Skin

The aircraft skin was modeled using 4-node, quadrilateral shell elements

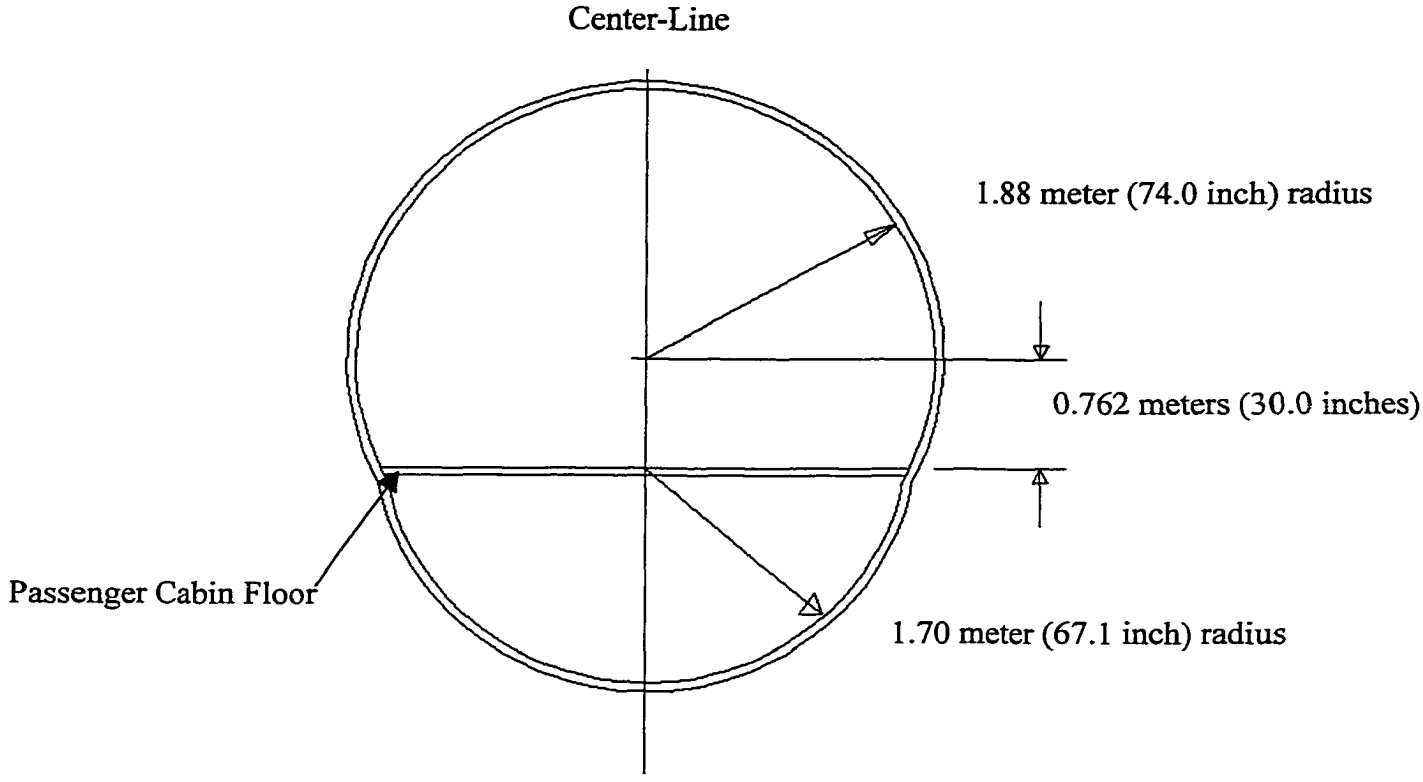

Figure 46. Typical Cross-Section of a Boeing 707-300. (Moon, Bharatram, Schimmels, and Venkayya,1995; 1996).

(ANSYS elements SHELL63 for elastic analysis and SHELL43 and SHELL181 for plastic large strain analysis). (Note: SHELL181 was used for the pressurized fuselage load case (B) since it accounts for changes in element thickness due to large changes in element geometry caused by plasticity (ANSYS, 1997)). The skin material was modeled as 2024-T3 aluminum with a thickness of 1.63 millimeters (0.064 inches). The material properties used to model the aluminum 2024-T3 skin, are given in Table 19.

For simplicity, details such as lap joints between adjacent skin panels and rivet joints were omitted from the model. An increased skin thickness (4.88 millimeters)

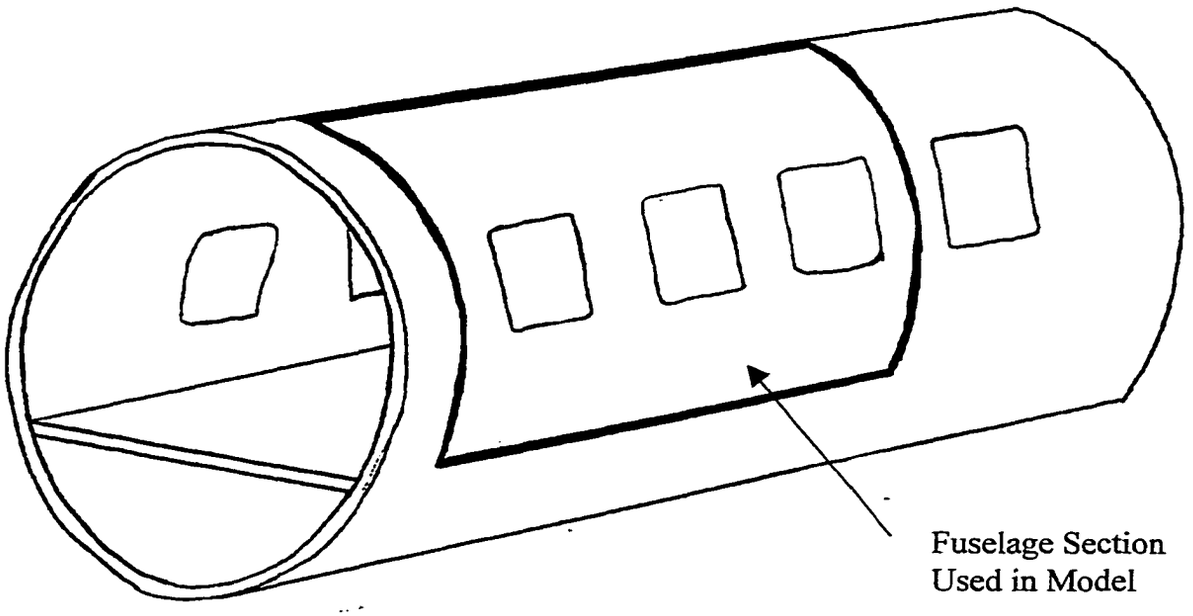

Figure 47. Location of Fuselage Section Used to Create the Finite Element Model.

was used to model the window belt area. This added material is used on aircraft to guard against fatigue failure in the vicinity of the passenger windows (Figure 48).

Stringers

The longitudinal reinforcing stringers were modeled as 3D beam elements (BEAM4 for both elastic and plastic structural analyses). The stringer material was modeled as aluminum 7075-T6 and the assumed stringer cross-section is shown in figure 49. The stringers were spaced at 0.203 meter (8.0 inch) intervals along the fuselage circumference (Figure 50). The material properties of aluminum 7075-T6 that were used to model the stringers are given in Table 20.

Table 19

Bi-Linear Material Properties for Fuselage Skin (Aluminum 2024-T3)

Property	
Yield Stress	0.345 GPa ($50x10^{+3}$ psi)
Young's Modulus	71.0 GPa ($10.3x10^{+6}$ psi)
Tangent Modulus	0.46 GPa ($67x10^{+3}$ psi)
Ultimate Stress	0.427 GPa ($62x10^{+3}$ psi)
Ultimate Strain	0.186 m/m
Density	2923 Kg/m^3
Poisson Ratio	0.334

Table 20

Material Properties for Frames and Stringers (Aluminum 7075-T6)

Property	
Young's Modulus	71.0 GPa ($10.3x10^{+6}$ psi)
Yield Stress	0.496 GPa ($72x10^{+3}$ psi)
Tangent Modulus	0.207 GPa ($30x10^{+3}$ psi)
Ultimate Stress	0.517 GPa ($75x10^{+3}$ psi)
Ultimate Strain	0.111 m/m
Density	2923 Kg/m^3
Poisson Ratio	0.334

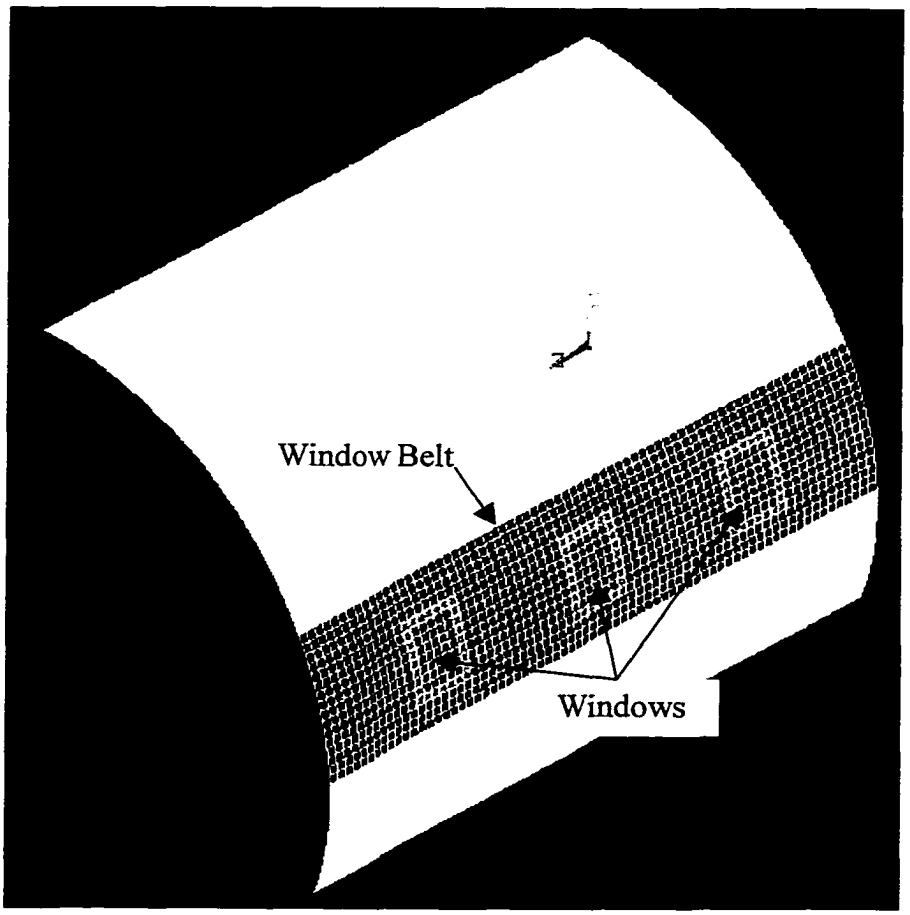

Figure 48. Location of Window Belt Area on the Modeled Fuselage Section.

Frames

The circumferential reinforcing frame members were modeled as 3D elastic beam elements (ANSYS element BEAM4). The frame material was modeled as 7075-T6 aluminum and the assumed frame cross-section is shown in Figure 49. The frame members were spaced at 0.508 meter (20.0 inch) intervals along the fuselage longitudinal axis (Figure 50). The material properties of aluminum 7075-T6 used to model the frames are given in Table 20.

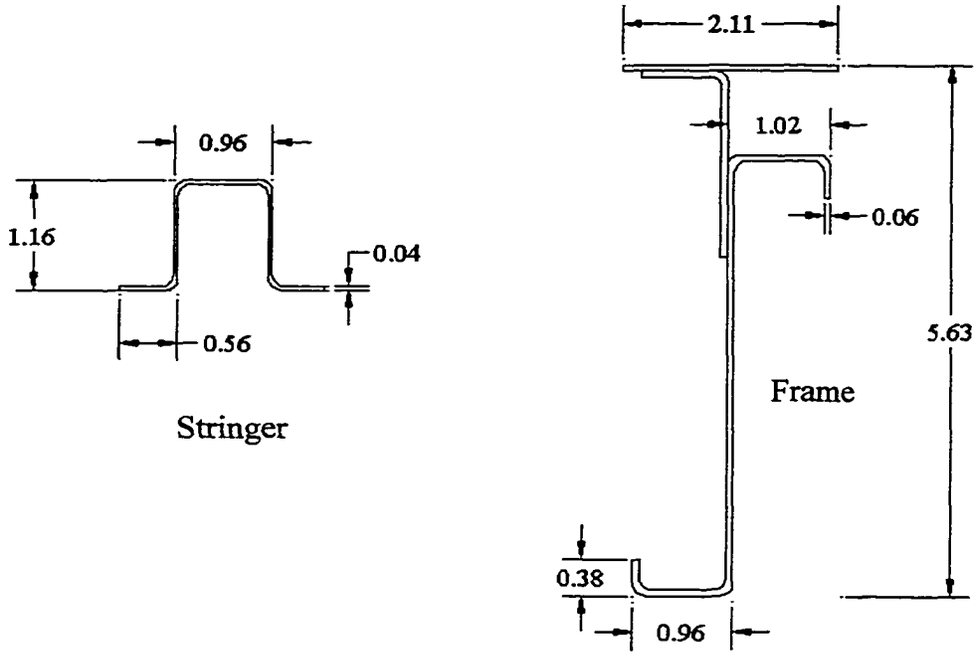

Figure 49. Stringer and Frame Cross-Sections. (All Dimensions in Inches.) (Roskam, 1985; Bruhn 1973).

Windows

The passenger cabin window assemblies were modeled as two components: the glass pane member and an aluminum window support frame. The glass pane, although actually two separate structural panels, was modeled as a single piece of soda-lime glass (10.0 millimeter thickness) using 4-node, quadrilateral elastic shell (SHELL63) elements. The supporting forged window frame, also meshed with elastic shell (SHELL63) elements, was modeled with the material properties of aluminum 7075-T6. The window frame attaches to the perimeter edge of the pane member and dimensions of 51 millimeters wide by 15 millimeters thick were assumed.

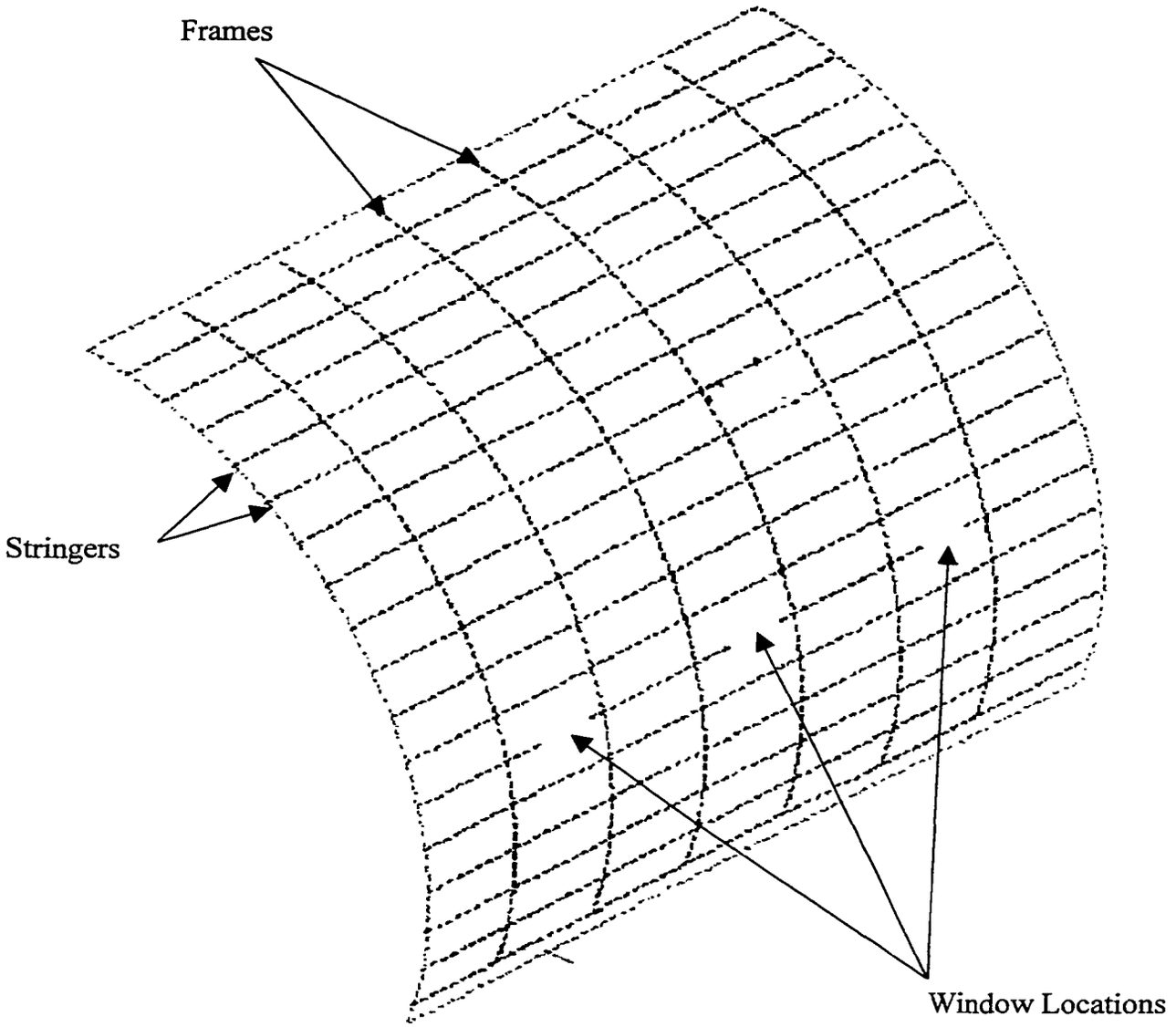

Figure 50. Depiction of the Stringer and Frame Arrangement Used for the Finite Element Model.

Finite Element Mesh Scheme

All of the shell elements used in the fuselage model (skin, glass panes, and window support frames) were modeled using 5.08 by 5.08 centimeter (2.0 by 2.0

inch) square elements (Figure 51). The stringer and frame members were modeled with beam elements with individual elements lengths of 5.08 centimeters (2.0 inches). These element sizes were selected based on the results of a convergence study which is included in Appendix A of this report. The stringer and frame elements were defined using skin nodes in order to minimize the total number of nodes required in the model.

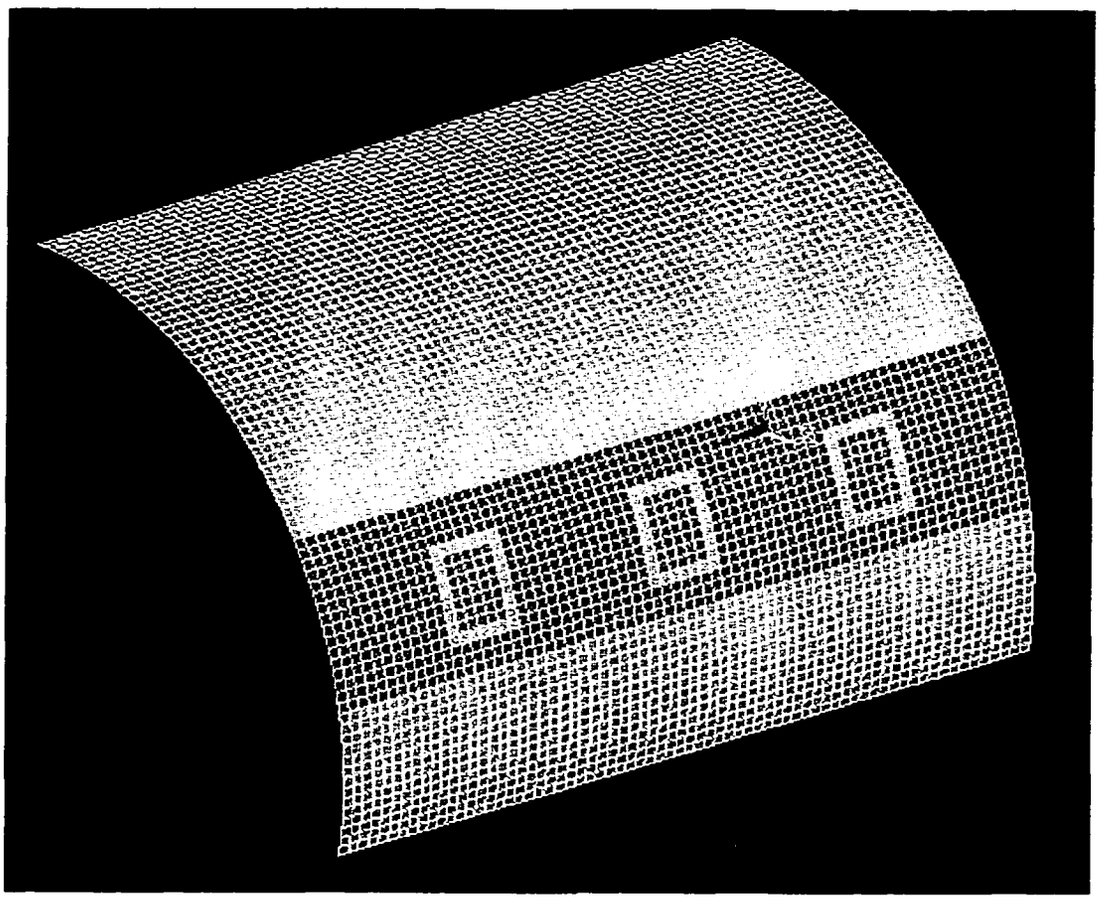

Figure 51. Depiction of Model of Fuselage Section Including Mesh Scheme for Skin, Glass Panes, and Window Support Frames.

Model Boundary Conditions

Appropriate boundary conditions for the finite element model were applied to the four edges of the fuselage panel. The fore and aft edges of the panel and the lower edge of the panel near the passenger cabin floor were modeled as simply supported edges. The upper edge of the fuselage panel was modeled using symmetry conditions.

Considerations of Strain-Rate Effects on Material Properties

In all of the finite element structural analyses presented, material properties are assumed to be constant regardless of strain rate. This assumption is based on tensile strength data at various strain rates as cited in literature. First, Felback and Atkins (1984) state that for a change in strain rate from 10^{-4} to 10^{0} seconds^{-1}, the stress level in Aluminum 2024 varies by less than 5%. These data apply to 2024 Aluminum in the temperature range of 28°C down to –195°C. Additionally, the tensile properties of 7075-T6 aluminum are, in essence, insensitive to strain rate as well. The tensile strength of 7075-T6 aluminum at a temperature of 30°C varies by only about 6% over the range of strain rates of from 10^{-5} to 10^{0} seconds^{-1} (Anon., 1979). For this reason, the materials under consideration are assumed to have constant material properties that are independent of strain rate.

It should be further noted, that for this analysis, all material properties are based on room temperature values (25 to 30°C). In actual practice, the fuselage skin of an aircraft flying at an altitude of 13,000 meters (36,000 feet) would be exposed to

ambient air at approximately –56°C (Thompson, 1972). Thus, the tensile strength of the 2024-T3 fuselage skin for these low temperatures would actually be about 4-6% higher than the values used in this analysis (Anon., 1979). Since the actual flight altitudes and ambient temperatures are not constant for all possible bombing scenarios, the room temperature values of material properties are considered a conservative estimate for this analysis.

Structural Analyses

Elastic Model - Static Fuselage Stress Under Cabin Pressurization

In order to evaluate the stress distribution of the fuselage under cabin pressurization loading, an outward pressure of 51.7 KPa was applied to the entire inner surface (ANSYS *SFE* command) of the elastic finite element model. A contour plot of the resulting radial displacements of the fuselage panel is shown in Figure 52. The maximum radial displacements (on the order of 2.0 millimeters) are seen in the upper fuselage in the aircraft skin at the center-most points between the stringer and frame members. As a comparison for this solution, consider the equation for the deflection of a uniform cylindrical shell under internal pressure (Timoshenko, Woinowsky-Krieger, 1959) (Equation 6.1).

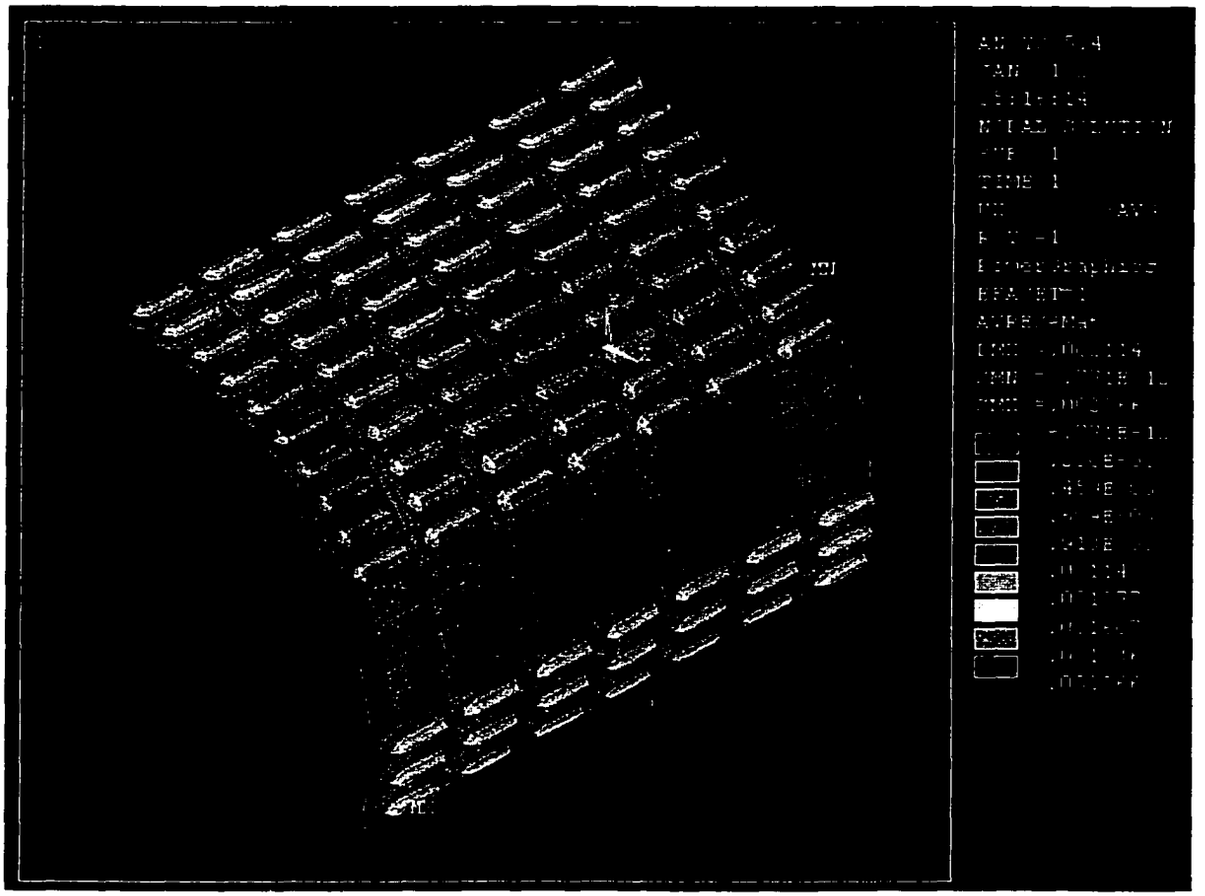

Figure 52. A Contour Plot of Radial Displacement for the Fuselage Model Under Internal Cabin Pressurization.

$$\delta = \frac{pa^2}{Eh} \tag{6.1}$$

Where:
- δ = Radial Displacement of Cylindrical Shell
- p = Internal Pressure on Cylinder
- a = Radius of Cylindrical Shell
- E = Modulus of Elasticity of Shell
- h = Thickness of Shell

Using this expression for the static pressurization (51.7 KPa) of a curved shell with the same radius (1.88 meters) and thickness (0.00163 meters) as the fuselage model gives a radial displacement of 1.58 millimeters. This result compares well with the finite element calculated radial deflection of the fuselage skin for a point in the upper fuselage mid-way between adjacent stringers and frames of 1.73 millimeters. As a point of reference, the finite element model predicts radial displacements of the frame and stringer members in the range of 0.5 to 0.6 millimeters.

It is interesting to note the relatively low radial fuselage displacements (approximately 0.8 millimeters) in the window belting area due to the increased skin thickness in that region. A closer view of the radial displacements in the upper fuselage model is given in Figure 53. The von Mises stresses in the fuselage model under static internal cabin pressurization of 51.7 KPa are also plotted (atop the deformed model) (Figure 54). The locations of maximum von Mises stress in the aircraft skin (on the order of 0.096 MPa) occur in the upper fuselage. A closer view of a portion of the fuselage illustrates that the maximum stresses in the fuselage skin occur at the skin-stringer interface (Figure 55).

Similar to the results observed for radial displacements, relatively low stresses (on the order 0.0183 MPa) are obtained in the window belting area due to increased skin thickness in that region. It is important to note that for the case of internal pressurization alone, stresses in the fuselage are significant when compared to the

material yield stress (Table 21). It should be further noted that actual service fuselage stresses will be considerably higher with the addition of flight loads.

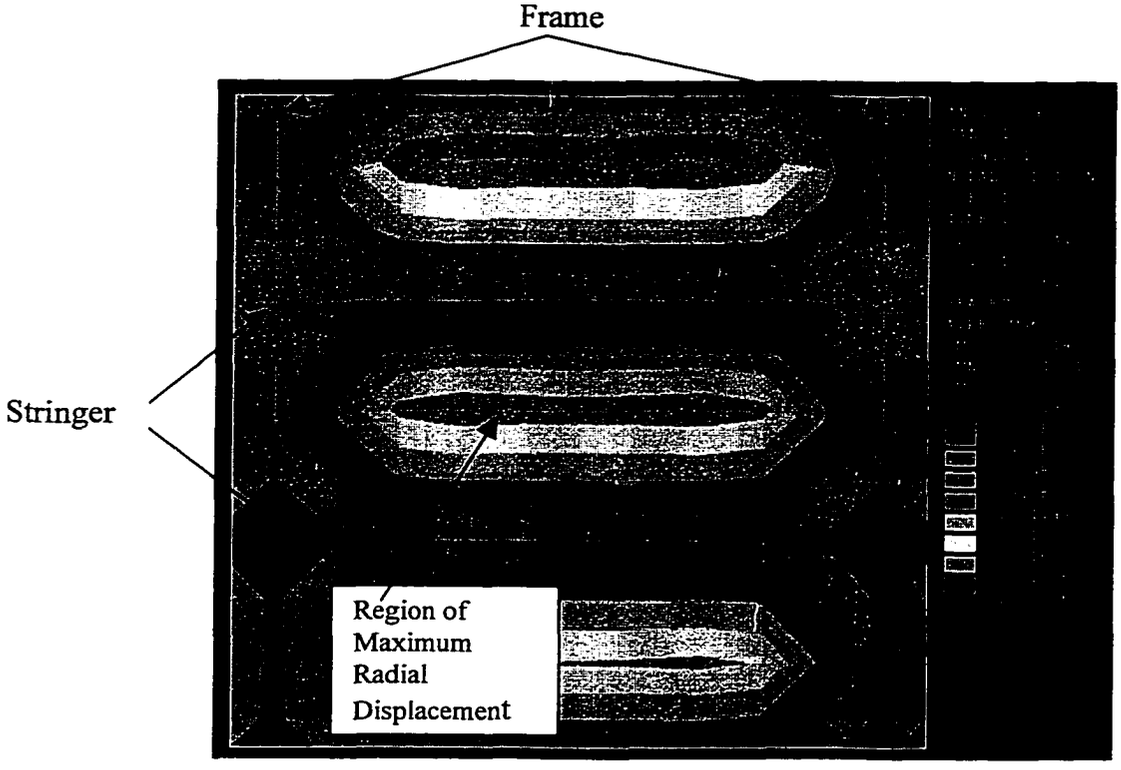

Figure 53. A Closer View of Radial Displacements in the Upper Fuselage Model Under Internal Cabin Pressurization.

These results illustrate the low safety margin exhibited by commercial aircraft structures. Although necessitated by weight minimization requirements, these low safety factors certainly contribute to aircraft damage vulnerability from unanticipated load cases such as internal explosive pressures.

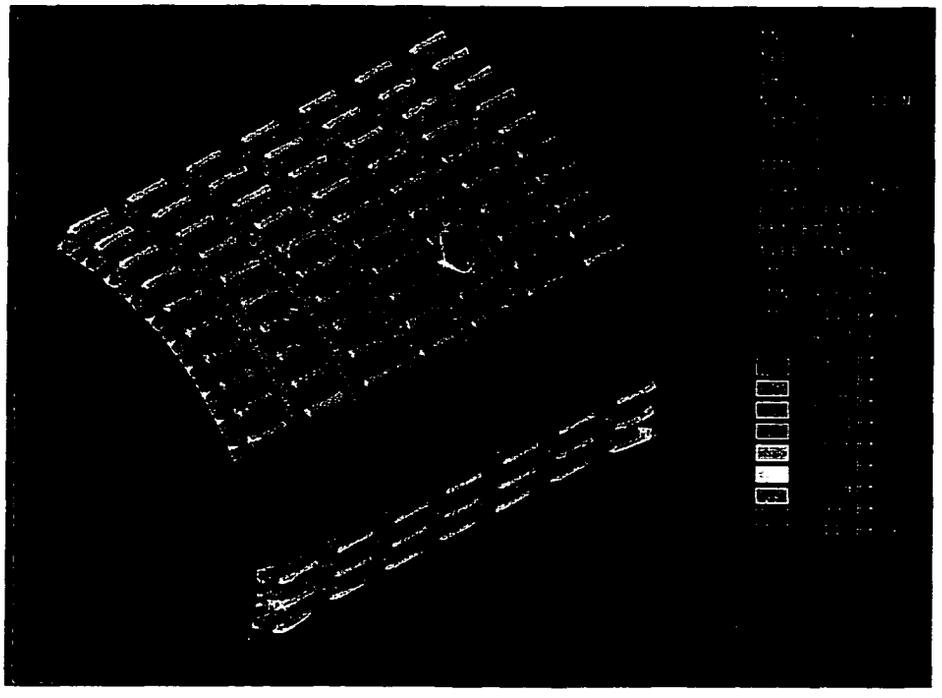

Figure 54. A Contour Plot of the Fuselage Skin von Mises Stresses Atop the Deformed Model for Static Internal Cabin Pressurization of 51.7 KPa.

Modal Analysis of Fuselage Model

In order to better understand the dynamic response of the fuselage model under transient loading, a modal analysis was first conducted. For this analysis, a modal analysis of the previously described fuselage model was performed using the ANSYS Block Lanczos solution method. In this case, the fuselage was modeled as an unpressurized structure and the first ten natural frequencies of the structure were found (Table 22).

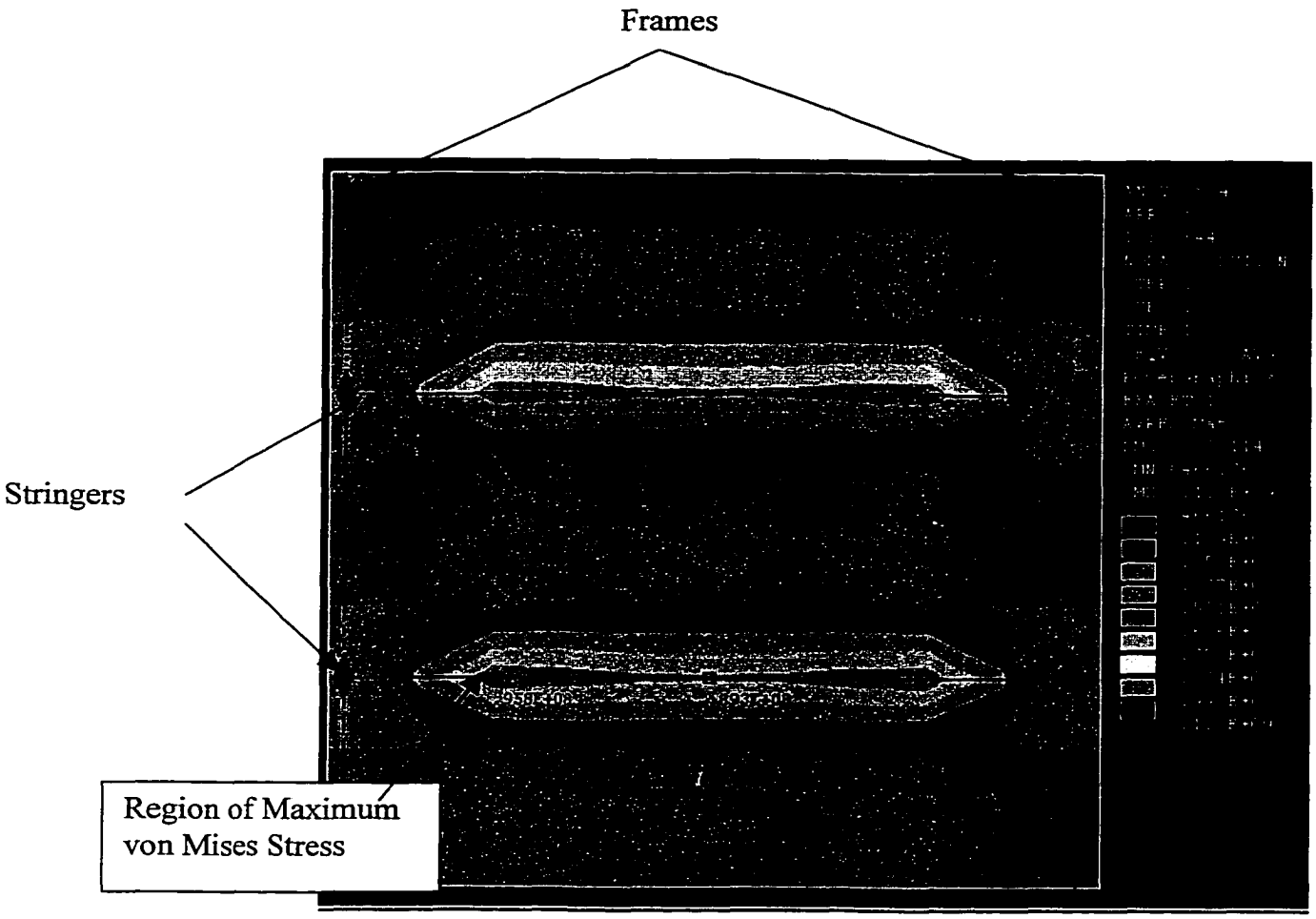

Figure 55. A Closer View of Fuselage von Mises Stresses in the Aircraft Skin in the Upper Portion of the Fuselage Model for Static Internal Cabin Pressurization of 51.7 KPa.

To determine the natural frequencies of a pressurized fuselage, a pre-stressed modal analysis was conducted. This process involved first solving the static finite element solution for the case of internal fuselage pressurization of 51.7 KPa. A modal analysis was then performed on the resulting pre-stressed model using the ANSYS Block Lanczos solution method and the first ten natural frequencies were determined (Table 22). As expected, the addition of cabin pressurization stiffens the structure resulting in an increase of the natural frequencies.

Table 21

Summary of Stress Results for Static Fuselage Pressurization of 51.7 KPA

Location	Maximum Calculated Stress for Internal Pressurization (51.7 KPa)	Material Yield Stress	% of Yield Stress
Skin (Al 2024T3)	0.096 MPa	0.33 MPa	29.1%
Frame (Al.7075 T6)	0.031 MPa	0.483 MPa	6.4%
Stringer (Al 7075 T6)	0.023 MPa	0.483 MPa	4.8%

Table 22

Summary of Modal Analysis of Unpressurized and Pressurized Fuselage Models

Mode	Unpressurized Fuselage Predicted Natural Frequency (Hertz)	Pressurized Fuselage (51.7 KPa) Predicted Natural Frequency (Hertz)	Difference	Cycle Duration Pressurized Fuselage (51.7 KPa) (milliseconds)
1	58.5	63.9	+9.2%	15.6
2	65.6	70.7	+7.8%	14.1
3	72.3	76.8	+6.2%	13.8
4	83.4	91.1	+9.2%	12.0
5	106.7	112.9	+5.8%	9.4
6	108.2	120.7	+11.6%	9.2
7	118.2	128.3	+8.5%	8.5
8	137.7	144.4	+4.9%	7.3
9	144.6	153.8	+6.4%	6.9
10	147.9	161.4	+9.1%	6.8
		Mean Difference	+7.9%	

For both pressurized and unpressurized models, the mode shapes associated with the first ten natural frequencies represent deformations of the full shell model. For modes five through ten, an increasing amount of localized deformation (in the fuselage skin between individual stringer and frame reinforcements) was observed. Even at the tenth natural frequency, however, the mode shape of the fuselage panel was still largely dominated by the global shell deformation behavior.

Transient Finite Element Analysis of Fuselage Model

In order to evaluate the structural response of the fuselage model to explosive pressure loading, a transient finite element analysis was conducted. The previously defined finite element model of a portion of a commercial aircraft fuselage was used to determine structural response under five different impulsive loading cases (Figure 45). The specific pressure pulse used to model the explosion was based on measured pressures reported by White, Bharatram, and Venkayya (1992) for blast testing conducted on a B-52 aircraft fuselage. Based on these measurements (recorded by a sensor at approximately 1.9 meters (75.0 inches) from the source of the explosion) a piecewise linear approximation of transient pressures was determined (Figure 56).

Case A – Pressure Pulse on an Unpressurized Fuselage

The first load case (case A) was intended as a control case to determine the response of an unpressurized fuselage and to predict the damage caused by an internal

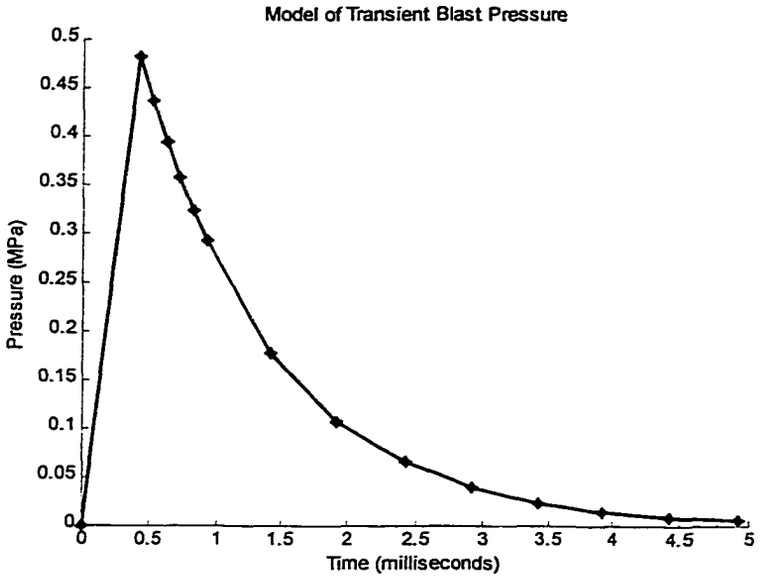

Figure 56. Piece-wise Linear Approximation of Explosive Pressures Based on Blast Test Measurements of a B-52 Aircraft Fuselage (White, Bharatram, and Venkayya,1992).

explosion. Based on the results of the static pressurization case, it was decided to track the transient displacements, stresses, and strains at three locations in the upper fuselage: 1) A node at the central point between frame and stringer reinforcements (for maximum displacements), 2) a node at the frame-skin junction mid-way between stringers (for stress concentrations at frame-stringer interface), and 3) a node at the stringer-skin junction mid-way between adjacent frames (for stress concentrations at skin-stringer interface), (Figure 57).

Case A Results - Assumed Elastic Material Properties

A transient analysis of the fuselage model was conducted using the ANSYS

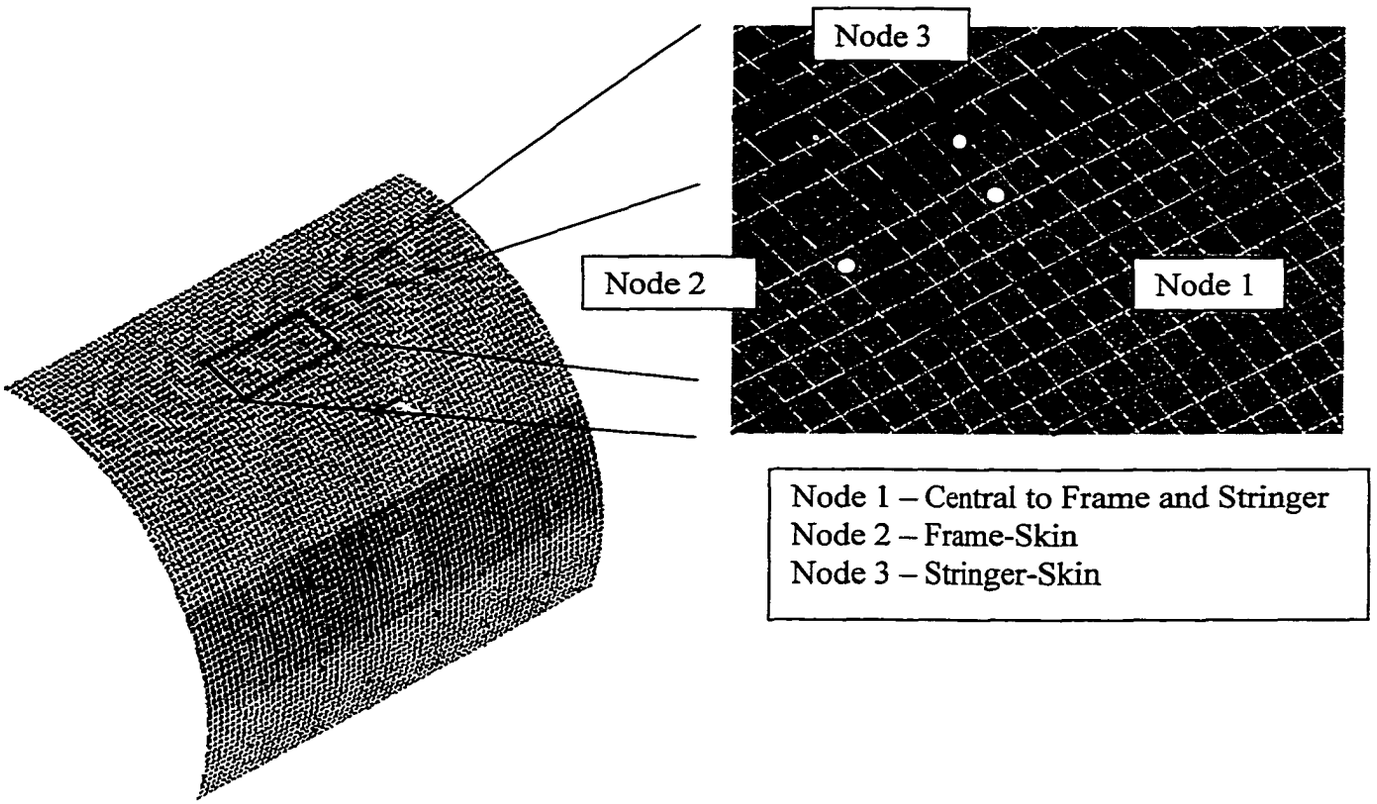

Figure 57. Depiction of the Three Nodes Used to Determine Transient Fuselage Radial Displacements and von Mises Stresses and Strains.

frontal solver. In order to account for large deformation effects, the non-linear geometry option was used. Initially, the solver parameters were set manually and some difficulty in reaching solution convergence was encountered. When the optimized non-linear solution default values suggested by ANSYS (ANSYS *Solcontrol* command) were used, however, the solution converged without difficulty. The analysis was conducted on a personal computer (Pentium 3, 500 MHz processor)

running ANSYS software (version 5.4) from a Windows NT network. The model contained 6775 total elements (4900 shell elements and 1875 beam elements) 5041 nodes, and 29,570 degrees of freedom. The analysis was conducted for a time duration of 50 milliseconds, and the solution time took approximately 23 hours on the computer. The average time step used by ANSYS in this analysis was 0.23 milliseconds.

The resulting radial displacements of the structure are shown for all three nodes of interest (Figure 58). The radial response of the three nodes appears to be the superposition of several sinusoidal functions with a significant response at a frequency on the order of 400 Hertz. The fuselage oscillation for this model with assumed elastic material properties occurs at a much higher frequency than as indicated by the previous modal analysis (where several peak frequencies in the range of approximately 60 to 100 Hertz were predicted – Table 22). This high frequency oscillation appears to be an artifact of the elastic linear property model, since significantly different displacement results were subsequently found using an elastic-plastic model.

It should be noted that natural frequency analysis of the fuselage shell leads to complicated results since the finite element modal analysis predicted literally hundreds of natural frequencies between 60 hertz and 400 hertz. At lower frequencies, the predicted vibrational mode shapes are found to involve global deformation of the full fuselage shell. At higher frequencies, however, the mode shapes are dominated by

various combinations of oscillations in localized areas of the fuselage skin between the surrounding frame and stringer support members. Since the elastic material

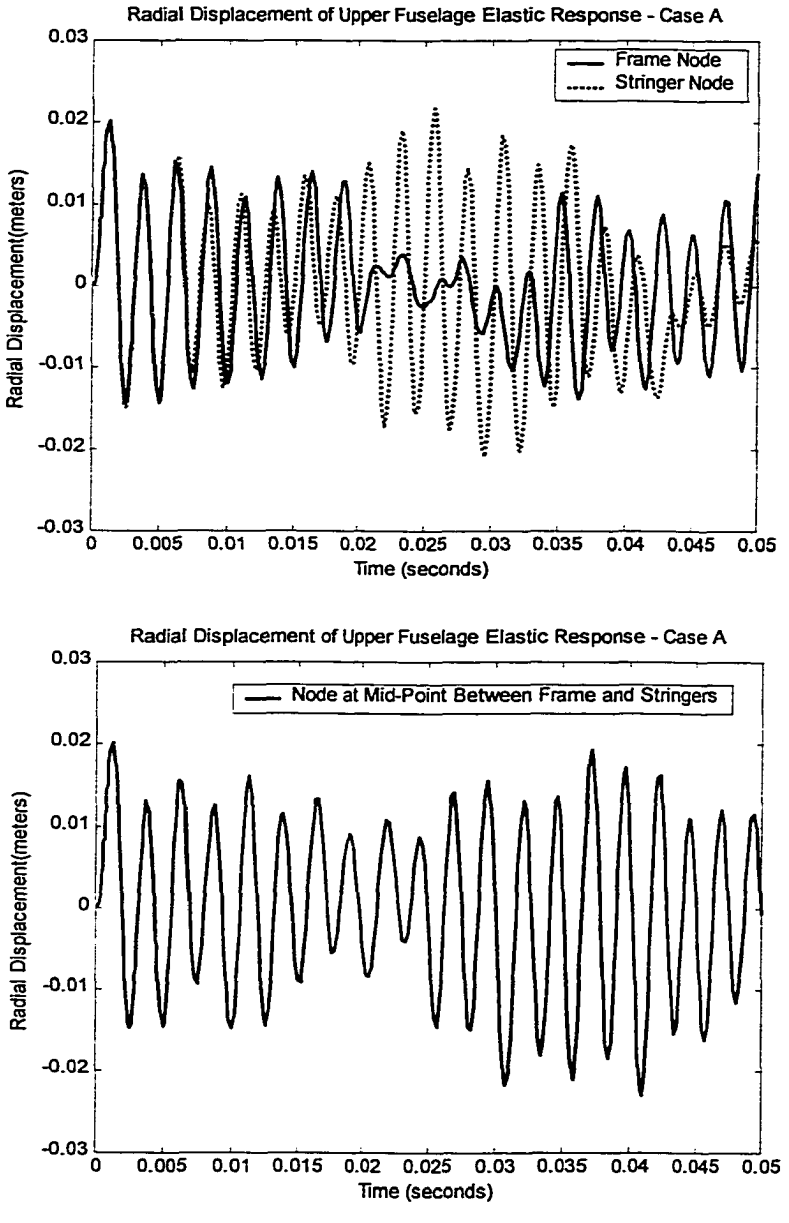

Figure 58. Predicted Elastic Radial Fuselage Displacements for a Pressure Pulse on an Unpressurized Structure.

property model is subsequently shown to be inadequate for this study, the predicted elastic fuselage frequencies (Figure 58) should also be questioned.

The transient von Mises stresses for the three fuselage locations of the elastic model were also calculated. The von Mises stress (using the distortional energy density criterion) is a means of converting the 3-dimensional stress components for a given element into an effective stress value. This effective stress (von Mises stress in this case) can then be compared to the uni-axial yield stress of a material in order to predict yield. The transient von Mises stresses for the stringer node and for the central node are shown in Figure 59. A summary of the peak von Mises for all three node locations is given in Table 23.

Since the fuselage skin stresses for the elastic model are well above the yield stress for the aluminum 2024-T3 (by a factor of approximately 2 to 4), it is apparent that the plastic nature of the material needs to be considered. Given the ductile nature of aluminum, the effects of plasticity were added to the model through the use of bi-linear isotropic material properties for the aluminum 2024-T3 (skin) and for aluminum 7075-T6 (frame and stringer) (Tables 19 and 20).

Case A Results-Assumed Elastic-Plastic Material Properties

The transient analysis of the fuselage model was re-run as described before with the use of non-linear (elastic-plastic) material properties. The skin, stringers and frames

were modeled as bilinear isotropic hardening materials using J2 incremental plasticity theory (Anon 19.12, 1997; Mendelson, 1968). Again, the optimized non-linear

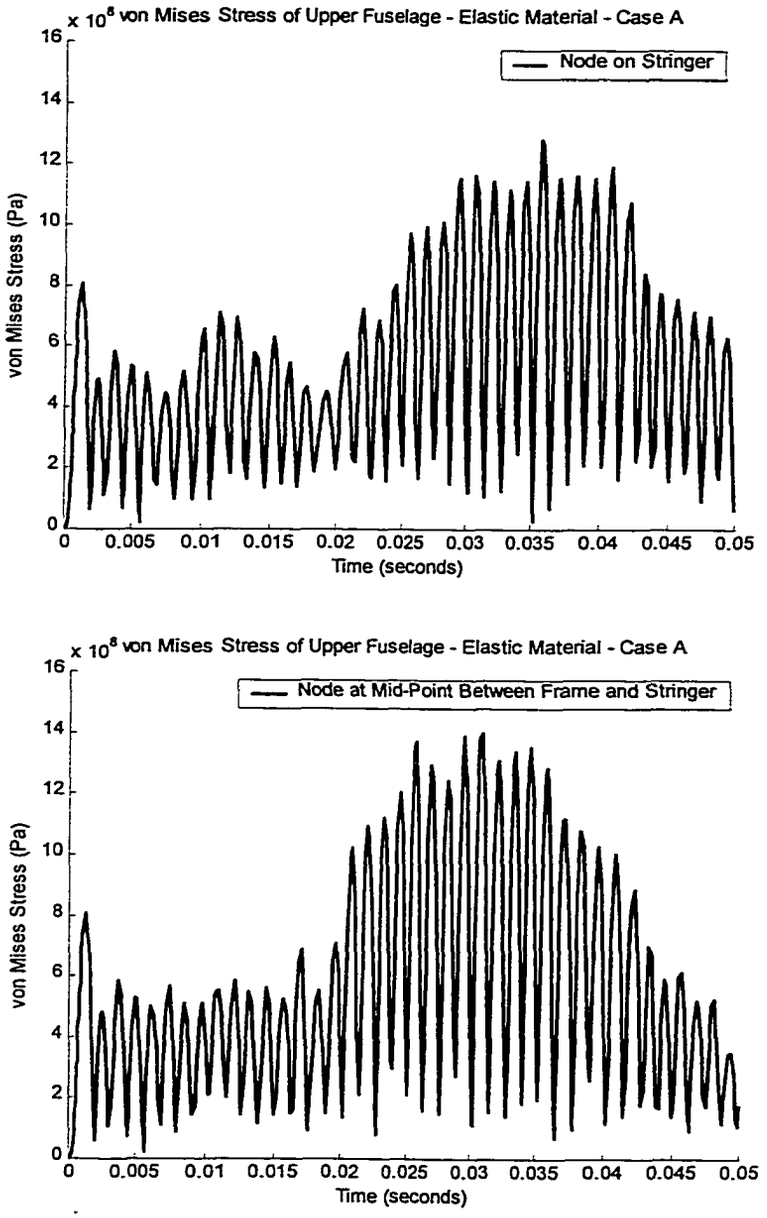

Figure 59. Transient von Mises Stress in the Upper Fuselage for Elastic Finite Element Model Under Load Case A.

linear solution default values suggested by ANSYS (ANSYS *Solcontrol* command) were used and the solution converged without difficulty. The total computer solution time for this analysis (50 millisecond time duration) was approximately 52 hours. The average time step size used by ANSYS in this analysis was approximately 0.24 milliseconds.

Table 23

Summary of Maximum Predicted von Mises Stress for Unpressurized Fuselage Elastic Analysis

Node Location	Maximum von Mises Stress	Material Yield Stress
Central to Frame and Stringer	1.4 MPa	0.33 MPA
Frame-Skin Interface	0.82 MPa	0.33 MPA
Stringer-Skin Interface	1.3 MPa	0.33 MPA

In order to illustrate the effects of considering material plasticity, the von Mises stress of the skin-stringer node is plotted for both the elastic and elastic-plastic analyses (Figure 60). The necessity of including material plasticity in the transient analysis was an expected result and correlates well with previous work by Kanninen, Marchand, and O'Donoghue (1992). Note that for the elastic-plastic case, the von Mises stress only briefly exceeds the material yield stress, since plastic deformation of the aluminum causes the stress to decrease. Accordingly, the maximum von Mises stress levels predicted in this analysis for the three nodes are very similar to the

material yield stress (Table 24). The radial displacements for the elastic-plastic fuselage model under load case A were also found (Figure 61).

For the elastic-plastic model, once the material has reached the yield stress and plastic deformation occurs, it is important to determine the total amount of strain in the structure. The total strain at a point in the structure is the sum of the elastic

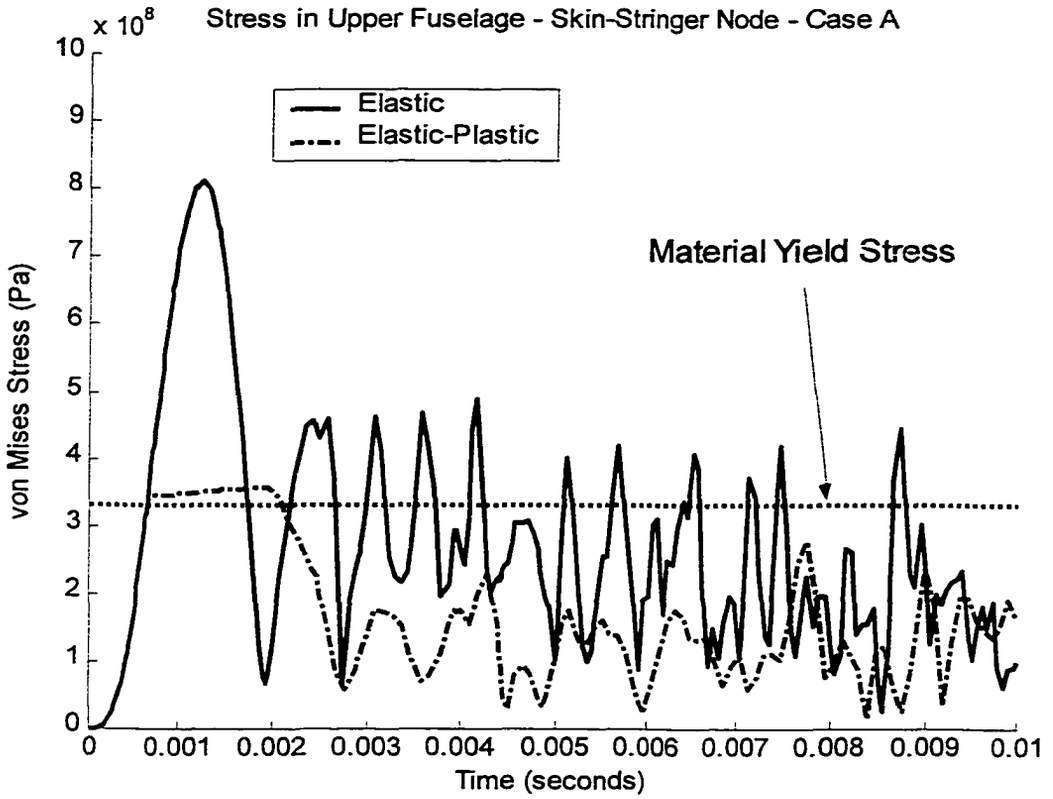

Figure 60. Transient von Mises Stress of Central Node in the Upper Fuselage for Elastic and Elastic-Plastic Finite Element Model Under Load Case A.

Table 24

Summary of Maximum Predicted von Mises Stress for Unpressurized Fuselage Elastic-Plastic Analysis

Node Location	Maximum von Mises Stress	Material Yield Stress
Central to Frame and Stringer	0.355 MPa	0.33 MPA
Frame-Skin Interface	0.354 MPa	0.33 MPA
Stringer-Skin Interface	0.358 MPa	0.33 MPA

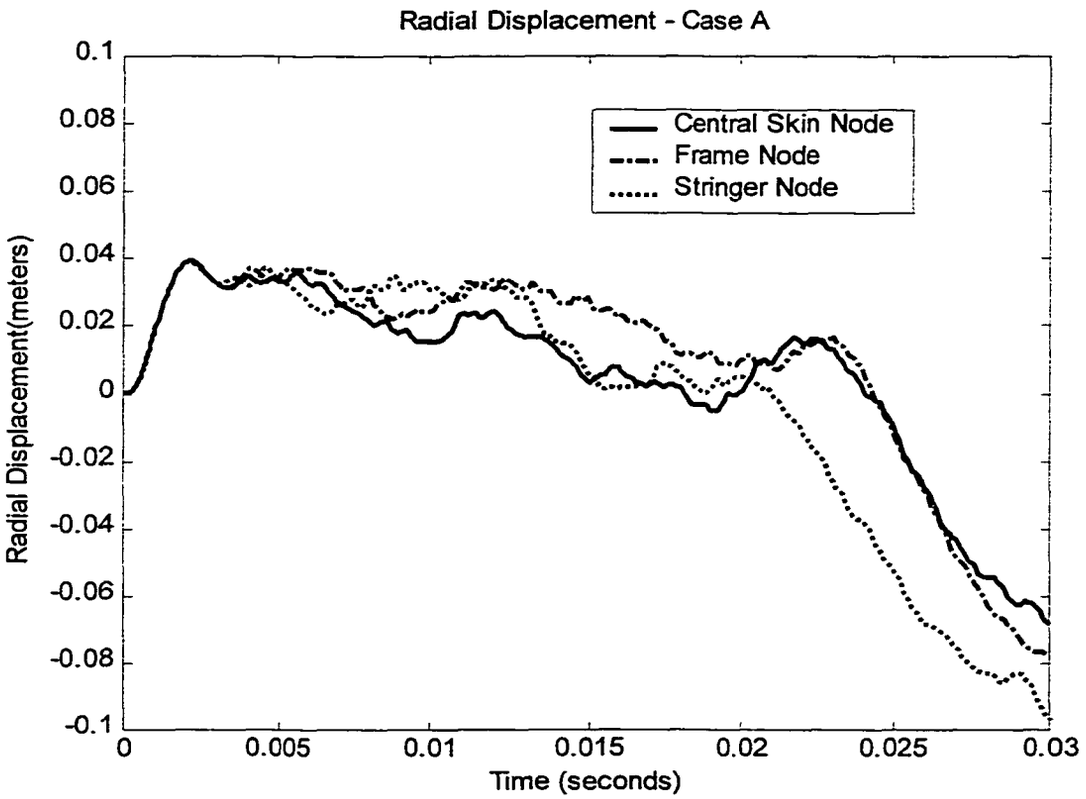

Figure 61. Radial Displacements of the Upper Fuselage for Elastic Finite Element Model Under Load Case A.

strain and plastic strain. For this analysis, the individual elastic and plastic strain components were first combined to give the total strain components, and the result was transformed into total equivalent strain using the von Mises criterion. The predicted total equivalent strains for the fuselage structure are given in Figure 62 and a summary of the maximum total equivalent strain values is given in Table 25.

From these results, it is clear that the total strain at the three selected locations in the fuselage remain quite low and do not approach the strain limit of the material. Thus, it can be concluded that although some plastic deformation of the material will occur, failure is not predicted.

Case B – Pressure Pulse on a Pressurized Fuselage

The second load case (case B) was used to determine the response of a fully pressurized fuselage (51.7 KPa) to an explosive pressure pulse. The same modeled pressure pulse was used in case B as in case A (Figure 56).

Case B Results-Assumed Elastic-Plastic Material Properties

For this load case, a pre-stressed transient analysis of the previously described fuselage model was conducted. This was accomplished by solving the static solution for the case of internal pressurization alone, and using the results as initial conditions for the transient pressure pulse loading.

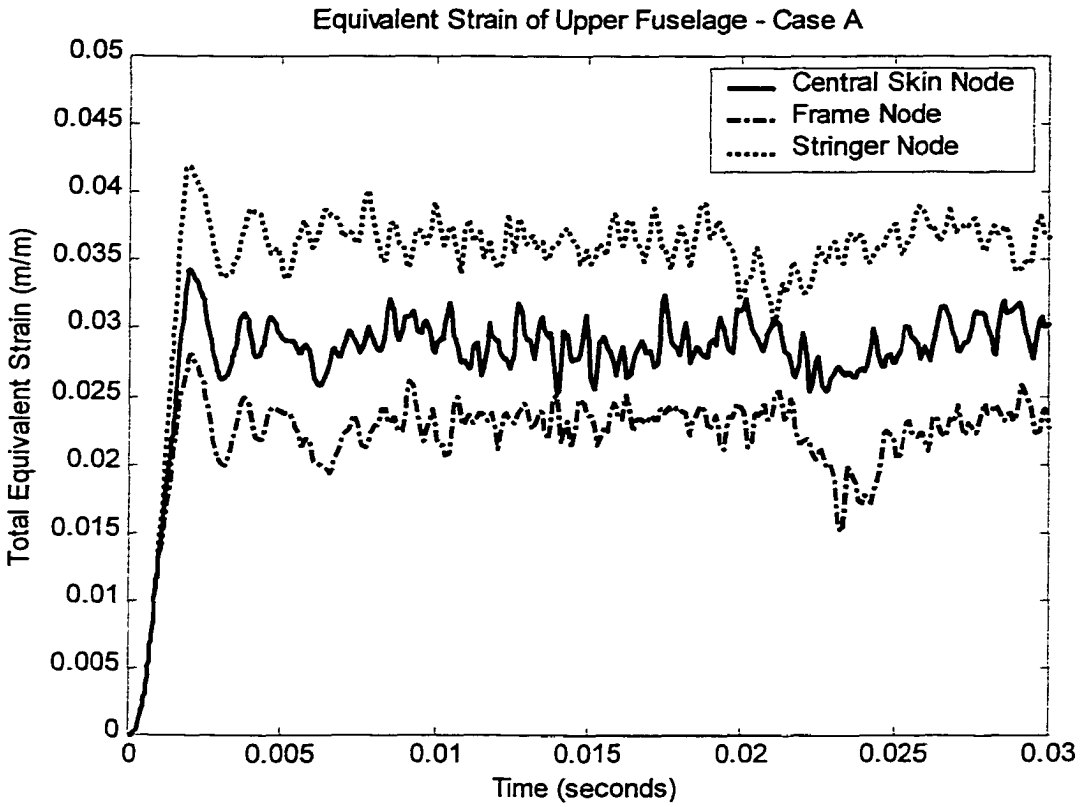

Figure 62. Total Equivalent Strains in the Upper Fuselage for Elastic-Plastic Finite Element Model Under Load Case A.

Table 25

Maximum Predicted Total Equivalent Strain for Unpressurized Fuselage Elastic-Plastic Analysis of Load Case A

Node Location	Maximum Total Equivalent Strain (%)	Material Strain Limit (%)
Central to Frame and Stringer	3.4 %	18.6 %
Frame-Skin Interface	2.8 %	18.6 %
Stringer-Skin Interface	4.2 %	18.6 %

The analysis was programmed to run for a 30 millisecond time duration and the optimized non-linear solution default values suggested by ANSYS (ANSYS *Solcontrol* command) were used. The solution converged without difficulty and the total computer solution time for this analysis (30 millisecond time duration) was approximately 52 hours.

The radial displacement results for case B show that all three nodes (on stringer, on frame, and mid-way between frames and stringers) exhibit a similar response (Figure 63). It also appears that the outward biased pressure on the fuselage ensures that the fuselage displacements remain primarily in the positive (outward) direction. From the displacement data (Figure 63) it is apparent that the dominant response frequency of the fuselage for load case B is on the order of 65 hertz, which compares favorably to the lowest natural frequency of the structure predicted by the finite element method (64 hertz) (Table 22).

The von Mises stresses of the model show that the material stresses reach the yield stress very quickly (about 1.0 milliseconds after the blast arrival) (Figure 63 and Table 26). Due to the relatively ductile nature of 2024-T3 Aluminum, the stresses are relieved through plastic deformation. The total equivalent strains in the fuselage for case B were also determined (Figure 64). Note that for all three fuselage locations, the equivalent strains reach their peak values fairly rapidly (within about 2.0 milliseconds after the blast arrival). It should be noted, however, that the although the maximum equivalent strains at all three nodal locations are 30-40% larger than for the

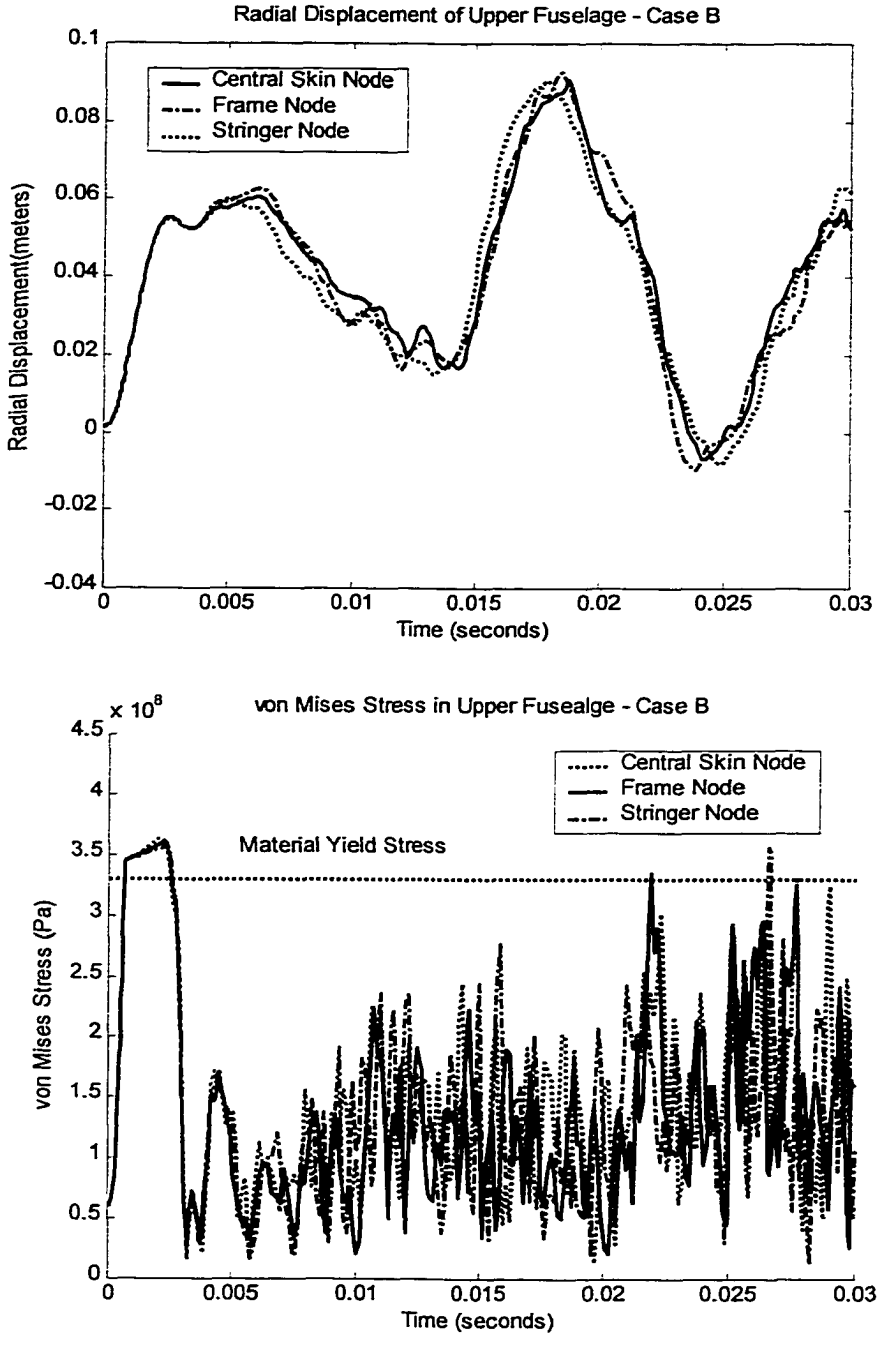

Figure 63. Radial Displacements and von Mises Stress in the Upper Fuselage for Elastic-Plastic Finite Element Model Under Load Case B.

Table 26

Summary of Maximum Predicted von Mises Stress for Pressurized Fuselage Elastic-Plastic Analysis of Load Case B

Node Location	Maximum von Mises Stress	Material Yield Stress
Central to Frame and Stringer	0.360 MPa	0.33 MPA
Frame-Skin Interface	0.357 MPa	0.33 MPA
Stringer-Skin Interface	0.363 MPa	0.33 MPA

unpressurized fuselage, these values still remain well below the ultimate strain limit of the material (Table 27).

This result is quite surprising considering the magnitude of the blast pulse used in this analysis (Figure 56). The blast pulse has a peak pressure of 482.6 KPa (70 psi) and an impulse, calculated as the area under the pressure-time curve, of 483.7 pascals·seconds (0.070 psi·seconds). This explosive blast at the assumed distance of 1 to 2 meters is equivalent to the detonation of a bare explosive charge quantity of 0.9 to 4.5 kilograms (2 to 10 pounds) (Baker, 1973). Considering the significant magnitude of the explosive pressure pulse used in this model, it was anticipated that the pressurized load case (B) would have resulted in structural failure as the fuselage skin reached the material strain limit. This finding will be addressed in more detail in the conclusions section of this chapter.

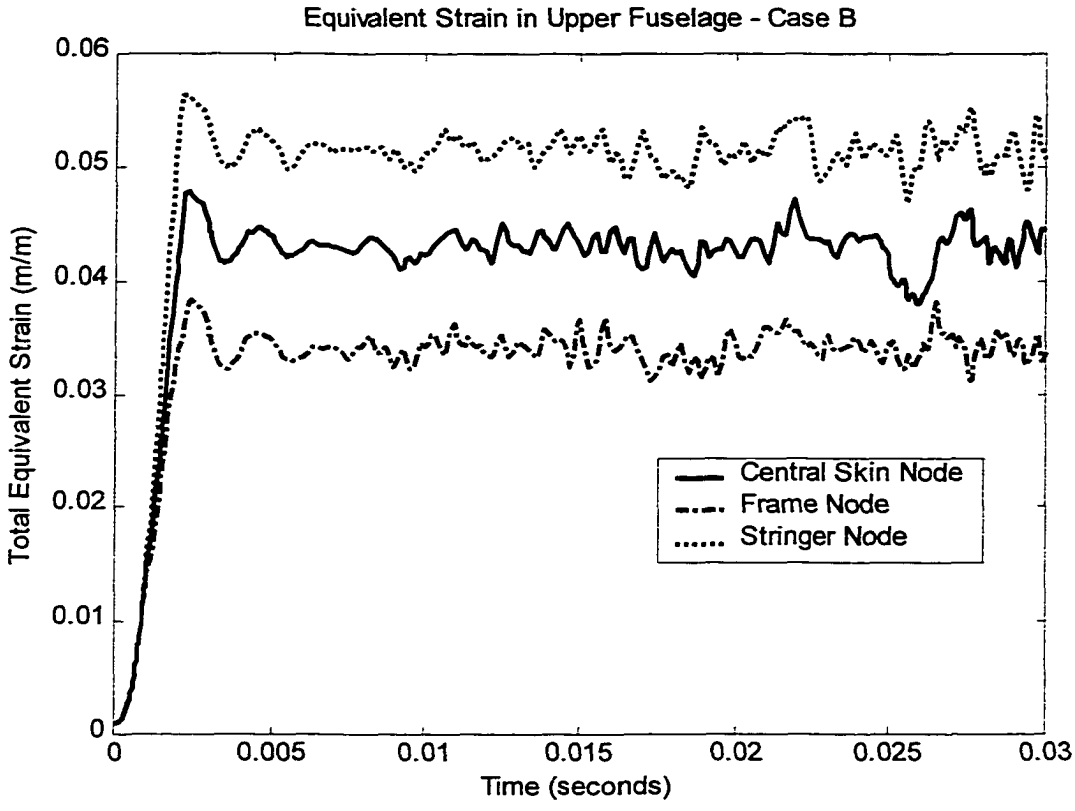

Figure 64. Total Equivalent Strain in the Upper Fuselage for Elastic-Plastic Finite Element Model Under Load Case B.

Table 27

Maximum Predicted Total Equivalent Strain for Pressurized Fuselage Elastic-Plastic Analysis of Load Case B

Node Location	Maximum Total Equivalent Strain (%)	Material Strain Limit (%)
Central to Frame and Stringer	4.8 %	18.6 %
Frame-Skin Interface	3.8 %	18.6 %
Stringer-Skin Interface	5.6 %	18.6 %

Case C – Pressure Pulse on a Pressurized Fuselage With Venting

After examining the results obtained from load case B, it was determined that the peak strain value for the pressurized fuselage model occurs rapidly (within about 2 milliseconds) after the pressure pulse contacts the structure. Recall that the original intent of analyzing load case C was to predict the blast response of the pressurized fuselage model in the event that the internal cabin pressurization is released starting at a conservatively estimated time of 7.3 milliseconds after detonation (or 5.7 milliseconds after blast contacts the structure). Thus, by a comparison of the time scale involved, it is concluded that the fuselage structure would reach its peak strain before the release of cabin pressurization could be initiated. For this reason, the results of load case C would be identical to those of load case B and the analysis of load case C as it was originally defined was not needed.

Case D – Pressure Pulse on Pressurized Fuselage with Simultaneous Venting

As previously mentioned, with the conservative assumptions used in this analysis, an active venting system could function to initiate fuselage venting only after the peak strain in the fuselage skin is reached. It is important, however, to consider the possibility that the assumptions made in this analysis may have been too conservative. For example, it would be possible to utilize more pressure sensors or a continuous line/strip sensor inside the aircraft fuselage in order to shorten the time needed for the control system to detect the explosive detonation. Additionally, it is

possible that the panel actuation times (as described in chapter IV) in the vicinity of the blast would be greatly reduced by the outward force of the explosive pressure acting on the panels. Also, it is conceivable that the pyrotechnic actuation device (as described in detail in chapter IV) could be designed to provide additional force to increase the speed of panel deployment and thus decrease the total time required to initiate venting.

Assuming these additional factors are considered in the analysis, it is reasonable to estimate that in the best case scenario, venting could begin at the instant the blast arrives (1.6 milliseconds as shown in Figure 44). Assuming (as calculated in Chapter V for the case of all 68 windows in a Boeing 737-700 used as vents) a fuselage decompression time of 0.190 seconds, the pressure pulse for case D can be considered (Figure 65).

Case D Results - Assumed Elastic-Plastic Material Properties

For this load case, a pre-stressed transient analysis of the previously described fuselage model was conducted. This was accomplished by solving the static solution for the case of internal pressurization alone, and using the results as initial conditions for the transient pressure pulse loading. The transient pressures used in case D were a combination of explosive pressures and the decaying cabin pressurization. The analysis was conducted for a 40 millisecond time duration and the resulting radial displacements and von Mises stresses (Figure 66 and Table 28) were calculated.

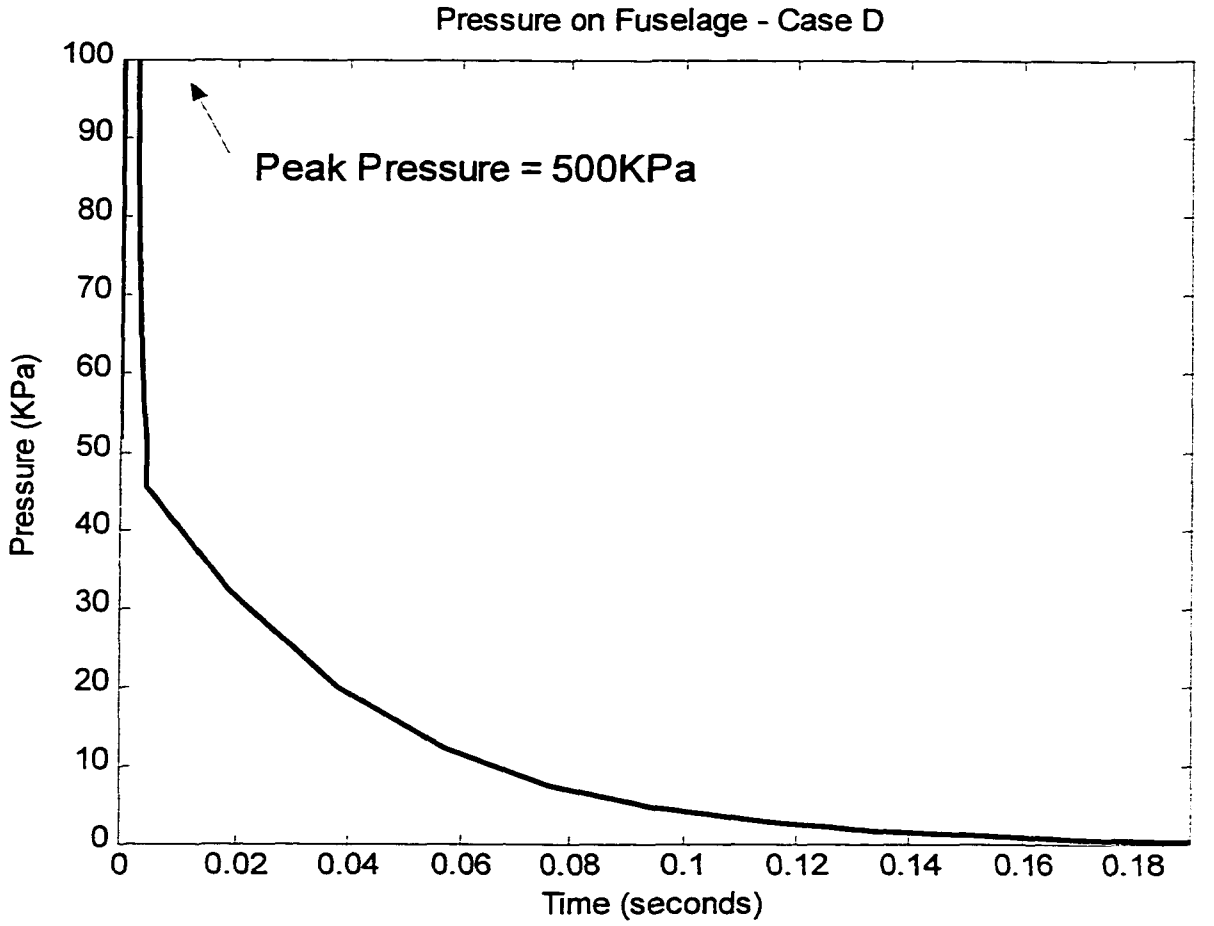

Figure 65. Transient Pressure on Fuselage for Case D in Which Explosive Blast Pressure Arrives at Instant of Venting Initiation.

The total equivalent strains in the fuselage for case D were also determined (Figure 67, Table 30). From the graphs and table presented, it is clear that the results of load case D (displacement, von Mises stress, and equivalent strain) are nearly identical to those found previously for load case B. This indicates that the initiation of venting under even the fastest imaginable scenario, would not decrease the fuselage deformation due to an on-board explosion. Again, it should be noted that for both pressurized and un-pressurized load cases, the peak strain (reached at approximately

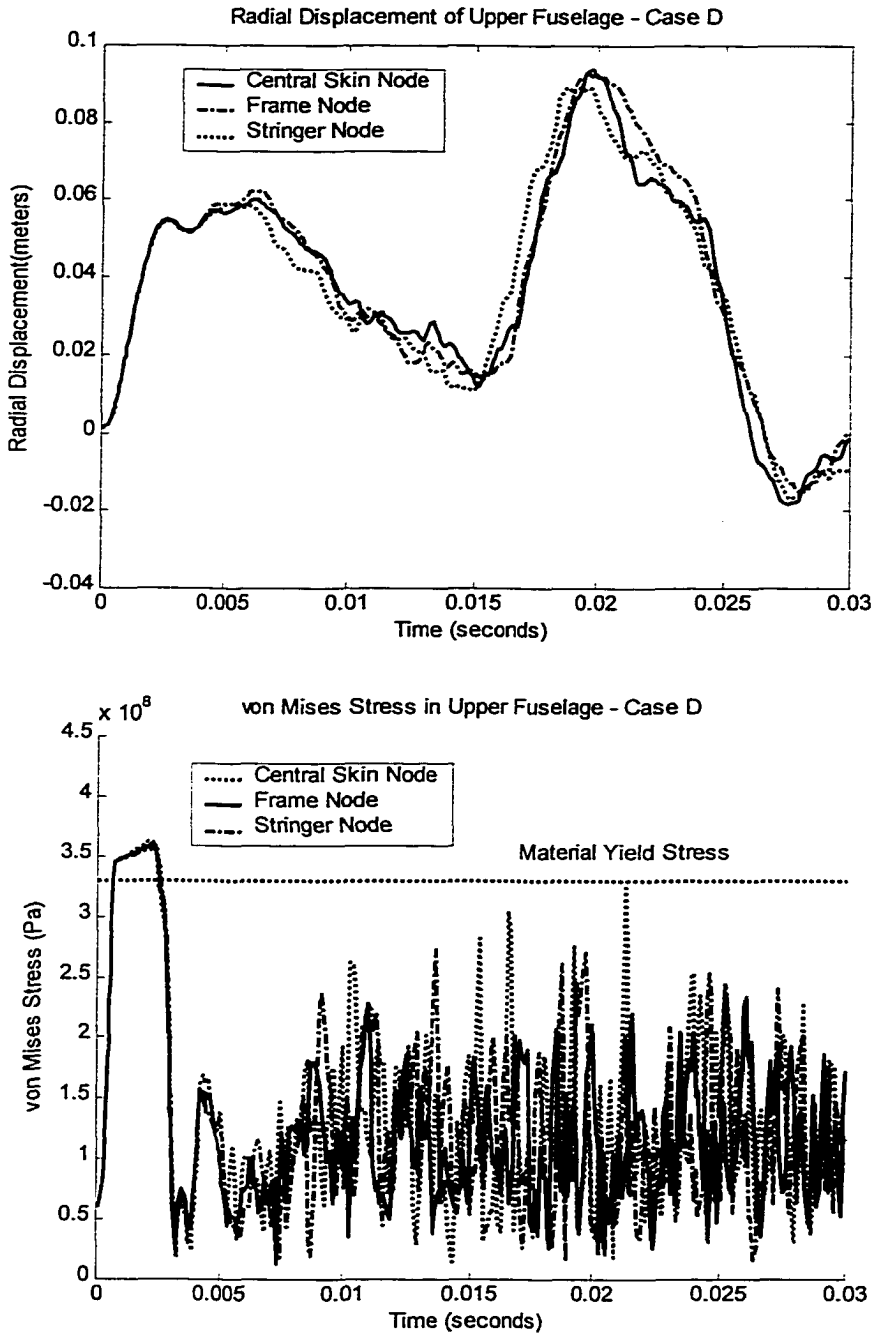

Figure 66. Radial Displacements and von Mises Stress in the Upper Fuselage for Elastic-Plastic Finite Element Model Under Load Case D.

Table 28

Summary of Maximum Predicted von Mises Stress for Pressurized Fuselage Elastic-Plastic Analysis – Load Case D

Node Location	Maximum von Mises Stress	Material Yield Stress
Central to Frame and Stringer	0.360 MPa	0.33 MPA
Frame-Skin Interface	0.357 MPa	0.33 MPA
Stringer-Skin Interface	0.363 MPa	0.33 MPA

2.1 milliseconds after the blast contacts the fuselage wall) is still well below the material strain limit for aluminum 2024-T3. The implications of this fact will be discussed later in the conclusions section for this chapter.

Case E – 50 Millisecond Delay of Pressure Pulse on Pressurized Fuselage While Venting

As previously mentioned (Chapter 1 – Background), the combination of venting an aircraft fuselage in conjunction with other methods of absorbing or slowing blast pressures has been proposed as a potential counter-measure to on-board explosions (Anon, 1990, and Ashely, 1992). With this in mind, a final transient pressure loading case is considered in which the explosive pressure loading of the aircraft structure is delayed for a brief time while the venting process acts to release cabin pressurization. Although the practical feasibility of this concept is not known, it

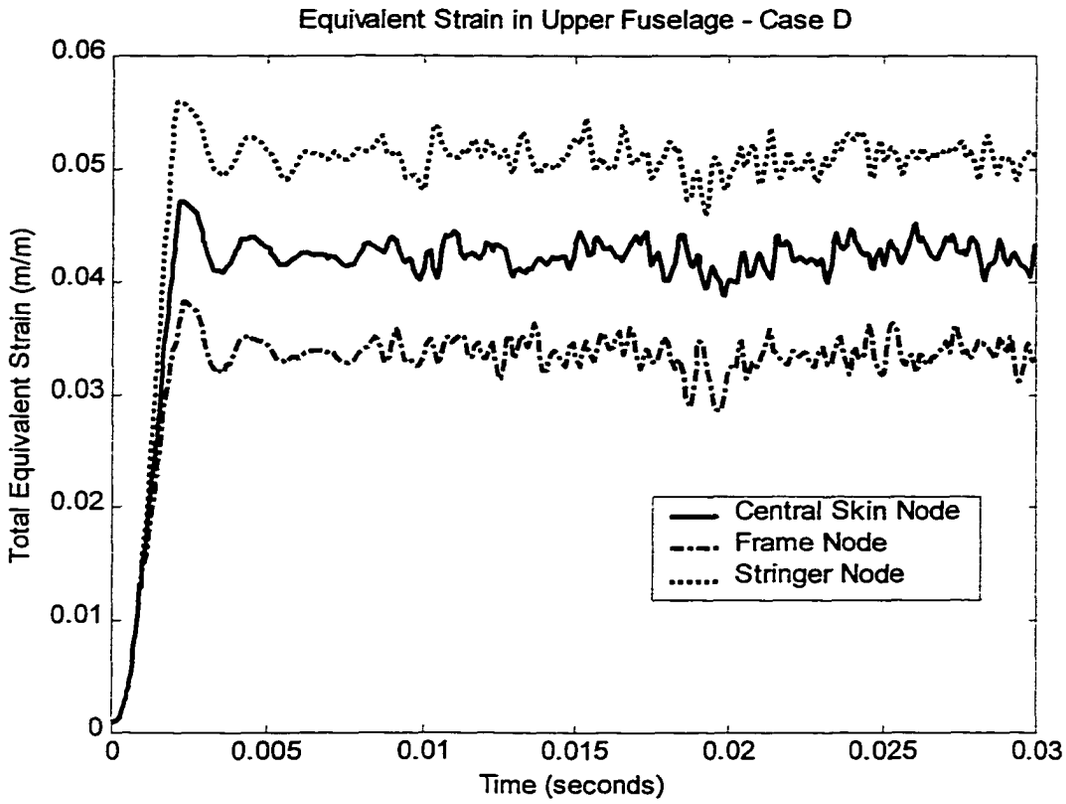

Figure 67. Total Equivalent Strain in the Upper Fuselage for Elastic-Plastic Finite Element Model Under Load Case D.

Table 29

Maximum Predicted Total Equivalent Strain for Unpressurized Fuselage Elastic-Plastic Analysis – Load Case D

Node Location	Maximum Total Equivalent Strain (%)	Material Strain Limit (%)
Central to Frame and Stringer	4.7 %	18.6 %
Frame-Skin Interface	3.8 %	18.6 %
Stringer-Skin Interface	5.6 %	18.6 %

is possible that energy absorbing structures inside the aircraft such as walls or luggage containers may be able to slow the blast loading of the structure enough to significantly reduce the pre-pressurization of the structure by venting cabin pressurization. For this final analysis (Case E), a time delay of 50 milliseconds has been arbitrarily selected to examine the effects of a delayed blast loading on the resulting structural damage. For the previously described 0.190 second decompression time (considering all 68 windows of a Boeing 737-700 are used as vents – Chapter V), the cabin pressurization will have dropped to approximately 22% of its original value (51.7 KPa to 11.5 KPa) by the time the pressure pulse arrives (Figure 68).

Case E Results-Assumed Elastic-Plastic Material Properties

For this load case, a pre-stressed transient analysis of the previously described fuselage model was conducted. This was accomplished by solving the static solution for the case of internal pressurization alone, and using the results as initial conditions for the transient pressure pulse loading. As in case C, the transient pressures used were a combination of explosive pressures and the decaying cabin pressurization. The analysis was conducted for a 60 millisecond time duration and the resulting radial displacements and von Mises stresses (Figure 69 and Table 30) were calculated. Note that the radial displacements and stress in the fuselage decrease initially as the cabin pressurization is vented. The subsequent blast loading occurs on a structure with a

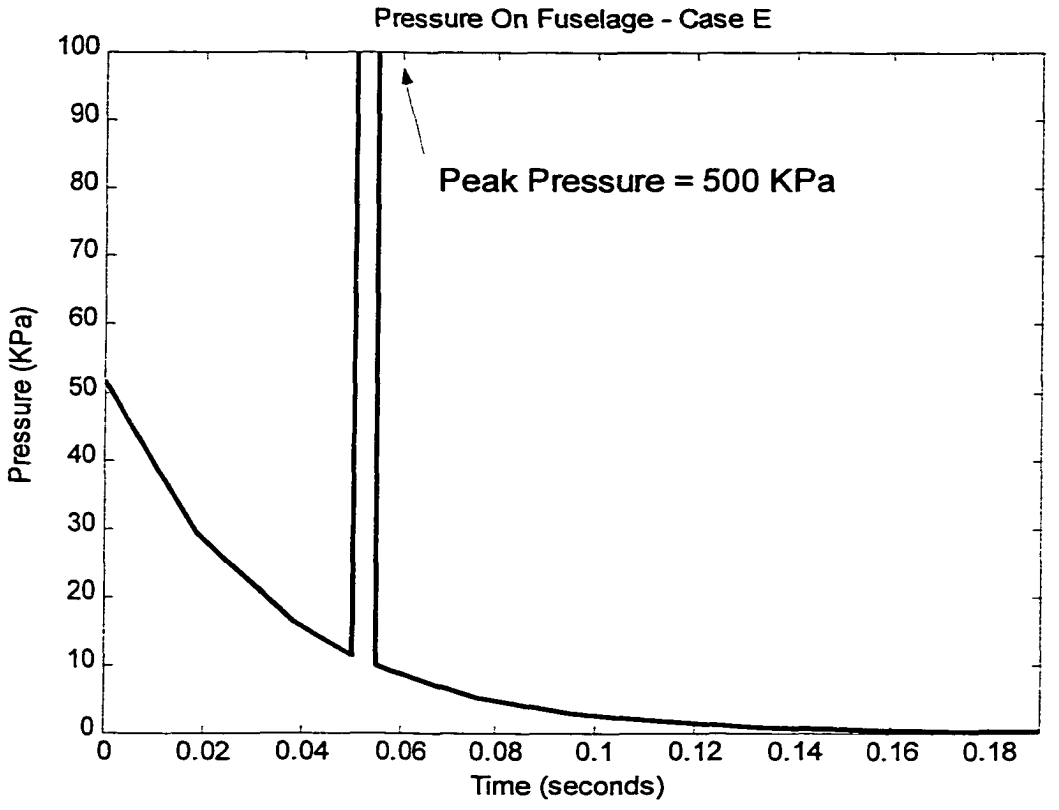

Figure 68. Transient Pressure on Fuselage for Case E in Which Explosive Blast Loading of Structure is Delayed by 50 Milliseconds.

significantly reduced amount of pre-loading.

The total equivalent strains in the fuselage for load case E were also determined (Figure 70, Table 31). Similar to previous load cases, the peak strain in the structure was reached rather quickly (within about 2 milliseconds after the blast arrival). It is also interesting to note that the peak strains in the fuselage for load case E are essentially the same as those found in the case of the unpressurized fuselage (Table 25). This indicates that a 50-millisecond delay in the arrival of the explosive

blast at the fuselage walls will allow the active venting system enough time to function to eliminate increased structural damage due to cabin pressurization.

Conclusions

Several important conclusions can be drawn from the results of the structural response analysis of the fuselage. First, it is important to note the difference in predicted structural blast damage for a pressurized and unpressurized fuselage. When subjected to the same pressure pulse, the unpressurized fuselage model has peak strains in the fuselage skin of 30 to 40 percent less than the pressurized model. Thus, pre-stressing the fuselage with cabin pressurization would increase the magnitude of aircraft structural damage from an on-board explosions.

A second conclusion that can be drawn from the structural analysis relates to the speed at which the pressurized structure reaches peak strains. The ANSYS model predicts that peak strains in the upper fuselage are achieved within about 2 milliseconds after the blast contacts the structure. When compared with the previously determined response time for an active venting system, it appears that even the fastest venting system imagined would not function quickly enough to reduce peak structural strains due to the initial explosive blast impact.

Another very important finding of this analysis is the fact that the initial blast loading of the structure did not lead to strains which exceeded the strain limits of the fuselage skin material. Thus, although the active venting system may not be effective in

reducing strains in the structure due to the initial blast impact (which occur within about 2 milliseconds after the blast contacts the fuselage), the overall strain levels for pressurized and unpressurized load cases remained below the failure threshold for the material. As mentioned previously this result was quite surprising considering the magnitude of the blast pulse used in this analysis. There are several possible explanations for this result. First, the finite element model used in this analysis did not include structural details such as rivet joints between reinforcing frames and fuselage skin and between adjacent skin panels. Also, the sole failure mode considered in this analysis was tearing of the fuselage skin. Thus, it is possible that an actual fuselage structure under explosive loading may suffer greater damage, through rivet pull-out or fracture or skin tearing at localized stress concentrations, than predicted for this model. The results of this model also suggest that the initial contact of the blast wave on the structure may not be sufficient on its own to impart catastrophic failure on the structure. After the initial blast wave contacts the structure, subsequent reflections and the significant overall increase in cabin pressure may pose the added loading which ultimately fails the structure. To this point, the report on the bombing of Pan Am flight 103 over Lockerbie, Scotland describes this process in detail as follows:

> "Following immediately behind the primary shockwave, a secondary high pressure wave – partly caused by reflections .... but mainly by the general pressure rise caused by the chemical conversion of solid explosive material to high temperature gas emerged" (from the location of the explosive detonation) (Anon., 1990).

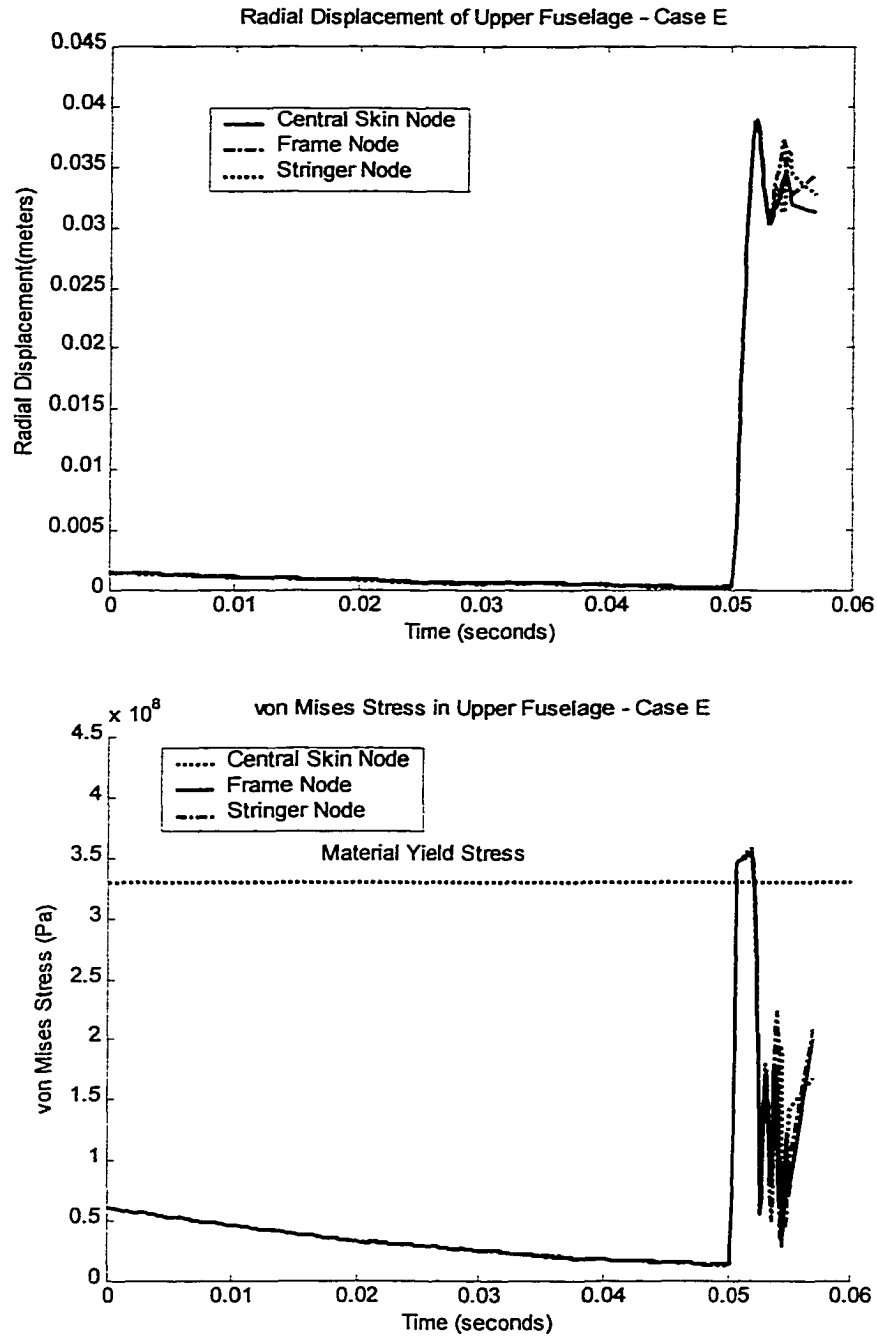

Figure 69. Radial Displacements and von Mises Stress in the Upper Fuselage for Elastic-Plastic Finite Element Model Under Load Case E.

Table 30

Summary of Maximum Predicted von Mises Stress for Pressurized Fuselage Elastic-Plastic Analysis - Load Case E

Node Location	Maximum von Mises Stress	Material Yield Stress
Central to Frame and Stringer	0.355 MPa	0.33 MPA
Frame-Skin Interface	0.353 MPa	0.33 MPA
Stringer-Skin Interface	0.358 MPa	0.33 MPA

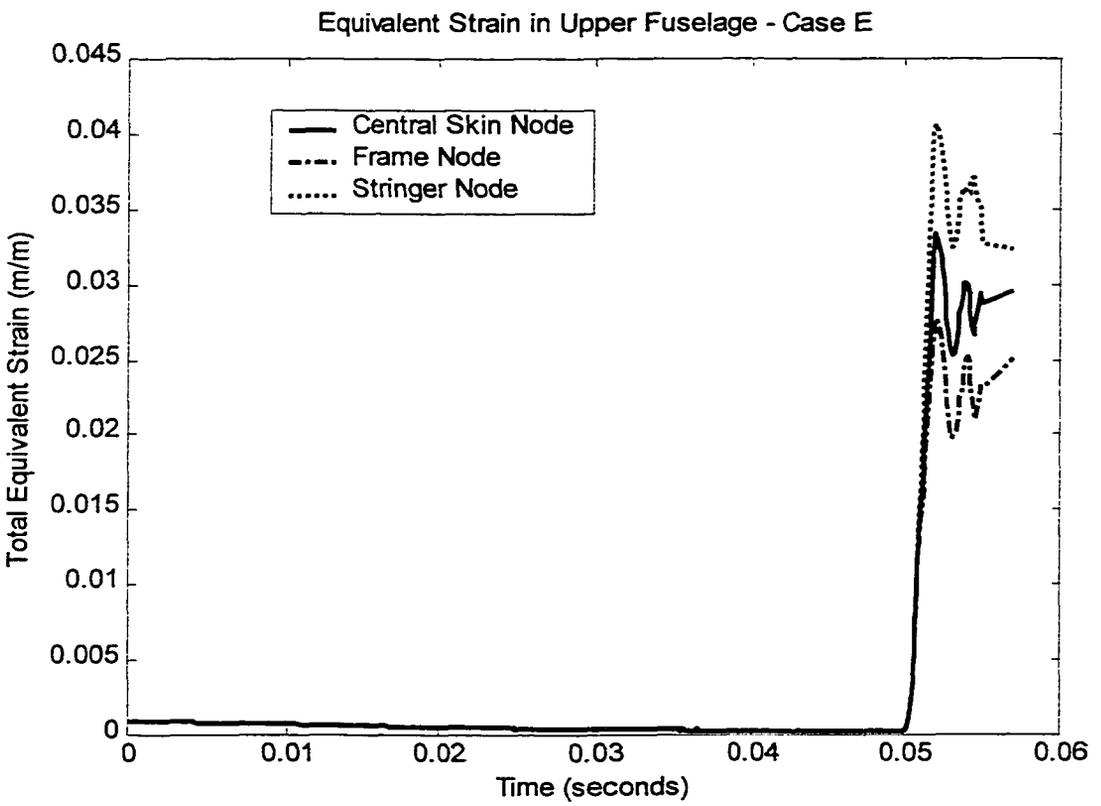

Figure 70. Total Equivalent Strain in the Upper Fuselage for Elastic-Plastic Finite Element Model Under Load Case E.

Table 31

Maximum Predicted Total Equivalent Strain for Unpressurized Fuselage Elastic-Plastic Analysis - Load Case E

Node Location	Maximum Total Equivalent Strain (%)	Material Strain Limit (%)
Central to Frame and Stringer	3.3 %	18.6 %
Frame-Skin Interface	2.8 %	18.6 %
Stringer-Skin Interface	4.2 %	18.6 %

For this reason, considering only the first contact of the explosive shock wave with the structure may not be adequate to predict the fuselage blast damage. This may also indicate that the actual catastrophic damage to the structure may occur later than originally thought. So, while peak incident strains are seen within about 2 milliseconds after fuselage contact, strains which exceed the material limits may not occur until some time later. If this hypothesis can be confirmed, an active venting system may indeed be capable of functioning rapidly enough to reduce the catastrophic fuselage damage.

Finally, it is important to conclude by stating the limitations of the current analysis. First of all, this study considered only a single pressure pulse which represents an explosive placed at the center of the fuselage radius. The resulting explosive shock front was assumed to pass freely through the interior aircraft cabin air without contacting solid objects such as seats, walls, and floors. In a real event, the

exact pressure loading on the fuselage would be altered by the original location of the explosive and by the effects of interaction with and reflections from solid and absorbent surfaces. The magnitude and time duration of the pressure pulse would also vary depending on the type and quantity of the explosive material used in the device. Additionally, the current study considered only a simplified portion of the aircraft fuselage for analysis without details such as riveted joint connections between adjoining fuselage panels and between the fuselage skin and reinforcing frames and stringers.

Even with these stated limitations (and others not mentioned), however, it is believed that the current study represents a reasonable analysis of the typical structural behavior that could be expected in an actual explosive loading of a commercial aircraft. The results are intended to serve as a guide for characterizing the damage and time scale of damage initiation for an explosive detonation inside an aircraft fuselage.

CHAPTER VII

CONCLUSIONS AND RECOMMENDATIONS

General Conclusions

In an effort to increase the resistance of commercial aircraft to damage caused by the on-board detonation of an explosive device, the current study examined the method of active fuselage pressure venting. Overall the study was successful in determining reasonable time estimates for the sequence of events involved in an explosive detonation and in the subsequent functioning of an active venting system.

The challenge of quickly and accurately sensing the detonation of an explosive device which could be located virtually anywhere inside an aircraft requires the use of an array of pressure sensors. In actual practice, the spacing of these sensors would be limited by cost, weight and the lack of physical mounting locations within the aircraft. For this study, the sensors were assumed to be placed at approximately 1.0 to 2.0 meter intervals. This resulted in a total estimated time required to detect an explosive event and to send the appropriate output signal to an actuation system of up to 3.0 milliseconds.

The actuation system analysis assumed the use of various styles of pyrotechnic actuators to achieve a rapid (on the order of 0.1 to 0.2 milliseconds) initiation of a vent opening. The response times of a scale-model hinged vent panel and a fracturable vent panel were predicted using simple differential equations of

motion and the results correlated well with experimental measurements. Additionally, the response time of three styles of full-size active vent panels (a hinged vent panel, a fracturable vent panel, and an edge-perforated vent panel) were considered. The predicted results for all three panels were generally quite similar with response times on the order of 5.0 to 7.0 milliseconds. These values are based on the time required for the vent panels to move from a rest position to a sufficient distance away from the fuselage in order to create an unobstructed vent opening. This inertia-based time of response made up the longest duration time event in the active venting process.

In order to establish the time required to vent an aircraft fuselage under a variety of conditions, scale-model experiments of two pressure vessels were used. The experimental results correlated well with an analytical model which related decompression time largely as a function of the initial air volume inside the fuselage and the cross-sectional area of the vent opening. With this method it was predicted that a total decompression of a typical commercial aircraft could occur within 0.5 seconds if 12 to 26 (depending on the aircraft altitude) of the 68 total aircraft windows were used as vent openings. For comparison purposes, if all 68 aircraft windows were used as vent openings, fuselage decompression times in the range of 0.09 to 0.19 seconds can be expected.

Finally, incorporating these time durations into a sequence of events, the structural response of a portion of a typical commercial aircraft fuselage was determined through a dynamic finite element analysis. From this approach, it was determined that the amount of structural damage of an aircraft from an internal explosion is increased by the pre-stressing of the fuselage due to in-flight cabin

pressurization. This result was anticipated and was the main impetus behind the active venting method explored in this study. Interestingly, it was determined that for both pressurized and unpressurized fuselage models considered, peak strains in the structure remained well below the ultimate limit of the aluminum skin material. Thus, although peak strains in the pressurized fuselage were 30 to 40 percent larger than for the unpressurized case, ultimate failure of the aluminum skin is not predicted in either case.

From these results it can be concluded that an active venting system can be designed to rapidly (within about 1.6 – 7.0 milliseconds of the explosive detonation) initiate the release of cabin pressurization in the event of an on-board explosion. Peak fuselage strains, however, which occur within about 3.6 milliseconds of the explosive detonation, are essentially the same as for an unvented fuselage under identical blast loading. For this reason, it is concluded that the proposed active venting system will not function rapidly enough to reduce the additional peak fuselage strains due to cabin pressurization. However, since the predicted fuselage strains for all load cases considered do not exceed the material limit of the fuselage skin, ultimate failure due to the incident blast wave is not predicted. From this data it is theorized that the ultimate failure in the fuselage under blast loading may be due to additional failure modes such as rivet joint separation (not considered in this model), or due to reflected blast pressures and the general rise in cabin ambient pressure following the detonation. Thus it is possible that the aircraft structure may survive the initial shock wave contact (occuring within the first 5 milliseconds after the blast) but fail under subsequent pressure loading, unless this loading is reduced through venting.

An additional conclusion regards the effects of delaying the blast loading of the fuselage structure by some small time duration in order to allow the fuselage to vent sufficiently. From this analysis, an arbitrarily selected time delay of 50-milliseconds between explosive detonation and blast-fuselage contact was sufficient to reduce the strain magnitude of a pressurized fuselage to that of the unpressurized case.

Recommendations for Future Work

The results of this study indicate the merit of pursuing additional work on the active venting concept. Future work should seek to determine realistic pressure profiles inside of an actual aircraft fuselage following an explosive detonation. It is likely that much of this transient pressure data already exists from prior explosive testing on full-scale aircraft, including the effects of pressure reflections and secondary shock waves. A logical extension of this work would be to then update the transient pressure load data in the existing finite element model from a simple exponential decay function to actual measured blast pressure data.

Additionally, the effects of adding more detail to the fuselage model would be helpful for evaluating additional failure modes of the structure. Although this may be difficult with the large model of the fuselage shell used in this study, a smaller model may still yield useful results. For example, explosive damage predictions could be conducted for a smaller stiffened shell panel that contains features which more closely resembles the construction of a commercial aircraft. The shell model could include rivet joints between the fuselage skin and reinforcing members and also

between adjacent skin panel members. In order to provide a realistic structural analysis, the pull-out strength and ultimate tensile strength of the rivets would need to be considered.

Another, more basic investigation involves determining the effects of peak explosive pressures and pulse durations on pressurized fuselage damage. Previously, Gefken, Simons, and Sanai (1993) studied the effects of explosive peak pressures and impulses on the damage to unpressurized aluminum plates (small flat plates were used to simulate aircraft skin and to allow for experimental verification of analytical predictions of blast damage). In order to extend this work to account for various flight altitudes, several levels of static pre-pressurization could be employed in a transient finite element analysis of aluminum plates subjected to explosive pressure pulses. By varying the peak pressures and impulses of the modeled shock wave, a damage threshold for aluminum aircraft skin can be plotted on a pressure-impulse (PI) diagram. Using the PI damage plot, an evaluation can be made of the altitude-dependant aircraft vulnerability to explosives of various sizes which are detonated in varying proximity to the fuselage.

A final area for future work involves the combination of methods for delaying explosive blast wave propagation and a venting system. It was shown in this study that a 50-millisecond delay in blast loading of the structure would be sufficient to reduce the damage magnitude of a pressurized cabin to that of an unpressurized fuselage. For this reason, methods which slow the release or propagation of an explosive pressure wave inside an aircraft should be considered as a means of improving the effectiveness of a venting system. Any system which increases the

elapsed time from the detonation of an explosion to the subsequent pressure loading of the fuselage (even by times as short as 50 milliseconds) could allow an active venting system to function effectively. Further research is needed to examine the effect of blast delay time on fuselage damage. In particular, various blast delay times between 0 and 50 milliseconds should be considered. Once a minimum delay time has been established which minimizes fuselage damage, an examination of methods for delaying the explosive shock loading of an aircraft fuselage such as energy absorbing members including luggage containers, internal walls, or wall linings should be conducted. Through this research it is proposed to verify the supposition that an active venting system used in conjunction with methods for delaying blast propagation could significantly decrease the vulnerability of a commercial aircraft to on-board explosions.

APPENDIX

Convergence Study for Number of Elements Used in the Fuselage Model

Finite Element Models of Fuselage Section

The structural response section of this document utilizes a finite element model with shell elements with dimensions of 0.0508 by 0.0508 meters (2.0 by 2.0 inches). Accordingly, the beam elements used to model the stringers and frames have a length of 0.0508 meters (2.0 inches). In order to evaluate the adequacy of this element size for predicting the static and transient behavior of the fuselage structure, two additional finite element mesh schemes were analyzed (Table A.1).

Table A.1

Description of Finite Element Mesh Schemes Used in This Convergence Study

FEA Model #	Element Size (for Shell Elements)	Total Number of Nodes	Total Number of Elements
1	0.1016 x 0.1016 meters (4.0 x 4.0 inches)	1,296	2,199
2	0.0508 x 0.0508 meters (2.0 x 2.0 inches)	5,041	6,775
3	0.0338 x 0.0338 meters (1.33 x 1.33 inch)	11,025	13,836

Results and Conclusions

Static Analysis

The radial displacements (Table A.2, Figure A.1) and von Mises Stress (Table A.3, Figure A.2) of the upper fuselage under static pressurization of 51.7 KPa were found using the three different mesh densities.

Table A.2

Static Loading Comparison of Radial Displacement for Three Mesh Densities

Nodal Location	#1 - Coarse Mesh (% Deviation From #2)	#2 - Fine Mesh	#3 - Very Fine Mesh (% Deviation From #2)
Mid-Stringer Node	0.59 mm (-9.2%)	0.65 mm	0.61 mm (-6.15%)
Mid-Frame Node	0.43 mm (-6.52%)	0.46 mm	0.44 mm (-4.35%)
Central Skin Node	1.78 mm (2.89%)	1.73 mm	1.69 mm (-2.31%)

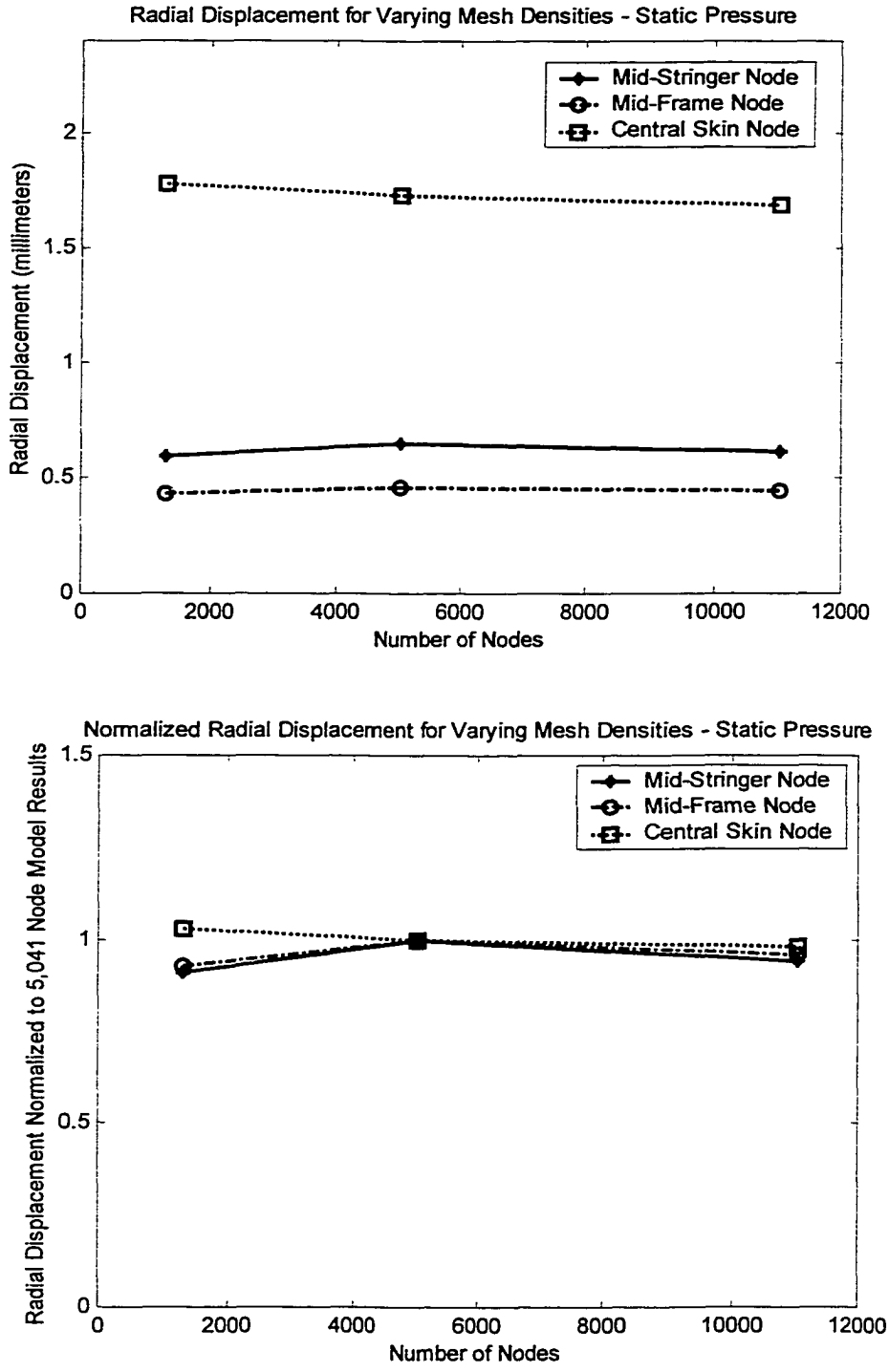

Figure A.1 Radial Displacements in the Upper Fuselage for Three Different Finite Element Mesh Sizes. Actual Displacements (Top) and Displacements Normalized to 5,041 Node Model (Bottom).

Table A.3

Static Loading Comparison of von Mises Stress for Three Mesh Densities

Nodal Location	#1 - Coarse Mesh (% Deviation From #2)	#2 – Fine Mesh	#3 - Very Fine Mesh (% Deviation From #2)
Mid-Stringer Node	0.0814 MPa (-8.95%)	0.0894 MPa	0.0928 MPa (3.80%)
Mid-Frame Node	0.0444 MPa (-26.62%)	0.0605 MPa	0.0639 MPa (5.62%)
Central Skin Node	0.0237 MPa (-7.78%)	0.0257 MPa	0.0257 MPa (0.0%)

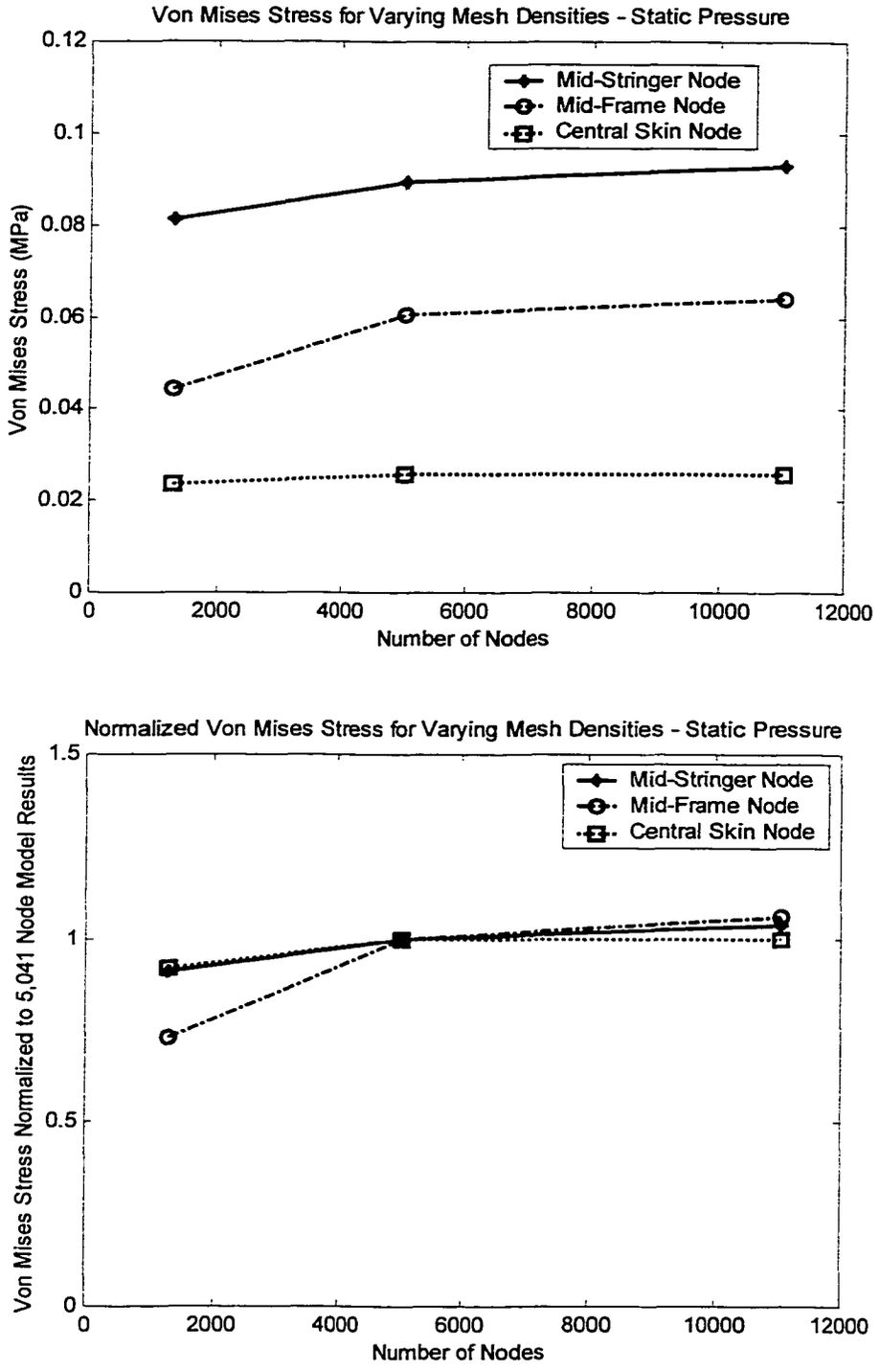

Figure A.2 Von Mises Stress in the Upper Fuselage for Three Different Finite Element Mesh Sizes. Actual von Mises Stress (Top) and von Mises Stress Normalized to 5,041 Node Model (Bottom).

In general, the results for static pressurization showed the use of a 0.0508 by 0.0508 meter (2.0 by 2.0 inch) element size to be adequate for this analysis. Significant changes in the element size used in the model resulted in result variations of less than 10 percent for calculated radial displacements. For calculating the secondary quantity of von Mises stress it appears that the element size of 0.0508 by 0.0508 meter (2.0 by 2.0 inch) is sufficient for reasonable accuracy. This is apparent in the fact that refining the mesh further results in less than five percent variation in predicted stress values. It is interesting to note from this study that the coarse mesh (mesh #1) does not appear adequate for calculating stress, especially for considering the results from the mid-frame node.

Modal Analysis

A modal analysis was also conducted on the fuselage model for the three different mesh densities (Table A.4 and A.5). In general, the first five natural frequencies for both pressurized and unpressurized fuselage models for all three mesh densities varied by less than 13%. Although a monotonic convergence was expected, this was not observed for the modal analysis and also for the radial displacements. This could possibly be effected by small deviations in the size of the fuselage windows and window frame members used in the three different mesh sizes.

Table A.4

Modal Analysis of Unpressurized Fuselage Models for Varying Mesh Densities

Mode	#1 - Coarse Mesh Predicted Natural Frequency (Hertz)	#2 - Fine Mesh Predicted Natural Frequency (Hertz)	#3 – Very Fine Mesh Predicted Natural Frequency (Hertz)
1	59.2	58.5	60.0
2	65.7	65.6	68.1
3	76.6	72.3	78.8
4	91.1	83.4	92.3
5	102	106.7	105.5

Table A.5

Summary of Modal Analysis of Pressurized Fuselage Models for Varying Mesh Densities

Mode	#1 – Coarse Mesh Pressurized Fuselage Predicted Natural Frequency (Hertz)	#2 - Fine Mesh Pressurized Fuselage Predicted Natural Frequency (Hertz)	#3 – Very Fine Mesh Pressurized Fuselage Predicted Natural Frequency (Hertz)
1	65.6	63.9	66.8
2	70.9	70.7	74.0
3	80.2	76.8	82.3
4	101.6	91.1	103.1
5	107.7	112.9	111.7

Transient Analysis

A final analysis was conducted to determine the effect of mesh size on the transient response of the fuselage model. Using explosive pressure loading (load case A from Figure 56), the transient stress and displacement response of the fuselage model was determined for element sizes of 0.1016 by 0.1016 meters (4.0 by 4.0 inches) and 0.0508 by 0.0508 meters (2.0 by 2.0 inches) (Figures A.3, A.4, A.5). Although no quantitative comparison of the responses is given, the transient values for both mesh densities appear to agree quite favorably.

Determination of Appropriate Mesh Density

By way of comparison, it is also interesting to note the reported element size used by others to model the transient behavior of commercial aircraft fuselage. Kanninen, Marchand, and O'Donoghue (1992) used 0.091 to 0.124 meter (3.6" to 4.9") element edge lengths. Moon, Bharatram, Schimmels, and Venkayya (1995) used an element size of 0.0508 by 0.0508 meters (2.0 by 2.0 inches).

Based on the results of this convergence study and on a comparison with previously reported finite element models, an element size of 0.0508 by 0.0508 meters (2.0 by 2.0 inches) was deemed adequate for use in this study. Additionally, it should be noted that a significant increase in computer solution time was observed for fuselage models with shell element sizes of less than 0.0508 by 0.0508 meters (2.0 by 2.0 inches). Thus, the small change in solution accuracy obtained from a finer mesh was not considered worth the associated expense of increased computer solution time.

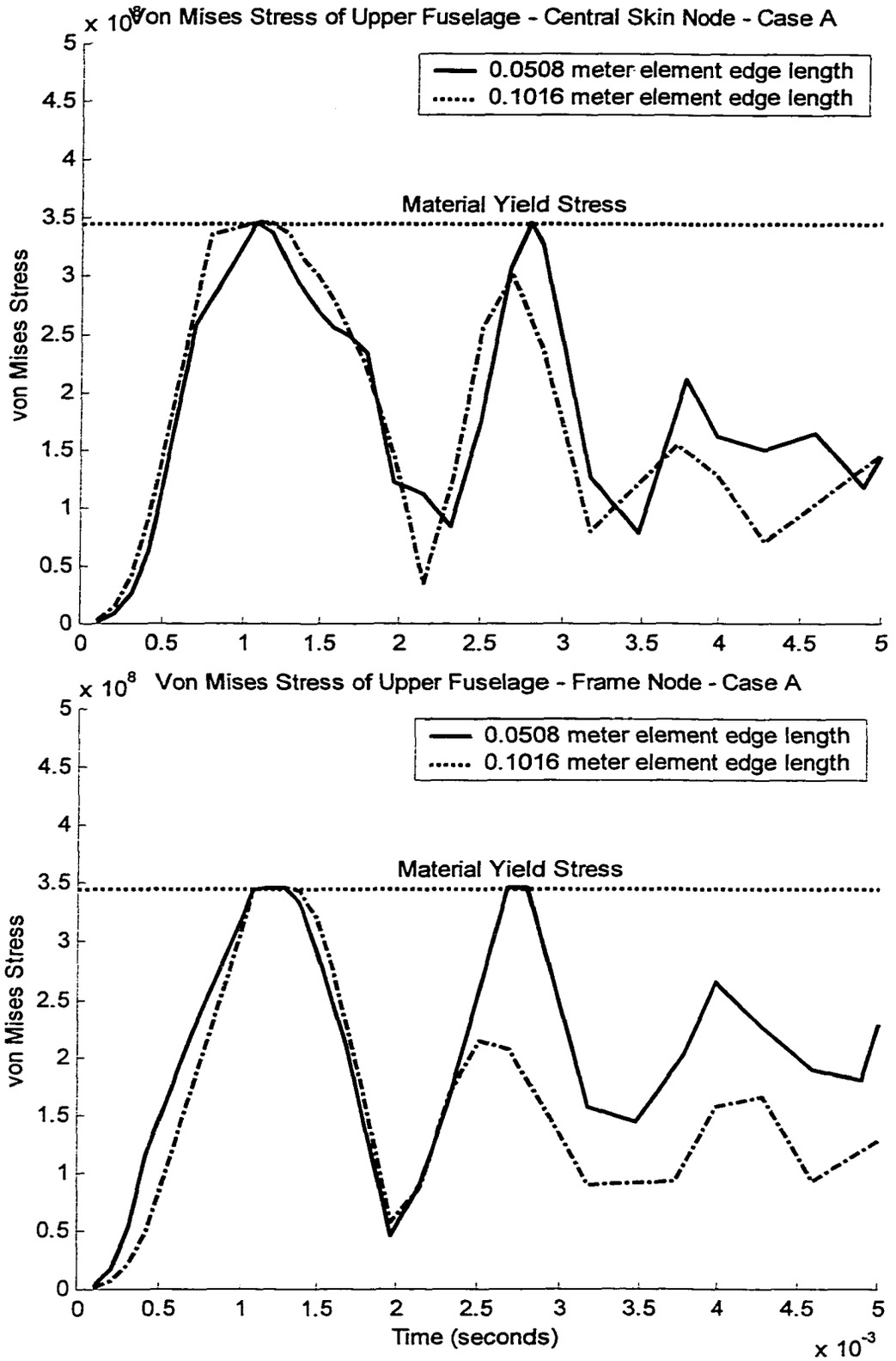

Figure A.3. Transient Von Mises Stress in the Upper Fuselage for a Central Skin Node (Top) and a Mid-Frame Node (Bottom) for Two Finite Element Mesh Sizes.

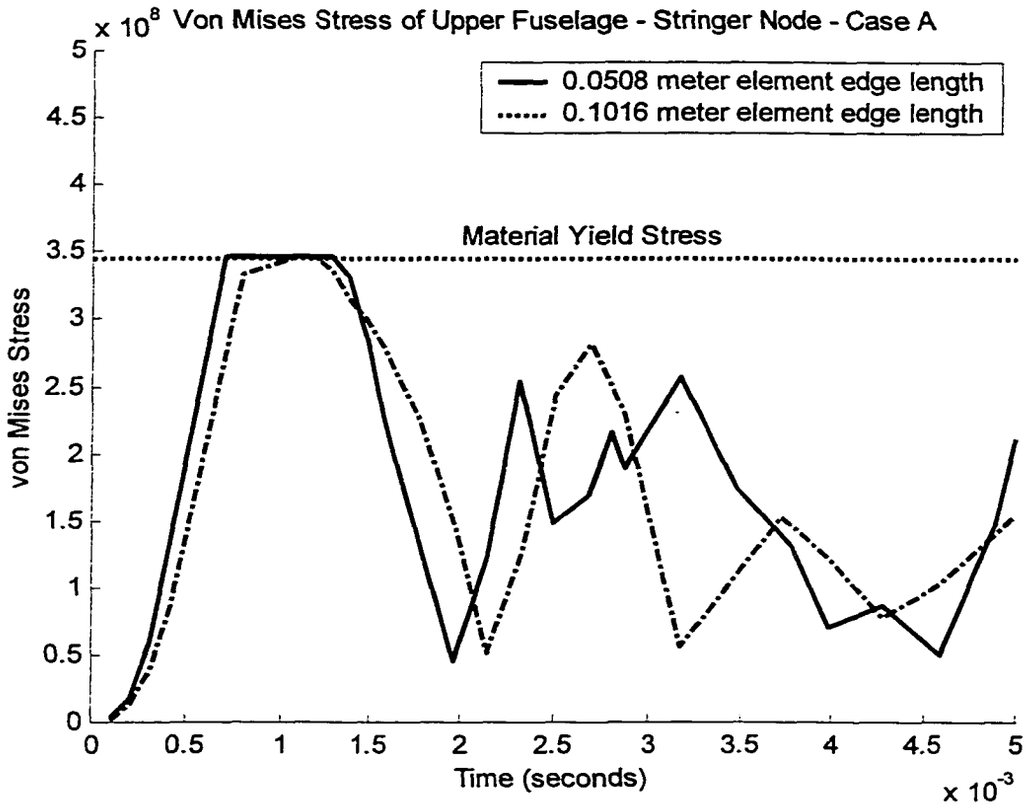

Figure A.4. Transient Von Mises Stress in the Upper Fuselage for a Mid-Stringer Node for Two Finite Element Mesh Sizes.

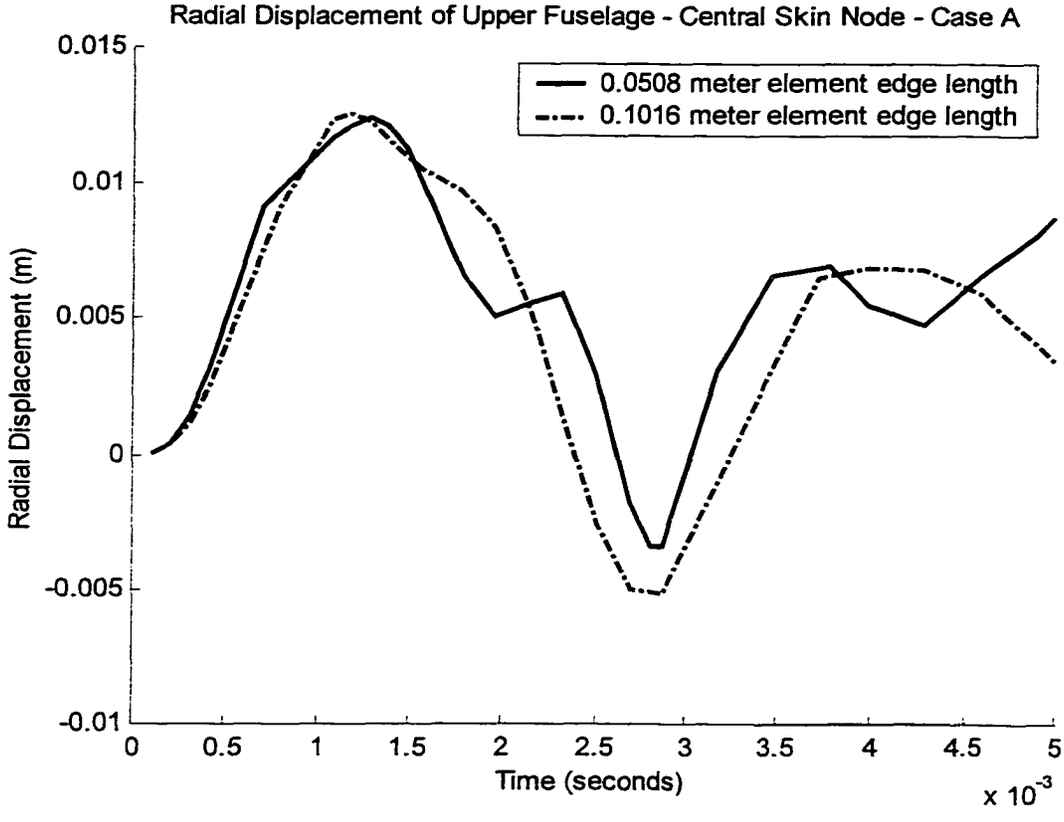

Figure A.5. Transient Radial Displacements for a Central Skin Node Under Explosive Pressure Loading.

BIBLIOGRAPHY

Anon. (1979). Metals Handbook – Ninth Addition, Volume 2. American Society for Metals: Metals Park, Ohio.

Anon. (1997). ANSYS Elements Reference Manual, 9th Edition. Section 4.181 – Finite Strain Shell. ANSYS Release 5.4, ANSYS Inc., Canonsburg, PA.

Anon. (1997). ANSYS Elements Reference Manual, 9th Edition. Section 19.12 – POST1 and POST26 – Interpretation of Equivalent Strains. ANSYS Release 5.4, ANSYS Inc., Canonsburg, PA.

Anon. (1994). Aviation Security: Development of New Security Has Not Met Expectations - Report GAO/RCED-94-142. U.S. General Accounting Office. Washington, D.C.

Anon. (2000). *The Boeing Corporation Home Page.* <http://www.boeing.com>. (2000, March 28).

Anon. (1993). Convention on the Marking of Plastic Explosives for the Purpose of Detection: 103d Congress - Senate Treaty Document 103-8..: U.S. Government Printing Office. Washington D.C.

Anon. (1958) Fusleage Stress Analysis for 707-300 and 400 Series Airplane, Vol. I, II, III, and IV. Seattle, WA.: Boeing Airplane Co.

Anon. (1990). Report on the accident to Boeing 747-121, N739A at Lockerbie, Dumfriesshire, Scotland on 21 December 1988, Aircraft Accident Report 2/90, United Kingdom Air Accidents Investigations Branch, HMO, London.

Ashley, S. (1992, June). Safety in the Sky: Designing Bomb-Resistant Baggage Containers. *Mechanical Engineering,* 81-86.

Auode, S. (1999). *The ultimate plane crash database.* <http://www.geocities.com/CapitolHill/5260/> (1999, September 7).

Baker, W.E. (1973). Explosions in Air. Austin: University of Texas Press.

Bangash, M.Y.H. (1993). Impact and Explosion. Boca Raton: CRC Press.

Bement, L.J. and Schimmel, M.L. (1995). A Manual for Pyrotechnic Design, Development, and Qualification. Hampton, Virginia: NASA.

Bement, L.J. (1980). Emergency In-Flight Egress Opening for General Aviation Aircraft, Hampton, Virginia: NASA.

Bruhn, E.F. (1973). Analysis and Design of Flight Vehicle Structures. USA: Tri-State Offset Company

Chan, P.C., and Klein, H.H. (1992, December). Study of Blast Effects Inside an Aircraft Fuselage. Proceedings FAA Aircraft Hardening and Survivability Symposium. (pp. 312-328).

Chen, V.L. (1997, February). First Sucessful Simulation of On-Board Explosion Will Aid in Aircraft Hardening Studies, Simulation, 107-110.

De Remer, D. (1992). Aircraft Systems for Pilots. Casper, Wyoming: IAP, Inc.

Ewing, M.S., Kivity, Y., and Lenselink, H. (1992, December). Internal Blast Response of a Ring-Reinforced Thin-Walled, Right Circular Cylinder: Analysis and Test. Proceedings FAA Aircraft Hardening and Survivability Symposium. (pp. 312-328).

Felback, D.T. (1984). Strength and Fracture of Engineering Solids. Englewood Cliffs, New Jersey: Prentice-Hall, Inc.

Fox, R.W., and McDonald, A.T. (1985). Introduction to Fluid Mechanics. New York: John Wiley and Sons.

Gefken, P.R., Simons, J.W., and Sanai, M. (November 1993). Blast Damage Assessment Methodology for Terrorist Bomb Attacks on Aircraft: Quarterly Progress Report. Menlo Park California: SRI International.

Glasstone, S., and Dolan, P.J. (1977). The Effects of Nuclear Weapons. US Government Printing Office. Washington D.C.

Greenwald, A.J., and McIver, R.G. (1967). Cabin Pressurization Characteristics of USAF and Commercial Transport Aircraft. Brooks Air Force Base, Texas: USAF School of Aviation Medicine.

Grubelich, M.C., and Bickes, R.W. (June 1992). A Semiconductor Bridge Ignited Hot Gas Piston Ejector. First NASA Aerospace Pyrotechnic Systems Workshop, (pp. 93-121).

Haber, F., and Clamman, H.G. (1953). Physics and Engineering or Rapid Decompression: A General Theory of Rapid Decompression. Randolph Field, Texas: USAF School of Aviation Medicine

Kanninen, M.F., Marchand, K.A., and O'Donoghue, P.E. (December 1992). An Advanced Fracture Mechanics Analysis of Deformation and Fracture in Aircraft Fuselages Subjected to On-Board Blast Loadings. Proceedings FAA Aircraft Hardening and Survivability Symposium. (pp. 57-89).

Kamoulakos, A., Chen, V., Mestreau, E., Lohner, R. (1996). Finite element Modeling of Fluid/Structure Interaction in Explosively Loaded Aircraft Fuselage Panels Using PAMSHOCK/PAMFLOW Coupling. <http://www.esi.fr/pubs/papers/explosiv/explosiv.html> (1997, December 4).

Kistler Product Literature (1995). Advanced Instrumentation for a World of Applications, Kistler Instrument Corporation.

Kurtz, A. (1993). Overview-Wright Laboratory Support. Proceedings of Transport Aircraft Survivability Conference. (pp. 61-83).

McFadden, E.B. (1979). Oxygen Equipment and Rapid Decompression Studies. Oklahoma City, Oklahoma: FAA Civil Aeromedical Institute.

Mendelson, A. (1968). Plasticity: Theory and Application. New York: The Macmillan Company.

Mlakar, P.F. (1997). U.S. Patent No. 5,595,431 – Hardened Aircraft Unit Load Device. Washington, D.C.: United States Patent and Trademark Office.

Mlakar, P. F., Klein, H. H., and Smith, J.L. (1992). Hardened Unit Load Devices. Proceedings FAA Aircraft Hardening and Survivability Symposium, (1-7).

Mlakar, P.F., and Smith, J.L. (1997). U.S. Patent No. 5,599,082 – Hardened Aircraft Unit Load Device. Washington, D.C.: United States Patent and Trademark Office.

Moon, Y., Bharatram, G., Schimmels, S., and Venkayya, V. (1995) Vulnerability and Survivability Analysis of Aircraft Fuselage Subjected to Internal Detonations. MSC 1995 World Users' Conference Proceedings. <http://www.mechsolutions.com/support/library/wuc95/index.html#Aircraft> (September, 1999).

Moon, Y., Bharatram, G., Schimmels, S., and Venkayya, V. (1996) A Vulnerability and Map of a Commercial Aircraft. MSC 1996 World Users' Conference Proceedings.<http://www.mechsolutions.com/support/library/wuc96/index.html#Aircraft> (September, 1999).

Moyer, E.T., McNaight, B.C., and Miller, R.D. (1992). The Reduction of Aircraft Panel Blast Loading by Venting. Proceedings FAA Aircraft Hardening and Survivability Symposium. (pp. 230-249).

Niu, M.C. (1988) Airframe Structural Design. Los Angeles: Conmilit Press Ltd.

Roskam, J. (1985). Airplane Design – Part III. Ottawa, Kan.: Roskam Aviation and Engineering Corp.

Sanai, M., and Greenfield, G.R. (1992) Improving Aviation Security Through Hardening of Luggage Containers. Proceedings FAA Aircraft Hardening and Survivability Symposium. (pp. 46-50).

Sanai, M. and Greenfield, G.R. (1993). U.S. Patent No. 5,267,665 – Hardened Luggage Container. Washington, D.C.: United States Patent and Trademark Office.

Shand, E.B. (1958). Glass Engineering Handbook.

Strang, W.Z. (1992, December) Numerical Simulation of a Charge Detonation Within an Axi-Symmetric Shell. Proceedings FAA Aircraft Hardening and Survivability Symposium. December 1992, (pp. 292-301).

Thompson, P.A. (1972) Compressible-Fluid Dynamics, New York: McGraw-Hill.

Timoshenko, S. and Woinowsky-Krieger, S. (1959), Theory of Plates and Shells, New York: McGraw-Hill.

Wald, M.L. (1997, May 18). Jetliner is Bombed in Test to Counter Terrorism in the Air. New York Times. p. 18.

White, C.E., Bharatram, G., and Venkayya, V.B. (1992, December) Finite Element Models of the B-52 Blast Tests. Proceedings FAA Aircraft Hardening and Survivability Symposium. (pp. 206-229).

Wilson, J. (1997 October). Blowing Up A 747. Popular Mechanics, 56-57.

Winters, L. (1990, January). High-Speed Flash Photography With Sound Triggers. The Physics Teacher, 12-19.

Zukas, J.A., & Walters, W.P. (Ed.). (1998). Explosive Effects and Applications. New York: Springer-Verlag.